PURIFICATION OF Cd, Zn AND Te FOR CdZnTe GROWTH

by

MICHAEL MEIER

B.S., Federal Institute of Technology, Lausanne, Switzerland, 2005

M.S., Federal Institute of Technology, Lausanne, Switzerland, 2007

_____

A THESIS

submitted in partial fulfillment of the
requirements for the degree

MASTER of SCIENCE

Department of Mechanical and Nuclear Engineering
College of Engineering

KANSAS STATE UNIVERSITY
Manhattan, Kansas
2009

Approved by:

Major Professor
Dr. Douglas S. McGregor

Copyright

Abstract

Purification of cadmium, zinc and tellurium was attempted to improve the quality of cadmium-zinc-telluride (CdZnTe) crystal growth. Specifically, vacuum distillation, zone refining and H_2 gas flow assisted zone refining were all investigated as methods to purify the constituent elements of CdZnTe. A unique multi-chamber ampoule was used to enable a purification sequence starting with double vacuum distillation followed by zone refining all without sample handling after the initial step. Modifications due to unique material properties of Cd and Zn were developed. Glow discharge mass spectroscopy (GDMS) analysis was used to measure impurity concentrations of 74 elements.

Cd purification using vacuum distillation proved to be an effective method to reduce the impurity level of 5N starting material to a purity between the range of 6N5 and 7N5, as measured using GDMS and laser ablation mass spectroscopy. Combined Zn double vacuum distillation and zone refining in an enclosed Ar atmosphere using 5N starting material yielded material with a purity between the range of 5N8 to 6N8. Tellurium purification using combined double vacuum distillation followed by zone refining under continuous H_2 flow of 4N specified raw material resulted in high purity tellurium between the range of 6N3 and 7N4.

Table of Contents

List of Figures

List of Tables

Acknowledgments

The author acknowledges the outstanding contributions to this work by Amy Hageman, Dr. Mark Harrison, Tyler Krehbiel and Steven Spalsbury.

Further thanks go to the entire Semiconductor Materials and Radiological Technologies (S.M.A.R.T.) Laboratory staff for their continuous support.

Special thanks go to Dr. Douglas S. McGregor for his guidance, encouragement and trust expressed throughout the entire project.

Chapter 1

Introduction

Cadmium Zinc Telluride (CdZnTe) has been shown to be the most promising material for room temperature X-ray and gamma ray spectroscopy grade detectors [1]. The combination of its high resistivity and relatively high photon absorption efficiency renders this crystal particularly advantageous.

McGregor et al. have developed spectroscopy grade CdZnTe detectors achieving 1% FWHM at 662 keV at room temperature operation [2]. A relatively simple Frisch ring design, based on an optimized geometry, achieved spectroscopy grade resolution without electronic correction (Fig. 1.1).
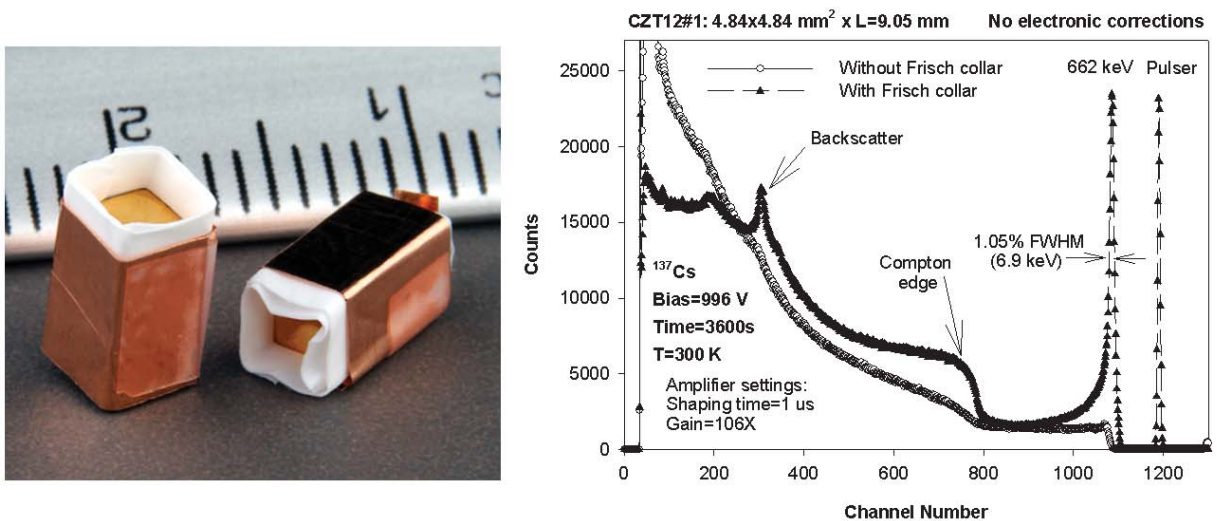
Figure 1.1: Frisch ring CdZnTe detector (left), gamma-ray energy spectrum (right) from [2].

However, impurities present in raw starting material can degrade device performance. Impurities change the conductivity and create charge carrier traps. Unfortunately, the S.M.A.R.T. Laboratory has experienced difficulty acquiring the raw materials Cd, Zn and Te at a consistent purity to develop reliable CdZnTe growth methods. Furthermore, prices for these three materials tend to increase drastically for purity levels higher than 4N-5N. These high costs are one motivation to develop in-house purification methods. Further, it is important to control the quality of the starting material for consistent results.

The following section address CdZnTe properties followed by the material purification section which illustrates the need for material purification for semiconductor radiation detectors. Finally, the chapter concludes with a thesis overview.

1.1   CdZnTe Properties

CdTe growth yield was limited by the low strength and the low thermal conductivity of the material, but adding Zn made the growth process easier, and the number of crystal defects could be decreased [3]. Typically, CdZnTe is grown as an alloy of CdTe and 4% to 20% of ZnTe.

CdZnTe is a direct bandgap semiconductor that is primarily used in electro-optic applications such as in infrared array technology as a substrate for HgCdTe epitaxial growth [4]. It has a band gap energy in the range of 1.4 eV to 1.65 eV, depending on the Zn concentration, which classifies it as a wide band gap semiconductor [5].

Semi insulation or intrinsic CdZnTe crystals have high intrinsic resistivities ($\rho_{CdZnTe} \approx 10^{10} - 10^{11}$ Ωcm^{-3} [5]) due to a low intrinsic charge carrier density and the relatively large band gap energy E_g. The free charge carrier concentration n_i for an intrinsic semiconductor, where background impurities have a negligible effect, can be determined with,

$$n_i = \sqrt{N_C N_V} \, \exp\left(-\frac{E_g}{2kT}\right),$$
(1.1)

where N_C and N_V are the effective density of states in the conduction and valence bands, respectively, k designates the Boltzmann constant, and T represents the absolute temper-

ature [6]. The intrinsic resistivity ρ_i can be calculated as a function of the intrinsic free charge carrier concentration as

$$\rho = \frac{1}{q\left(n\mu_n + p\mu_p\right)} \tag{1.2}$$

where $q = 1.6 \times 10^{-19}$ As is the elementary charge, μ_n and μ_p are the electron and hole mobilities, and n and p are the free electron and hole concentrations, respectively. For an intrinsic semiconductor, p and n are equal to the intrinsic free charge carrier density n_i. If no impurities are present, the relatively high band gap energy E_g of CdZnTe (1.4 eV to 1.65 eV) yields high resistivity, according to Eqs. (1.1) and (1.2).

Silicone or gallium arsenide based semiconductor detectors with lower intrinsic resistivity are typically constructed with blocking contacts to reduce leakage currents. They are operated in reverse bias to form a depletion layer (the active region of the detector) to reduce generation current. Only under these circumstances can Si and GaAs based devices operate as spectrometers. CdZnTe high resistivity material, however, can be used without blocking contacts mainly because leakage currents are already low. Ohmic contacts are typically applied so that the voltage drop is spread out over the entire crystal, which ensures a large active region, thereby improving gamma ray detection efficiency.

The probability of photoelectric absorption, described by the photoelectric cross section, can be estimated based on the atomic number (Z-number) of the material and the gamma-ray energy. The "probability that a photoelectric absorption will occur per unit distance traveled by the photon" τ can be approximated by

$$\tau \approx K\frac{Z^n}{E_\gamma^{3.5}}, \tag{1.3}$$

where E_γ is the gamma-ray (photon) energy, Z is the atomic number of the material and K is a proportionality constant independent of E_γ and Z. The exponent n is generally between 4 and 5 [7]; hence photoelectric energy deposition efficiency is a strong function of the atomic number. Heavy materials are therefore preferred for gamma-ray detectors to provide adequate absorption efficiency. Ultimately, CdZnTe detectors ($Z = 48$, 30, 52) offer

comparable energy deposition efficiency to that of commonly referenced NaI ($Z = 11, 53$) scintillator detectors.

CdZnTe material charge transport characteristics are quite different for electrons and holes. Electrons have a mobility μ_e of approximately 1350 cm^{2}V^{-1}s^{-1} and a mean free drift time τ_e ranging from 100 ns to 1μ s, whereases holes have a mobility μ_h of approximately 120 cm^{2}V^{-1}s^{-1} and a mean free drift time τ_h ranging from 50 to 300 ns [5]. The low mean drift time of holes is mainly due to hole trapping at crystal imperfection locations, such as Te precipitates.

The induced charge $Q(x)$ for a planar semiconductor detector is dependent on the position of the radiation interaction location (distance from the anode x) due to non-symmetric charge transport characteristics of electrons and holes. The measured induced charge can be described by the Hecht equation [8]:

$$Q(x) = Q_0 \left[\rho_e \left(1 - \exp\left(\frac{-x}{W\rho_e} \right) \right) + \rho_h \left(1 - \exp\left(\frac{-(W-x)}{W\rho_h} \right) \right) \right], \qquad (1.4)$$

where Q_0 is the initial charge created by the radiation interaction event, W is the width of the detector region, and ρ_e and ρ_h are the charge carrier extraction factors for electrons and holes, respectively, defined as

$$\rho_{e,h} = \frac{\mu_{e,h} E \tau_{e,h}}{W}, \qquad (1.5)$$

where E is the electric field strength, $\mu_{e,h}$ the respective mobility, and $\tau_{e,h}$ is the mean free lifetime for electrons and holes, respectively. The product $\mu_{e,h} E$ is equal to the respective charge carrier drift velocities $v_{e,h}$.

McGregor and Knoll et al. [8] showed that generally low values or unequal charge extraction factors for holes and electrons lead to poor energy resolution. In those cases, the induced charge becomes a function of the radiation interaction location. In particular, CdZnTe crystals suffer from a much lower hole charge extraction factor mainly due to a lower mean free drift time from hole trapping. Mean life time of charge carriers is strongly dependent on the impurity concentration since impurities create deep energy levels and

scattering centers in the band gap. Thus carrier mobility is a function of crystal perfection and purity [9].

To improve the energy resolution of CdZnTe detectors, the detector width W could be reduced, which, however, leads to a lowered intrinsic detector efficiency and a higher capacitance. Alternatively, single charge carrier devices, where the induced signal is due mainly to the electron motion, have been successfully demonstrated by McGregor et al. [2]. For example, the Frisch-collar CZT detector design, with a corresponding energy spectrum, is shown in Fig. 1.1. The non linear weighting potential produced by the Frisch collar suppresses the charge induced by the hole movement, thereby rendering the device a quasi single charge carrier device.

High quality CdZnTe crystals nevertheless remain the key factor for high resolution spectroscopy grade detectors. Accordingly, motivation to reduce hole and electron trapping in CdZnTe therefore remains, and raw material purification is the key objective of this research. Further, crystal properties change as a function of starting material; hence, in-house purification adds an important control step for CdZnTe growth.

1.2   Raw material purification

Along with introducing or increasing charge trapping, impurity atoms that become electrically active adversely affect the electrical properties of a semiconductor. For example, impurities acting as donors or acceptors introduce free charge carriers to the crystal bulk, thereby affecting leakage current and reducing the energy resolution.

However, impurity atoms are not necessarily in an ionized state and therefore electrically active. The energy level of the respective impurity atom, and the thermal energy available (kT), determine whether an impurity atom becomes electrically active. Such impurities fall broadly into two categories: donors and acceptors. A donor impurity is an atom (or a molecule) that releases valence electron into the conduction band, denoted as an n-type (negative charge carriers) semiconductor. An acceptor atom attracts an electron from the

semiconductor valence band and binds it, denoted as a p-type (positive charge carrier) semiconductor. The empty valence band state (designated as hole) acts as a charge carrier for p-type semiconductors.

The ionized impurity concentration (N_D^+ for donors, N_A^- for acceptors) can be calculated using the Fermi-Dirac probability distribution function,

$$N_D^+ = \frac{N_D}{1 + \frac{1}{g_D} \exp\left(\frac{E_D - E_F}{kT}\right)} \tag{1.6}$$

and

$$N_A^- = \frac{N_A}{1 + g_A \exp\left(\frac{E_A - E_F}{kT}\right)}, \tag{1.7}$$

where N_D and N_A are the donor or acceptor concentrations, respectively, and E_D and E_A designate the respective energy levels. The degeneracy factors, $g_D = 2$ and $g_A = 4$ account for the different possible permutations that the energy states can be filled, due to two different spins and over lapping valence bands [10]. E_F is the Fermi energy level, defined as the energy state at which the probability of occupation by an electron is exactly one-half [6]. Also, at 0 K, all states below E_F will be filled, all above will be empty. E_F itself is a function of the charge carrier concentrations n and p, defined by,

$$\frac{E_F - E_i}{kT} = \ln\left(\frac{N_D^+}{n_i}\right) \tag{1.8}$$

and

$$\frac{E_i - E_F}{kT} = \ln\left(\frac{N_A^-}{n_i}\right). \tag{1.9}$$

Equations (1.6) through (1.9) can be used to find E_F, iteratively.

In CdTe, the electrically active impurities are reported to be Li, Na, K, Al, Ga, In, N, P, As, Sb, Bi, Cl, Br, I, Cu, Ag and Au [11]. It is believed that the same impurities are likely to be electrically active in CdZnTe. Finally, according to [12], nearly all impurities are reported to be ionized down to liquid nitrogen temperatures in CdTe. Since CdZnTe detectors are designed to operate at room temperature, the interest in reducing impurity concentration (N_D and N_A) to reduce bulk leakage current is evident.

1.3 Research Scope

The scope of this work was to integrate two methods to purify Te, Zn and Cd for CdZnTe crystal growth, those being vacuum distillation and zone refining. The vacuum distillation stages were designed by Dr. Mark Harrison and were later characterized by Amy Hageman. The author then added a zone refining system to the purification chain. The intent was to purify the three relevant materials with both methods without handling the material between steps. Due to particular material properties of Cd and Zn, modifications had to be carried out. Ultimately, the research goal was to develop purification recipes that consistently yield high purity materials suitable for CdZnTe crystal growth.

The thesis contains a theory chapter, where vacuum distillation and zone refining are discussed, and a numerical code is described for predicting the impurity distribution after an arbitrary number of purification passes. The theory chapter concludes with a literature review covering Te, Zn and Cd purification using vacuum distillation and zone refining techniques. Described in the system design chapter is the equipment used for the purification processes, mostly dedicated to the zone refining equipment built by the author. The remaining chapters describe the experimental procedure, results and discussion and are followed by a conclusion talking about improvements and future work.

Additional information is reserved as part of the appendix, for example the zone refining Matlab code and the impurity analysis results. Also, significant effort was put into vapor pressure fit equations for relevant materials, and these equations along with the parameters are in appendix B, where the vapor pressure for common impurities is plotted for the respective pre-distillation and distillation temperatures.

Chapter 2

Theory

Material purification can be defined as the separation of a chemical substance of interest from contaminating substances. Depending on the purity level desired and the material of interest, different technologies based on different physical mechanisms are employed. In the context of the present work, vacuum distillation and zone refining were chosen to generate high purity material (6N-8N). Specifically, this chapter focuses on vacuum distillation, zone refining and on general ultra-high purification efforts reported in literature on Cd, Zn and Te.

Purity levels are typically expressed in percentages weight. An abbreviated nomenclature states the number of nines in the percentage figure. For increased precision, the fist non-nine digit is added so that 99.9983 is given as 4N8 purity, for instance.

2.1   Material Purification Techniques

Distillation is the most widely applicable and a very commonly used method of purification [13] based on the difference in volatility (vapor pressure) of impurities and that of the material of interest. Many subcategories exist, one of which is vacuum distillation, which is employed for materials with particularly high melting temperatures.

Also, partial recrystallization is commonly used for inorganic material [13]. It is based on the fact that the crystallization (solidification) process generally tends to reject or attract impurities. Zone refining is one subcategory of recrystallization purification methods.

Other purification methods are chemical where the differences in attraction to chemical, agents between contaminants and the substance of interest are exploited. Contaminants may be removed by a compound formation that leads to precipitation, for instance. Electrolytic purification is another example, where an electric current is passed through an ionic substance and cation material builds up at the cathode while anion material builds up at the anode. Natural separation such as filtration based on different material particle size is mostly used in early stages in the purification chain.

The quality of the purification process can be characterized based on the separation coefficient S_C computed as

$$S_C \ [\%] = \frac{C_i - C_f}{C_i} \cdot 100 \tag{2.1}$$

where C_i is the initial concentration, and C_f designates the concentration after purification. Furthermore, S_C is a dimensionless number that expresses the absolute purity improvement relative to the designated starting purity.

If purities greater than 6N are required, such as for different electronic applications of cadmium, conventional purification methods such as electrolysis are not sufficient [14]. In those case, the term ultra (high) purification is typically used.

2.2 Vacuum Distillation

Distillation in general is a commonly utilized method for separating mixtures based on different volatilities of the constituents. In particular, distillation performed under a vacuum allows for lower distillation temperatures and avoids chemical reactions of the product with gases present (i.e. oxygen in air). Vacuum distillation therefore is preferred where high purity material is desired and for substances with particularly high atmospheric boiling points.

In a closed system, there is an equilibrium between between solid phase and its vapor phase. Thermodynamics describes the equilibrium coexistence as a function of temperature. Liquids and solids have a tendency to evaporate whereas gases have a mutual tendency to

condense to solid or liquid phase. For a set temperature, there is a set pressure (its vapor pressure) at which the gas of that substance is in dynamic equilibrium with its liquid or solid form. Also, the vapor pressure of any substance increases non-linearly with temperature according to the Clausius-Clapeyron relation [15]. Therefore, as the temperature rises, atoms have a stronger tendency to leave the solid or liquid phase due to the increased thermal agitation so that the vapor pressure generally increases with rising temperature.

The boiling point of a liquid is defined as the temperature where the vapor pressure equals the surrounding pressure. From this temperature, with an incremental increase in temperature, the vapor pressure becomes sufficient to overcome the surrounding pressure and lift the liquid to form bubbles inside the bulk of the substance. Bubble formation deeper in the liquid requires a higher pressure, and therefore a higher temperature. The boiling point temperature is therefore clearly a function of the surrounding pressure. The commonly used atmospheric boiling point is defined for standard atmospheric surrounding pressure (i.e., 101.325 kPa).

For temperatures lower than boiling temperature, evaporation from a liquid is limited to the surface exposed to the vapor phase, whereas exceeding the boiling temperature allows material from within the body to evaporate. As a result, the evaporation rate increases drastically when the boiling temperature is reached. Most materials are distilled from the liquid phase. Materials producing significant vapor pressure from the solid state exhibit sublimation distillation.

In a mixture of elements, partial pressure evolution governs the evaporation process. Dalton's law states that the total pressure is the sum of the vapor pressures of each individual constituent [15]. The pressure in a vacuum system is determined by the capacity of the vacuum pump, the rate of leakage and the sum of the individual vapor pressures of each component of the mixture. Therefore, only the fractional number and not the absolute number of vapor molecules of each constituent present in the "vacuum" can be determined by the respective vapor pressure.

By controlling the system temperature during evaporation, vacuum distillation can be used to harvest material characterized by a distinct vapor pressure. However it is not possible to completely purify a mixture by distillation since the impurities always present a non-zero vapor pressure at any given distillation temperature.

The distillation step is typically preceded by a lowered temperature pre-distillation step where highly volatile particles are outgassed. Clearly, selection of pre-distillation and distillation temperatures are critical to successful purification [9]. A distillation temperature too low results in slow vaporization, which in turn causes slow condensate deposition and a correspondingly slow purification rate. However, higher temperatures than necessary will cause impurities with lower vapor pressures to vaporize and condense on the deposition surface, minimizing the purification effect.

2.2.1 Evaporation in Vacuum

Under high vacuum, it can be assumed that the vapor atoms leave the emitting surface relatively unimpeded. The rate at which atoms leave the liquid can therefore be assumed to be the same as that of atoms evaporating from the surface of the substance in dynamic equilibrium with its saturated vapor [16]. Recall that in the case of the dynamic equilibrium described in Section 2.2, evaporation and condensation occur at the same rate. Based on those assumptions, Irwin Langmuir derived an equation for the rate of evaporation R [$\text{gcm}^{-2}\text{s}^{-1}$] in vacuum:

$$R \equiv \frac{1}{S}\frac{dM}{dt} = 0.0585 P_v a \sqrt{\frac{\tilde{m}}{T}} \tag{2.2}$$

where M is the mass being evaporated, a is the probability an atom remains on the molten surface, typically assumed to be equal to unity, P_v is the vapor pressure in torr, $\tilde{m}$ is the molecular weight of the substance being evaporated, and T is the absolute temperature in K. Where the material evaporates in molecular form, Eq. (2.2) has to be adapted. Generally, however, metals are evaporated as atoms, dissociated from each other.

Note that the rate of evaporation no longer depends on the overall pressure in the

enclosure as the gaseous phase does not exert significant pressure on the substance to be evaporated [16]. In vacuum distillation, typically the temperature is not raised above boiling point, so that evaporation is limited to the surface exposed to the vacuum. Notably, the evaporation rate calculated with Eq. (2.2) typically overestimates the actual evaporation since the evaporation surface often may be covered with an impervious coating, such as an oxide layer.

2.2.2 Transport and Deposition Process

Once vaporized, the mean free path of a suspended particle (atom, molecule), as well as the temperature of the enclosure and the material, determine whether the particle will condense in solid form, in liquid form, or will remain in the vapor state.

The average distance traveled by a vapor particle in between collisions with a residual gas particle is known as the mean free path λ which expressed in cm can be calculated using the Sutherland formula given as

$$\lambda = 2.33\text{E-}20\frac{T}{\xi^2 P} \tag{2.3}$$

where ξ is the diameter of evaporation atom in cm, T is the absolute gas temperature in K, and P is the pressure in torr.

The transport of particles in a vacuum can be categorized as either *molecular*, where the mean free path is larger than the characteristic distance L between evaporation and distillation ($\lambda > L$), or *viscous*, where the mean free path is shorter than the characteristic distance ($\lambda < L$). In a molecular type situation ($\lambda > L$), the atoms travel in straight lines, and few collisions occur with the residual gas. Viscous type distillation ($\lambda < L$), however, occurs at higher pressures where chains of atoms may still be intact in the vapor phase [17]. The transport characteristics in vacuum are an important factor affecting the efficiency of the distillation process.

Langmuir later formulated the concept of a critical temperature for condensation that was a function of the intensity of the impinging vapor stream. Langmuir showed that

low condensation rates could not be attributed to reflection but to condensation and re-evaporation on the receiving surface [16]. His theory assumes that an atom spends an *average life* on the surface before being re-evaporated due to thermal energy provided by the receiving surface. However, if a second atom collides while the first atoms is attached to the receiving surface, an atom pair is formed, and the energy required to re-evaporate an atom-pair is considerably increased. This concept explains the combined influence of surface temperature and the intensity of the vapor stream on the deposition process.

Cadmium atoms were experimentally found to condense on non-metallic surfaces with difficulty unless the surface temperature was greatly reduced [16]. However, once a first layer had been formed, the cadmium condensed readily at room temperature.

2.3 Zone Refining

Zone melting and its related techniques emerged in the early 1960s. The first important application of zone melting was to purify of germanium for transistors [18]. The usage was soon extended to any substance that can be safely melted and exhibits a difference in impurity concentration between liquid and freezing solid.

The general term zone melting describes the family of methods controlling the distribution of soluble impurities in crystalline materials. Other than purification, zone melting techniques are also applied as methods to distribute dopants uniformly throughout a crystal, a technique referred to as *zone leveling*.

Zone melting methods have in common that a part of a charge is melted, and the freezing interface is moved along the charge. The freezing interface has a tendency either to reject or accumulate impurities, which is the basis of separation or purification by zone melting.

The term *zone refining* designates a zone-melting method with the purpose of purification. A molten zone is moved along a solid charge in one direction pushing certain impurities along and rejecting others. The extremities of the charge accumulate impurities as the number of passes is increased. However, the purification efficiency of each pass decreases, and

the external contamination of impurities starts to become significant.

The impurity distribution can be mathematically expressed in terms of geometrical parameters such as zone length, ingot length, the number of passes and the distribution coefficient k. The distribution coefficient (segregation coefficient) is the key material property related to zone melting techniques. k is defined as the ratio of impurity concentration in the freezing solid to the impurity concentration in the main body of the freezing liquid. The equilibrium value of the distribution coefficient can be taken from the phase diagram's liquidus and solidus line if available. A non-unity distribution coefficient indicates either an attraction or rejection effect of the freezing interface. The value for k for typical impurities for commonly zone refined materials can be found in literature but typically presents a large discrepancy among sources.

2.3.1 Impurity Segregation in Zone Refining

Equilibrium between liquid and solid phase of a binary system shows that the solute concentration in the freezing solid differs from that in the liquid. Binary phase diagrams describe the effect of the solute concentration on the phase of a substance and distinguish homogeneous liquid zones, heterogeneous two phase zones, and homogeneous solid zones where the solute is in solid solution. The three zones are separated by the liquidus and the solidus line. An idealized phase diagram with its three zones is shown in Fig. 2.1. Notably, phase diagrams are drawn for thermodynamic equilibrium, which is never entirely attained during a solidification process. It can, however, be assumed that the concentrations close to the freezing interface in the solid and liquid closely approach equilibrium state [18] so that considerations based on phase diagrams are viable.

The equilibrium value of the distribution coefficient (also designated segregation coefficient) k_0 for a certain solute (impurity) / solvent (bulk material) combination can therefore be taken from the respective phase diagram. The equilibrium segregation coefficient k_0 is defined as the ratio between the concentration of impurity atoms in the growing crystal

14

(solidus concentration) and that of the melt (liquidus concentration) as shown in Fig. 2.1,

$$k_0 \equiv \frac{C_S}{C_L}. \tag{2.4}$$

Typically, the equilibrium segregation coefficient has a value lower than unity because impurity atoms tend to be rejected by the solute in the growing crystal lattice. The presence of such impurities lowers the melting point of the mixture as compared to that of the pure material.

Consider Fig. 2.1 where a melt with an impurity concentration C is cooled down below liquidus temperature. The first crystal to appear will have a solvent concentration $C_S = k_0 C$ according to the definition of k_0 in Eq. (2.4). As the solidification continues, the solid shrinks in proportion, but its impurity concentration increases according to the solidus concentration. The impurity concentration in the remaining liquid increases (liquidus concentration) until the last liquid drop reaches an impurity concentration of C/k_0. Under perfect equilibrium, however, the impurity concentration throughout the entire formed crystal will be uniform and equal to the initial C_L concentration due to diffusion in the solid. This idealized scenario is known as equilibrium freezing, which is not achieved in practice.

Since the diffusion of solute in the solid is slow, the part of the crystal formed first will have a smaller impurity concentration, and the last fraction of the crystal formed will have a greater impurity concentration than the initial melt. Therefore, the freezing interface has a tendency to reject impurities where k_0 is lower than unity.

When impurities raise the melting point ($k_0 > 1$), the case can be treated as the solid tending to attract impurities. The simplified case where k_0 is independent of impurity concentration is characterized by solidus and liquidus being straight lines; however in practice, k_0 depends on the impurity concentration, which is reflected in curved liquidus and solidus lines.

As opposed to calculating the equilibrium segregation coefficient k_0 from existing equilibrium phase diagrams, the effective segregation coefficient is often calculated from a fractional crystallization experiments such as a zone melting run. The effective segregation coefficient

15
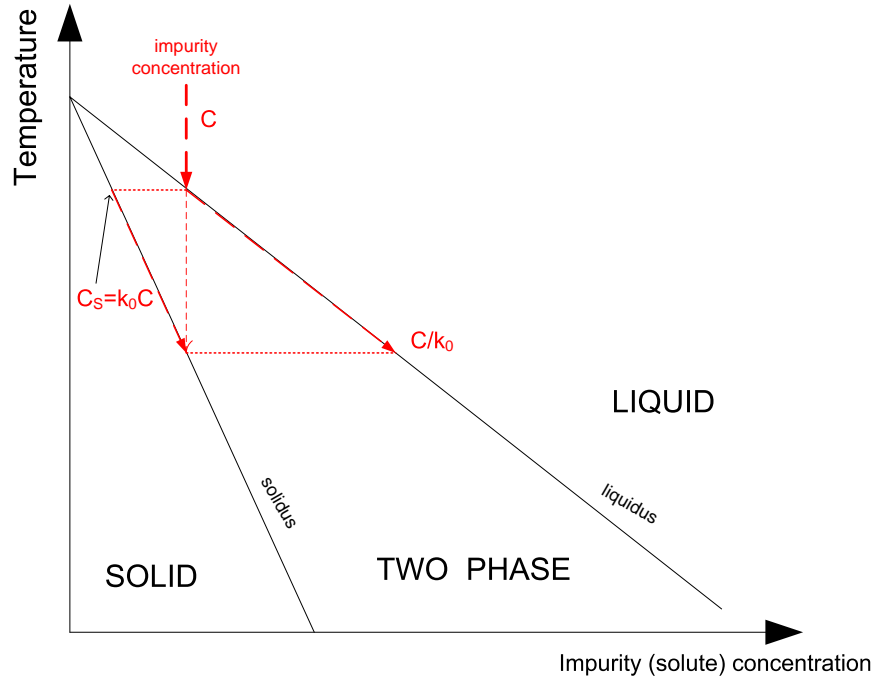
Figure 2.1: Equilibrium freezing shown in an idealized phase diagram.

calculated from *measured* impurity distributions is designated k or k_{eff}.

2.3.2 Mathematical Description

A mathematical description of the zone refining process illustrated in Fig. 2.2 is given in the present chapter. The mathematical description increases understanding and allows predictions of the effects caused by different parameters such as zone length, charge length and segregation coefficient.

a) Single-Pass Distribution

In order to derive an expression for the impurity concentration distribution after n zone refining passes, the following assumptions apply:

- Diffusion and convection erase concentration gradients within the melt.
- The concentration of a specific impurity in the newly crystallized solid C_S is k times that in the melt C_L, namely $C_S = kC_L$.
- The impurity concentration is small so that k is assumed to be invariant of the impurity concentration.

16
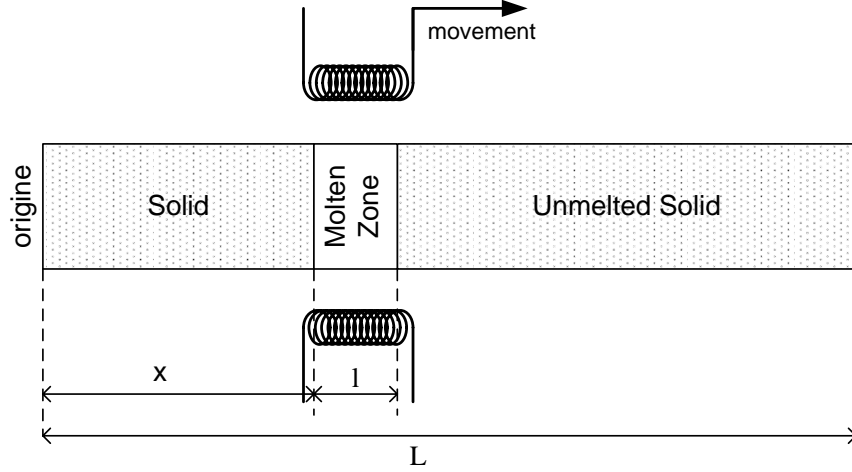
Figure 2.2: Schematic representation of zone refining process.

- The zone length l and rod cross section A are constant. For simplicity, without restricting the generality, the cross section is set equal to one.

- The initial impurity distribution of the charge is uniform and designated C_0.

As an intermediate variable, the number of impurities in the molten zone is defined as I. Thus, the molten zone advancing by an infidecimal distance of dx will experience a change dI of the number of impurities, which is equal to the initial concentration entering the melt C_0 minus the concentration rejected to the solid C_S, which is equal to kC_L so that

$$dI = (C_0 - kC_L)dx. \tag{2.5}$$

Assuming perfect mixing in the melt, the impurity concentration in the liquid for an unitary cross section per definition can be written as

$$C_L = I/l \tag{2.6}$$

and accordingly, the initial concentration is given as

$$C_0 = I_0/l. \tag{2.7}$$

Integrating Eq. (2.5) using Eqs. (2.4), (2.6) and (2.7) leads to the theoretical single zone distribution:

$$\int_0^x d\tilde{x} = \int_{I_0}^I \frac{d\tilde{I}}{C_0 - \frac{k\tilde{I}}{l}} \tag{2.8}$$

17

$$\frac{C_S(x)}{C_0} = 1 - (1 - k)\exp\left(-\frac{kx}{l}\right). \tag{2.9}$$

As the freezing interface rejects impurities for $k < 1$, the solid close to the origin will be purified, and the liquid in the molten zone will be solute enriched. The concentration in the molten zone builds up and approaches C_0/k_0 from where the concentrations entering and leaving the zone are approximately equal, and no more purification effect is achieved.

Eq. (2.9) is mathematically valid up to the point where the melting interface reaches the end of the charge $x < (L - l)$ from where *normal freezing* equations analytically describe the impurity distribution after the zone pass. The situation is illustrated in Fig. 2.3.
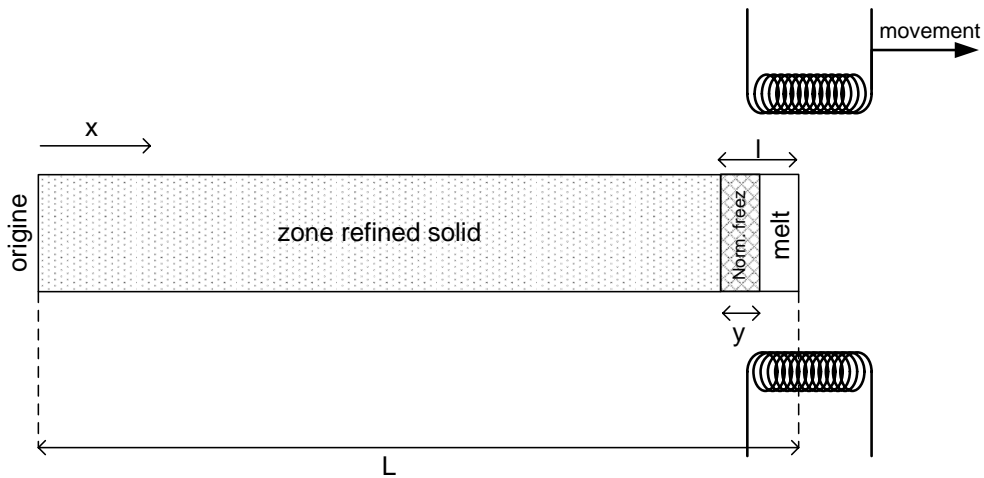
Figure 2.3: Schematic representation of normal freezing process.

Normal freezing is where the freezing interface is moved along an initially entirely molten charge, as opposed to zone refining where the molten zone shrinks and *no* new material enters the molten zone. Instead, the impurities build up in the melt as the solidification front advances, and the last parts to solidify will contain a high concentration of impurity.

Normal freezing, also known as directional solidification, can be used as a purification process by itself. However, the last part to solidify has to be discarded before a successive normal freezing cycle can be attempted. This is relatively wasteful, and the cut procedure potentially introduces contamination, which makes normal freezing relatively unattractive for ultra-high purification [19].

The distribution after a normal freezing cycle can be analytically calculated [18] and is given by

$$\frac{C(\tilde{y})}{C_0} = k(1 - \tilde{y})^{k-1} \tag{2.10}$$

Where $\tilde{y}$ is the fraction of the original liquid that has crystallized given as

$$\tilde{y} \equiv \frac{y}{l} = \frac{x - (L - l)}{l}. \tag{2.11}$$

Equations (2.9) and (2.10) are basically dimensionless since they are ratios just as the segregation coefficient, k. Concentrations can be expressed in atom fractions (mol fractions) or weight fractions. If volumetric units are used such as "atoms per cm^3", then it is necessary to introduce a density ratio of the solid density to the liquid density or to simplify by assuming the densities of liquid and solid to be equal [18].

b) Multi-Pass Distribution

Impurity distributions after a finite number of passes $(n > 1)$ have to be computed numerically. No explicit analytical solution has been found; only approximate analytical solutions for semi-infinite ingots exist [18]. However, the author wrote a numerical code to illustrate the effect of different parameters such as distribution coefficient, zone length and number of passes on multi pass distributions.

The code calculates the purity of the freezing material for two different situations. The initial position 0, where the full extent of the melt zone is reached (position 0), has to be treated differently from a generic position i, where material enters the melt zone through the melting interface and purified material exits through the freezing interface (position i).

Position 0: Performing a n-th zone refining pass, the heaters start to cover one side of the charge, and a molten zone starts to form until it attains its full extension l as illustrated in Fig. 2.4. The number of discrete space steps (length ϵ) is given as l/ϵ. The impurity concentration of the melt at the initial position $(i = 0)$ during the n-th pass $C_{liquid,0}^n$ is given as the average of the concentrations from the previous pass C_i^{n-1}:

19
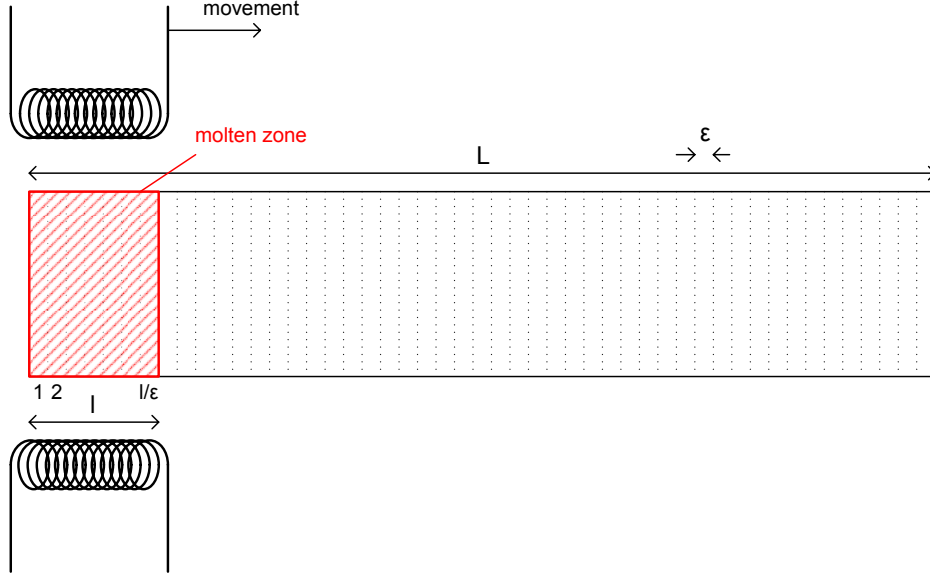
Figure 2.4: Spatial discretization of zone refining rod.

$$C_{liquid,0}^n = \frac{\sum_{i=1}^{l/\epsilon} C_i^{n-1}}{l/\epsilon}. \tag{2.12}$$

Here, researchers assume diffusion and convective mixing in the melt erases any concentration gradient and no material has frozen out at this stage.

Position $i > 0$: At position i ($i = 1, 2, 3, ..., \left(\frac{L-l}{\epsilon} - 1\right)$), the ith zone presently froze with a concentration C_i^n as shown in Fig. 2.5. The concentration of the recrystallized solid is equal to k_0 times the impurity concentration of the liquid right before the ith zone froze,

$$C_i^n = k_0 C_{liquid,i-1}^n. \tag{2.13}$$

The concentration of the new melt $C_{liquid,i}^n$ is found from a species balance: the concentration of impurity species in the liquid immediately before the ith zone froze $C_{liquid,i-1}^n$ plus the concentration from the newly melted zone at $i + l/\epsilon$ must be equal to the concentration of the ith liquid zone $C_{liquid,i}^n$ plus the concentration of the zone that most recently froze with C_i^n. The respective concentrations must be weighted by the extension of their respective
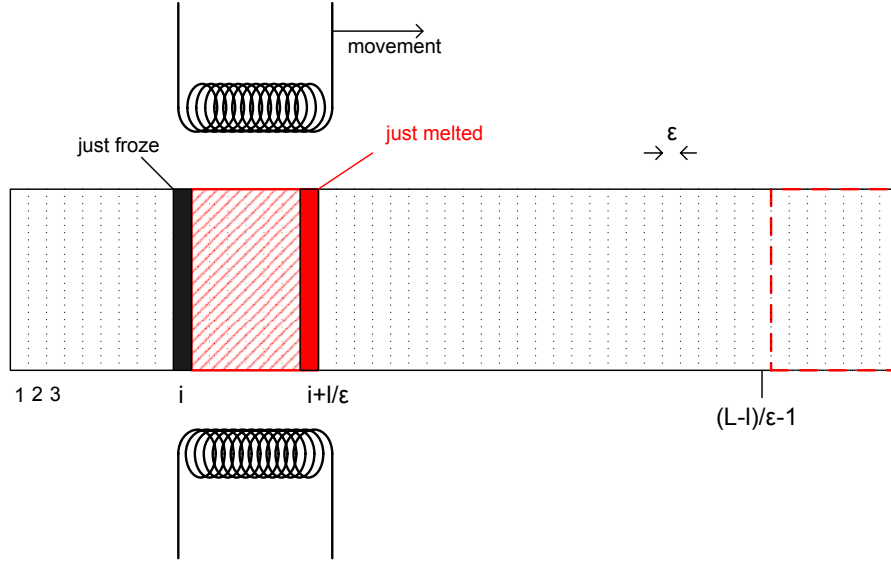
Figure 2.5: Zone refining heaters at discrete position i.

zones so that

$$lC_{liquid,i-1}^n + \epsilon C_{i+l/\epsilon}^{n-1} = lC_{liquid,i}^n + \epsilon C_i^n. \tag{2.14}$$

Solving for $C_{liquid,i}^n$ yields,

$$C_{liquid,i}^n = C_{liquid,i-1}^n + \epsilon/l \left[C_{i+l/\epsilon}^{n-1} - C_i^n \right]. \tag{2.15}$$

A loop can be implemented covering the different positions $i = 1, 2, ..., (\frac{L-l}{\epsilon} - 1)$ to calculate the impurity distribution after one pass based on the impurity distribution resulting from the $(n-1)$-th pass. A superimposed loop over different number of passes n allows one to compute the distribution after an arbitrary number of passes.

c) Ultimate Distribution

The impurity distribution mathematically reaches a steady state situation that characterizes the maximum attainable purification effect. The forward flux of impurities due to the rejection/attraction of impurities at the freezing interface is balanced by the backward flux due to the mixing effect in the molten zone [18]. An approximation for this ultimate

21

distribution can be calculated analytically as [18]

$$C(x) = Ae^{Bx}, \qquad (2.16)$$

where B is given implicitly by Eq.(2.17) and A is given explicitly by Eq. (2.18) as,

$$k = \frac{Bl}{e^{Bl} - 1}, \qquad (2.17)$$

$$A = \frac{C_0 BL}{e^{Bl} - 1}. \qquad (2.18)$$

Once the impurity distribution reaches the equilibrium situation of the ultimate distribution, further purification can be achieved only by cropping the extremities of the charge. By doing this, a "non-equilibrium" is externally introduced, allowing for further purification.

The ultimate distribution is an approximation because it does not take into account the back contamination effect from the last zone length described in Section 2.3.3. Also, a large number of zone passes is inefficient since contamination inevitably introduced over time starts to become relevant. The mathematical ultimate distribution description therefore remains purely mathematical. However, the ultimate distribution can be used to determine a reasonable number of zone passes by comparing measured purity levels of some well chosen impurities to the ultimate purity levels. Once impurity levels approach the ultimate distribution levels, additional passes become ineffective. However, impurities with segregation coefficients close to unity are often used as control impurities in order to check how far away the purification effect is from its best attainable result.

2.3.3   Parameter Study

The purification efficiency of the zone refining process mainly depends on the segregation coefficient of the considered impurity. As shown in the zone refining single pass Eq. (2.9), the purification effect also depends on the zone length of the molten zone. However, the mathematical description developed in Section 2.3.2 simply assumes a molten zone moving

along a charge without modeling any heat transfer aspects. Therefore, effects from parameters such temperature gradients, charge cross section and zone velocity can not be predicted with the given model. Those parameters have to be experimentally optimized or taken from literature, which this research has done. The code for multi pass distribution could, however, be used to illustrate the effect of the basic parameters: segregation coefficient k, zone length l and number of passes n.

a) Segregation Coefficient k

A set of computed impurity distribution curves for different values of k is shown in Fig. 2.6. The normalized zone refining solute concentration is plotted as a function of the normalized distance x/L from the charge origin where the zone moved from 0 to 1. As indicated in Eq. (2.9) k strongly affects the purification effect after one pass. Impurities with k smaller than unity will be rejected from the freezing interface building up in the normal freezing extremity. Meanwhile, impurities attracted by the freezing zone ($k > 1$) accumulate at
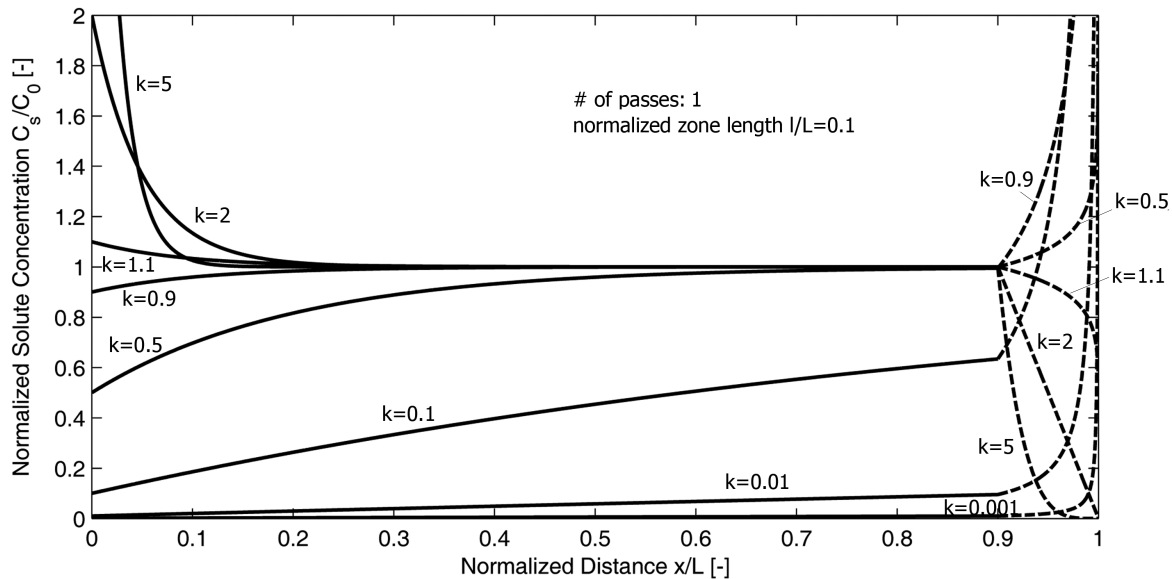
Figure 2.6: Numerical computation of impurity distribution for different segregation coefficients k. Solid line represents zone refining region; dashed line represents normal freezing region.

23

the origin of the charge. Fig. 2.6 clearly shows that if k is close to unity, the exponential concentration distribution flattens out within the rod, and the purification effect does not penetrate the entire charge, so a relatively large number of passes is required. In this example, the distribution in the normal freezing zone ($x/L > 0.9$) is hypothetical, and the predicted concentration distribution is far from achieved results. The reason is that the segregation coefficient changes as the impurity concentration in the melt builds up, which is not taken into account in the used model. However, since the extremities on both sides of the charge will be chopped off after zone refining purification, the true distribution in the extremities is of little interest.

b) Number of Passes n

The advantage of zone refining over techniques such as zone melting lies in the possibility of multiple passes. The distribution after different numbers of passes is illustrated in Fig. 2.7. Clearly, increasing the number of passes increases the purification effect. Impurities with $k < 1$ build up in the normal freezing zone. When the melt zone just barely reaches a part of the normal freezing zone in a consecutive pass, the melt becomes enriched with impurity concentration from the previously built-up impurities in the extremity. This effect leads to a back contamination effect clearly visible after 5 passes at $x/L \approx 0.8$ where a discontinuity appears.
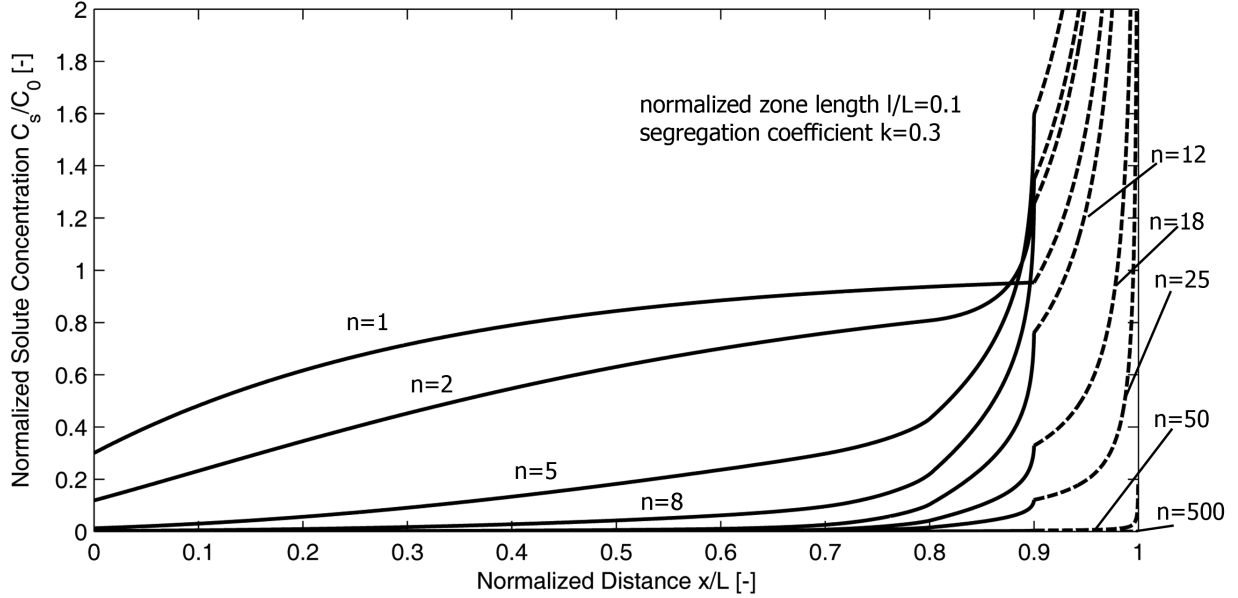
Figure 2.7: Numerical computation of impurity distribution for different number of passes n. Solid line represents zone refining region; dashed line represents normal freezing region.

The segregation coefficient ($k = 0.3$) value chosen to illustrate the effect of multiple passes is comparably high to typical k-values of common impurities. As mentioned before, the effect of changing k as the impurity concentration significantly increases (normal freeze region) or decreases (highly purified material) leads to a distorted estimation of the purification efficiency. Eventually, as high purity levels are reached, external contamination becomes significant, which limits the reasonable number of passes. Introduction of impurities from quartz, for example, may include Al, Li, Ca [17].

c) Zone Length l

The zone length l is determined mainly by the temperature profile imposed by the heating system and the conductive heat transfer in the charge. In a well-controlled thermal environment, l is relatively constant. As indicated in Eq. (2.9), the larger the zone length l, the better the purification efficiency for the initial pass. Fig. 2.8 shows a set of impurity distributions after a single pass for different l/L ratios. Note that to convey the effect of zone length influence a segregation coefficient of $k = 0.2$ was chosen, which is a lot closer to

25

unity than most of the common impurities.

After multiple passes, the back contamination effect described above becomes significant so that smaller zones become advantageous. The effect of zone length variation has been studied theoretically by [20]. For multipass operations, considerable improvement are reported by adjusting zone lengths in each pass separately.

Heat transfer in the charge tends to flatten out the applied temperature profile, which makes very short melt zones not feasible. This fact marks a lower boundary for the feasible zone length. To increase the l/L ratio, the length of the charge L is therefore increased often.
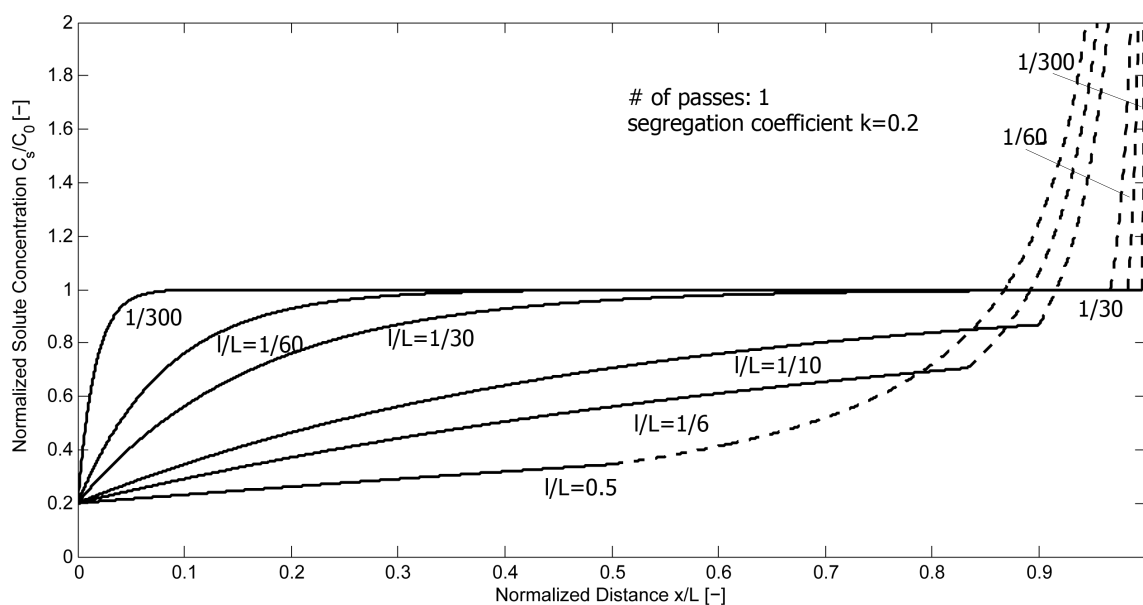
Figure 2.8: Numerical computation of impurity distribution for different zone lengths l. Solid line represents zone refining region; dashed line represents normal freezing region.

d) Initial Concentration C_0

The derived expressions (Eqs. (2.9), (2.10)) and the numerical code do not predict any purification efficiency dependency on starting impurity concentration. This is explained by the fact that the segregation coefficient is assumed to be independent of the solute concentration.

2.3.4 Matter Transport

The Change in density during the melting process could be ignored for impurity distribution calculations. However, contraction of the material on melting causes a forward material transport in the direction of zone travel, whereas melt expansion causes reverse transport motion.
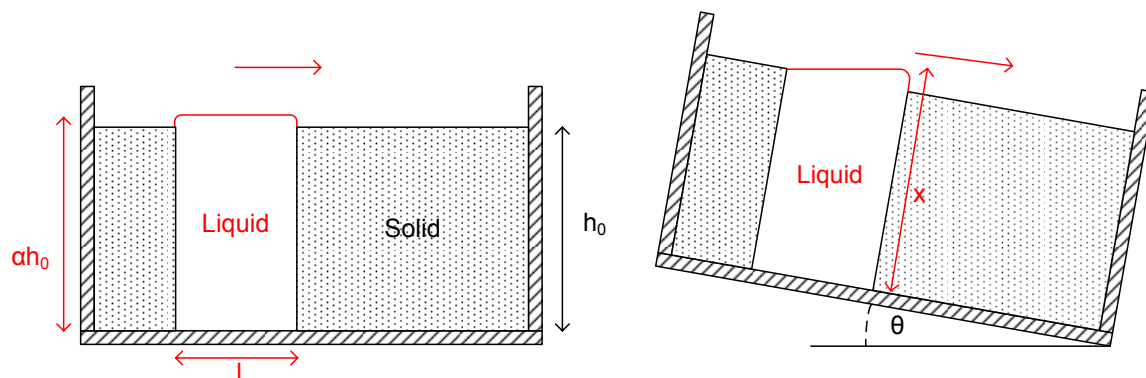
Figure 2.9: Density change from solid to liquid state (a), calculation of inclination angle θ to avoid matter transport (b). Upward zone movement for materials that contract while melting, downward zone movement for expanding materials passing from solid to liquid.

Matter transport can be reduced largely by tilting the boat to the appropriate angle [18]. The tilting angle θ is found by aligning the top of the freezing interface with the solid height h_0 shown in Fig. 2.9 where expansion of the material passing from solid to liquid is illustrated. Overflowing of the molten material is typically prevented by the surface tension of the liquid material. The height of the liquid at the melting interface can be found by equating the liquid volume (unitary depth) in the tilted and horizontal case as,

$$\alpha h_0 l = \frac{h_0 + x}{2} l, \tag{2.19}$$

where α is the ratio of the density of the liquid phase to that of the solid phase, so that the height x becomes

$$x = h_0 \left(2\alpha - 1\right). \tag{2.20}$$

Aligning the freezing interface to h_0 using basic trigonometry and Eq. (2.20) yields

$$tan(\theta) = \frac{h_0 - x}{l} = \frac{2h_0\left(1 - \alpha\right)}{l}.$$ (2.21)

Fig. 2.9 shows the material expanding as it melts (i.e. Cd, Zn and Te). Also, the same reasoning and mathematical expression for materials that contract on melting are viable. Where the material contracts on melting, the direction of travel of the zones is supposed to be upwards to avoid matter transport.

Note that the tilt angle depends on the zone length l and the height of the charge h_0. Both parameters basically can be chosen to greatly reduce the necessity for a tilt angle. Furthermore, interface phenomena between boat and liquid metal strongly affect the tilt angle so that Eq. (2.21) only provides a rough estimation.

2.4 Material purification for CdZnTe growth

This section is a brief literature review of ultra purification of the three elements Cd, Zn and Te. Material properties relevant to the purification processes used for this work are summarized in Appendix C.

2.4.1 Cadmium Purification

Cadmium is a naturally occurring element typically appearing in the crust of the earth along with zinc. Cadmium is therefore isolated during the extraction process of zinc. The main impurities in cadmium typically are zinc and copper.

Cadmium is toxic to humans such that long-term occupational exposure can cause adverse effects on the lungs and kidneys. It also exhibits a relatively high vapor pressure so that special care has to be taken when handling cadmium vapor. Furthermore, cadmium vapors readily turn into oxides, which are particularly harmful.

The extraction process for cadmium production depends on the procedure for zinc extraction. If zinc metal is extracted by *smelting*, cadmium is isolated by distillation, taking

advantage of cadmium's low melting point and high volatility. Smelting is a generic method in metallurgy, where heat and a chemical reducing agent are used, commonly a fuel that is a source of carbon. The carbon or carbon monoxide derived from the combustion removes oxygen from the ore, by changing the oxidation state, to leave the metal.

If zinc is extracted by electrolysis, cadmium sulfate is precipitated out of the electrolysis solution. Electrolysis is a chemical reaction that is driven by an electric current inducing a red ox reaction which results in the deposition of zinc at the cathode.

Higher grade cadmium is typically obtained by electrolytic refining with intermediary purification of the electrolyte solution itself. Ultra-purification aimed at purities greater than 5N is typically achieved by vacuum distillation, zone refining, or a combination of both. Reportedly, Cd may be distilled from solid phase due to the substantial vapor pressure exhibited in the solid phase [16]; however, it does not readily condense unless the vapor intensity is extremely high or if the substrate is pre-coated [16]. The potential for zone refining is challenged due to cadmium's high thermal expansion coefficient, high thermal conduction and high volatility. Early investigations listed in [18] report successful zone refining of Cd performed in carbon coated fused silica boats in H_2 atmosphere and in oxidized sheet tantalum boats in a protective He atmosphere.

More recently, different research groups have attempted ultra purification of cadmium using zone refining or vacuum distillation. The research groups associated with S.T. Ali [14, 21–23] and S.V. Kovalevski [24, 25] are involved in cadmium ultra purification as well as in tellurium ultra purification due to the common applications of those two metals. A publication by Marthur et al. [26] has been reviewed as well. First, Table 2.1 summarizes the expected vacuum distillation purification efficiency for common impurities in Cd based on the vapor pressure differential. Highly volatile impurities removed during pre-distillation are listed separately. Finally, elements that were successfully purified by vacuum distillation but do not fall in either of the two other categories are listed separately as well. Table 2.2 summarizes the expected zone refining purification efficiency for common impurities based

on their respective segregation coefficients. Impurities chemically removed by the H_2 flow are listed separately. Elements that were successfully purified in experiments without theoretical data are also listed separately.

Table 2.1: Vacuum distillation purification potential for different impurities in cadmium according to literature.

Purification:	effective	ineffective
Theoretically	Mg, Sb, Bi, Se, As, Pb [22]	Sb, As, Zn [14]
Pre-Distillation	K, Na [21, 22] Cs, Rb, S, Cl [21], Li, P, Si [22]	
Experimentally	Fe [21–25], Zn, Ag [21, 23–25], Cu [14, 23–25], Ni [22, 23, 25], Al [24, 25], Ca [21, 25], Tl [14, 22], Sn, Co, Mn [25], Ge [21], C [14]	Ni, Cu, Se, Sb, Pb [21], Zn, Ag, Cu [22], B, Mg, Ti, V, Mn, Sn [23]

Table 2.2: Zone refining purification potential for different impurities in cadmium according to literature.

Purification:	effective	ineffective
Theoretically	Tl, Pb, Bi, Ag, Sb [14, 26], As, Pb, Cu, Fe, Ni [14]	Si, O, Se, Zn [14]
H_2	Se [14]	
Experimentally	Zn [14, 26], Co, B, Sn [26]	Si [14]

Cadmium vacuum distillation as described in [14, 21, 22] was attempted by S.T. Ali et al. A distillation system that contains raw Te in a graphite crucible and collects the distilled Cd at the bottom of the cooled collector was used. The distillation was carried out in a vacuum of 2.1×10^{-3} torr, which generally leads to viscous-type distillation characteristics where atoms in vapor phase collide before condensing. A pre-distillation step at 350 C was conducted. Afterwords, the chamber was purged and the collectors were cleaned. The actual distillation step was performed at 450 C, and the yield was between 80% and 90%. The deposited material was removed from the collector and placed in the graphite crucible for subsequent distillation steps. The temperature of the collector surface is reported to be a

key factor for high purification efficiency such that the condensation rate should fall between 1% and 5% of the present evaporation rate. Droplets regularly fall back from the collector to the crucible, washing out the condensing surface of impurities [21]. Results showed the following findings: 5N purity was reached in one distillation step from 3N raw material [21]; Triple-distillation reported in [22] lead to 6N purity starting with 3N8 material; a combined purification effort was conducted in [14] where the distillation step was followed by 25 zone refining passes; 3N7 raw material was purified to 4N9 purity in one distillation step where the soaking temperature was 500 C and the collector temperature was set to 330 C with a yield of 80%; 6N purity was achieved after 25 zone refining passes with a molten zone length of 2 cm, a charge length of 20 cm and a displacement rate of 3 cm/hr using a pyrocarbon coated quartz boat. Ultimately, research determined that 25 passes represents the upper limit for zone refining purification after which the ultimate distribution is achieved. Furthermore, oxides were generally separated during distillation due to their low volatility. Finally, the zone refining was performed under H_2, which reportedly removes remaining oxides and removes nitride impurities by out-diffusion [14].

Marthur et al. [26] performed Cd quadruple zone refining under H_2 flow. Zinc, with its segregation coefficient close to unity, was used to monitor the purification efficiency and determine the number of passes necessary to approach the ultimate distribution, after which the impurity enriched ends have to be removed. Four cycles consisting of 20 passes each were performed, after which 4 cm on each extremity were chopped off. A graphite crucible of 30 cm length was used and a molten zone of 55 mm - 60 mm length was moved along the charge at a rate of 3 cm/hr. Consequently, 6N purity was achieved using 4N+ starting material.

Kovalevski et al. [24, 25] successfully performed Cd purification using vacuum distillation in the presence of cadmium oxide using a single quartz tube with indentations separating the different zones. The inner surface of the quartz tube was coated with a carbon film. The evaporation temperature was set to 325 C approximately, and the condenser temperature

31

was at 150 - 200 C. Initially, only a slight vacuum of 0.1 torr was pumped forming an oxide film. Later, the tube was evaporated to 1×10^{-5} torr for the actual vacuum distillation step. With respect to the 14 analyzed elements, two distillation steps with the presence of CdO purified 3N cadmium to 5N5 purity. Introducing CdO into the system reportedly improved impurities removed with greater affinity to cadmium-oxide than to elemental cadmium.

An extensive list of impurity segregation coefficients is in Table 2.3. Please refer to Section 2.3.1 for the respective definitions of k and k_0. Predicted values for segregation coefficients k_0 based on the equilibrium phase diagram may differ from the measured segregation coefficient k if equilibrium freezing conditions were not attained during the process.

Table 2.3: Various segregation coefficients of different impurities in cadmium. k_0 was calculated from equilibrium phase diagrams [9]; $k = k_{eff}$ was determined from an experimental normal freezing impurity distribution [9].

Impurity	k_0 Kuchar et al. [9]	k Kuchar et al. [9]
Li		2.62
Na		0.14
Mg		1.28
Co		< 0.1
Ni		0.04
Cu	0.088	0.058
Zn	0.11	0.4
Ga	0.1	0.091
Ge	0.037	0.008
As	0.002	< 0.1
Pd		< 0.2
Ag	2.96	2.52
In	0.12	0.081
Sn	0.016	0.13
Sb	0.004	≈ 0.02
Pt		0.027
Au	0.65	0.55
Hg	0.32	0.41
Tl	0.13	< 0.1
Pb	0.06	0.053
Bi	0.53	0.056

2.4.2   Zinc Purification

Zinc is a relatively abundant element in the crust of the Earth, Zinc in nature is normally bound to sulfur, typically as sphalerite, a form of zinc sulfide. To purify, first, the zinc oxides are separated from the zinc sulfide by a process called "roasting". In a next step, the zinc oxide is mixed with fine ground coal, and the zinc oxide is reduced until the elemental zinc can be collected by condensation. At this point, purified zinc typically contains Pb, Fe and Cd impurities in significant proportions, so next the zinc is purified by fractional distillation where Pb and Fe remain in the residue due to their low volatility. Then, Cd and Zn are separated from each other by their distinct condensation temperature.

Greater purification is often performed using electrolyte purification. Electrolysis is a chemical reaction that is driven by an electric current inducing a red ox reaction separated to the annode and the cathode which results in the deposition of zinc at the cathode. The zinc deposits are stripped from the cathodes every 24 to 48 hours and remelted into ingots.

Unfortunately, little literature has been published on the ultra purification of zinc using vacuum distillation and zone melting techniques. While the zone melting book by Pfann [18] reports zone refining being performed by a few groups using carbon coated fused silica boats, those reported works are presently unavailable to the author; hence only three works regarding vacuum distillation / zone refining results are reviewed at this point.

Zinc presents a great affinity for oxygen, which is reflected by the low standard enthalpy of formation for ZnO of 278.4 kJmol^{-1} [27]. Therefore, zinc is typically covered by a barely volatile oxide film during evaporation. However, due to the low solubility of oxygen in liquid zinc (7×10^{-7} [27]), zinc oxide does not contaminate the zinc bulk. Furthermore, Zn may be distilled from solid phase due to the substantial vapor pressure exhibited in solid phase [16].

Zinc with its atomic number of 30 has many prominent impurities with comparable atomic weights. Furthermore, zinc presents five significantly abundant isotopes. Both facts explain why the quantitative analysis of impurities in zinc using mass spectroscopy is partic-

ularly challenging and results in relatively high detection limits, and therefore low precision results.

Zinc is reportedly one of the most difficult elements to purify because many impurities present segregation coefficients close to unity and comparable vapor pressures [25]. The artificial introduction of ZnO during the vacuum distillation process was consequently proposed as a solution. Table 2.4 summarizes the results of zinc purification by vacuum distillation and zone refining according to [25, 27, 28].

Table 2.4: Vacuum Distillation / Zone Refining potential for different impurities in zinc according to literature.

Purification:	effective	ineffective
Distillation (experimental)	As, Bi, Mg, Sb, Pb [25, 27], Mn [25, 28], Ag, Ni, Sn [25], In, Fe [28], Ca [27]	
Zone Refining (theoretical)	Cd, Cu, Pb [28]	Fe [28]

Zinc vacuum distillation was performed by Kovalevski et al. [25] whereby a layer of zinc oxide was intentionally grown prior to the distillation step to evaporate the zinc in the presence of its oxide. Thus. impurities with greater affinity to the ZnO than Zn would be absorbed by the oxide and thereby efficiently removed.

Shelpakova et al. [27] addressed the difficulty of impurity analysis in zinc. Specifically, a zinc sample was distilled to concentrate the impurities on collectors previously coated with ZnO, taking advantage of the affinity of many impurities to zinc oxide. The method was verified using zinc with intentionally introduced impurity concentrations and then applied in a vacuum distillation purification run of zinc: Purification was performed in a three zone quartz tube where the inner surface was covered with a pyro-carbon. The loaded Zn was first melted in a 10×10^{-1} torr atmosphere, where an oxide layer was intentionally grown. Distillation was then performed at 10×10^{-5} torr at 425-430 C, and the condensation zone was set to 250 - 300 C. The distillation duration was timed to leave a 10% residue containing

the non-volatile oxide layer where the impurities could be absorbed.

Isshiki et al. [28] performed zinc vacuum distillation and zone refining. Vacuum distillation was performed in a vertically oriented Pyrex ampoule where the zinc raw material was located at the bottom, and the condensation occured at a constricted part of the Pyrex tube. The material was distilled four times, the material reloaded to the bottom position in between distillation steps. Additionally, zone refining was performed under high purity Ar with a zone refining width of 50 mm and a translation rate of 5 cm/hr in a graphite boat. The zone refining range was progressively shortened to where only the first 10 passes were performed over the entire charge length. Also, the zone refining range was restrained twice to approximately 70% of the previous range to avoid redistributing of the accumulated impurities at the extremities. This study performed 20 passes taking relative purity measurements using resistivity measurements; however, no explicit impurity concentration numbers were published.

2.4.3 Tellurium Purification

Tellurium is a relatively rare material in the crust of the Earth whose production is associated with the electrolysis of copper, where tellurium accumulates in the anode slime [29]. The process comprises mixing the slimes in sulphuric acid to form soluble tellurium sulphate, and the solid fraction is removed by filtration. Metallic copper is then added to the filtrate to form a copper-tellurium cementation product containing tellurium particles [30]. A first purification step typically consists of a refining process based on an acid or alkaline solution precipitating the TeO_2 from Na_2TeO_3 [9]. In a second step, TeO_2 is decomposed to elemental Te by H_2SO_4 electrolysis. However, this step does not eliminate Se, and especially S impurities. Instead, impurities such as Se, Cu, Ag and Au are significantly reduced in a second electrolysis step [9].

Several research groups have attempted the ultra purification of tellurium. For example, zone melting techniques were considered promising in the 1960s by Pfann [18] due to tel-

lurium's relatively high melting point and low thermal conductivity. Consequently, Table 2.5 summarizes the expected vacuum distillation purification efficiency for common impurities in Te based on the vapor pressure differential. Highly volatile impurities removed during pre-distillation are listed separately. Finally, elements that were successfully purified by vacuum distillation (experimentally) and do not fall in either of the two other categories are listed separately as well. Next, Table 2.6 summarizes the expected purification efficiency for common impurities based on segregation coefficients for zone refining. Impurities chemically removed due to the H_2 flow are listed separately.

Table 2.5: Vacuum distillation purification potential for different impurities in tellurium according to literature.

Purification:	effective	ineffective
Theoretically	Al, Ag, Bi, Fe [9, 31], Ca, Pb, Mn, Sn, Ni [31] Au, Cu, Sb, Si [9]	As, K, Na, S, Se [9, 31] As, Cd, Cs, Hg, Mg, P, Se, Zn [31]
Pre-Distillation	Cs, K, Li, Na, P [31]	
Experimentally	As, B, In, Mg, Na, Pb, V [17]	Pd, Ti [17]

Table 2.6: Zone refining purification potential for different impurities in tellurium according to literature.

Purification:	effective	ineffective
Theoretically	Bi, Sb [32, 33], Cd, Ge, In, S, Si, Pb, Zn [32] Fe, Sn [33]	Se [9, 17, 32–38], Co, Cu, Mg, Zn [33]
H_2	O, Se [33, 37], Cu, S [37], N [33]	
Experimentally	Cu [17, 32, 36], Pb [17, 32] Ag, Al, Ni [17] Be, Mg [32], Cr, Zn [36]	Cd, Cr, Hg, Na [32]

In the last decade, the research group of N.R. Munirathnam et al. has published several papers on the ultra purification of tellurium using vacuum distillation and zone melting techniques. For instance, triple Distillation under a 5×10^{-3} torr vacuum allowed for the purification of 4N starting material to 5N5 material [31]. A multiple distillation system

was used to triple-distill tellurium in a single run without material handling between steps using a horizontally oriented quartz ampoule with four different temperature zones. The temperature of the evaporation zone was set to 500 C and the condensation temperature to 270 C. For the second and third distillation step, back distillation was prevented by setting the original zones to 550 C.

A zone refining setup to prevent matter transport by an appropriate inclination angle was built by Munirathnam et al. [32–36]. A 56 cm long boat with inner diameter of 2.5 cm was used. One cycle was defined as a certain number of passes (15 according to [36]) after which the extremities (7 cm on each side) were cut off to physically remove the impurity enriched material before the next cycle was launched. The particular challenges in removing selenium from tellurium were addressed in [34]. Specifically, tellurium is not easily purified of selenium by fractional crystallization methods such as zone refining due to its segregation coefficient close to unity ($k = 0.44$-0.50 [34]). To address this problem, the liquid tellurium was exposed to a H_2 atmosphere under which Se gets converted to hydrogen selenite, which is carried away in the H_2 gas flow. Thus, the zone refining process was performed under a H_2 gas flow to simultaneously purify by the segregation effect and the chemical effect described above. The gas flow was set in opposite direction to the heater movement and the gas flow was set to 4.8 l/h (80 cm^3/min), which passes over the molten tellurium converting selenium into hydrogen selenite gas as

$$H_2(g) + Se(l) \rightarrow H_2Se(g). \tag{2.22}$$

The hydrogen selenite gas produced was neutralized as the gas passed through a bubbler containing a sodium hydroxide solution before being released into the atmosphere. Results show that the Se removal efficiency was highest at the gas inlet side decreasing linearly along the bar [33]. Because the process of zone refining only exposes the molten zones to the chemical purification, research found [33] that it was necessary to reduce the Se content to about 1ppm before initiating zone refining to reach 7N purity. Therefore, a pretreatment of the Te charge with H_2 exposure before zone refining is suggested. It is stated in [34] that

the selenium concentration dropped from 1100 ppb to 120 ppb after 15 passes (1 cycle) and to 30 ppb after 2 cycles. Thus, 7N purity was achieved with 5N starting material.

The ideal number of zone passes, zone length and translation ratio was investigated in [33], determining ideal zone lengths in the range of 3 cm - 6 cm and 30 mm/h as the optimal zone traveling speed. The ideal number of zone passes is reported to strongly depend on the initial impurity concentration, but generally a considerable reduction was observed after 60 passes according to the literature [33].

Other research groups such as A. Zaiour et al. [17, 37] combined vapor distillation and zone refining under H_2 and N_2 flow conditions using a horizontal quartz tube arrangement connected to a vacuum system pumping at 3×10^{-3} torr vacuum. The collector ampoule was water cooled and maintained at 0 C while the pre-distillation step was performed with the furnace temperature at 500 C, after which the atmosphere was purged before the actual distillation step. The temperature was raised to where the tellurium surface reached its melting point (i.e. 450 C under atmospheric pressure). Results found low evaporation rates to improve the separation effect and viscous type distillation due to the moderate vacuum level, which means that the Te atoms experienced some collisions while traveling in the vapor phase. The distilled tellurium was then melted into a semicircular quartz boat (ID: 20 mm, L: 21 cm) in a hydrogen atmosphere where an appropriate tilt angle prevented matter transport in the zone refining boat. The hot-zone temperature was maintained at 500 C and was moved at 6 cm/h. Three cycles (each of which consisted of three passes) were performed after which the extremities (2 cm) were chopped off.

Additional findings show the zone temperature affects the purification efficiency such that a lower zone temperature increases the efficiency of purification. Thus, Ag, Cu, As, Mn, Ti and Pd were most negatively affected by an increased zone temperature [17], and the experiment demonstrated the chemical removal of impurities such as O, Cu, S and Se during zone refining with an H_2 flux [37]. Evaporation coefficients for 15 impurities in tellurium were calculated but no actual purity number are published.

Finally, an extensive list of impurity segregation coefficients is given in Table 2.7. Predicted values for segregation coefficients k_0 based on the equilibrium phase diagram are rarely achieved after zone refining since equilibrium freezing conditions are not achieved [39]. In some cases, multi-component systems to appear where major impurities interact with other impurities, so impurity segregation can not be treated independently of other solutes present, which makes k differ further from k_0 [39].

Table 2.7: Various segregation coefficients of different impurities in tellurium. k_0 was calculated from equilibrium phase diagrams [9]; $k = k_{eff}$ was determined from an experimental normal freezing impurity distribution [40], [9].

Impurity	k_0 Kuchar et al. [9]	k Kuchar et al. [9]	k Schaub et al. [40]
Na	6×10^{-6}	< 0.1	
Mg	0.0001	< 0.1	0.0002
Al	0.004	< 0.1	0.0005
Si	0.1	< 0.1	
S	0.23	0.29	
Ca		0.01	0.001
Cr		< 1	0.2
Fe		< 0.1	0.005
Ni		< 0.1	0.0009
Cu	0.013	< 0.1	
Zn	0.0025	< 0.1	
Ge	0.000		0.0006
As	0.003	0.0002	0.0008
Se	0.38	0.44	0.2
Ag	3×10^{-5}		0.0003 [41]
Cd	0.0006		2
In	0.013		0.0005
Sn	0.17		0.0003
Sb	0.96		0.005
I	0.04		0.002
Au	0.21	0.1	
Hg	0.017	0.14	0.05
Tl	0.002	< 0.1	0.00002
Pb	0.0005	0.12	0.001
Bi	0.0007	0.0004	0.001

Chapter 3

System Design

This chapter details the design of system components: Vacuum distillation apparatus, zone refining system and ampoule. Primarily, the zone refining furnace and its electric system is describes as it was designed and built by the author.

The vacuum distillation stages (one and two) were designed and built by Dr. Mark Harrison. Tyler Krehbiel wrote the LabView virtual interface (VI) to program the vertical movement of the furnace relative to the ampoule. Along with Amy Hageman's contributions, the vacuum system was characterized, and the stationary ampoule design was improved. Extensive results for the tellurium purification and preliminary results for the Cd and Zn purification were generated. The author was assigned to develop the vacuum distillation of Cd and Zn further and add a zone refining step to the purification chain. Therefore, a zone refining apparatus was built, with the help of Steven Spalsbury. Tyler Krehbiel programed the temperature control and the horizontal furnace movement control using LabView software. Finally, a novel ampoule design integrated the zone refining into the purification chain thereby removing any material handling between the vacuum distillation and zone refining steps.

3.1   Vacuum Distillation Stage

A schematic representation of the basic vacuum distillation apparatus in Fig. 3.1 shows its two sub systems: the vacuum system and the furnace system. The vacuum system includes

a stationary, single-use quartz ampoule coupled to a permanent vacuum system and an Edwards ERM18 roughing pump is coupled to an Alcatel ATP 80 turbo pump. With the cold trap filled with liquid nitrogen (LN2), the vacuum system can achieve ultra low vacuums of approximately 3×10^{-7} torr with an empty (non out-gassing) ampoule attached. The vacuum pressure is measured by a MKS cold cathode ion gage transducer and recorded by the LabView interface software.
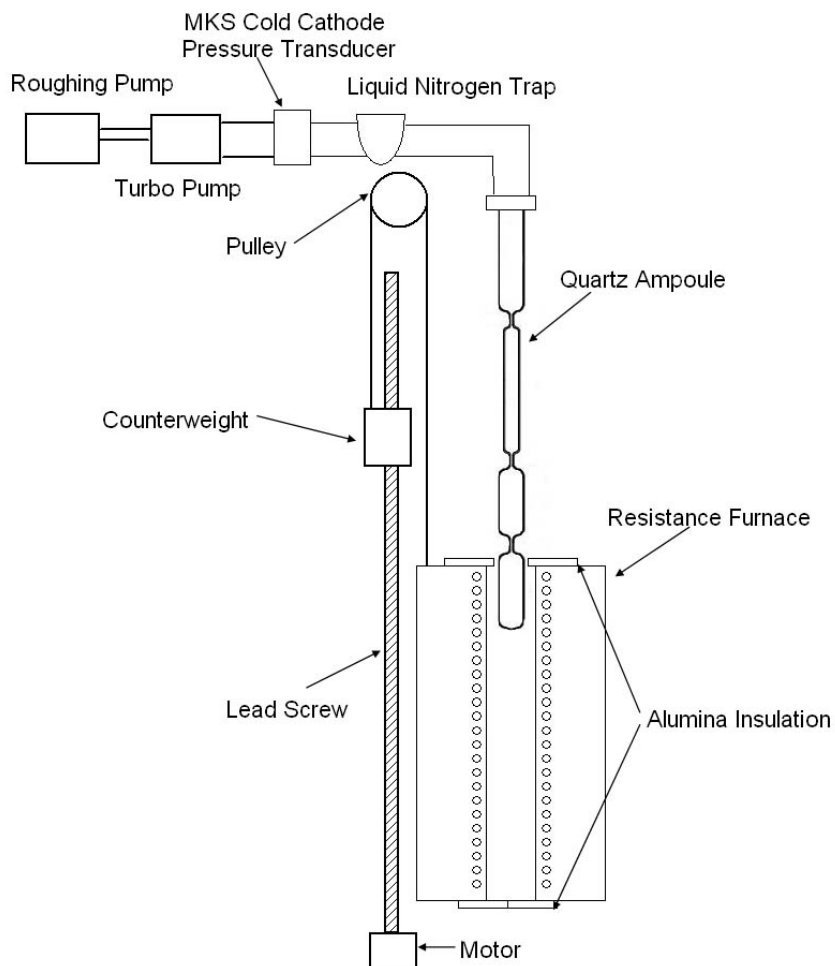
Figure 3.1: Schematic representation of the vacuum distillation system.

The furnace system consists of a single zone resistance furnace with temperature and horizontal motion controls. A Honeywell 3204 temperature controller with an analog input accuracy of $\pm 0.20\%$ provides temperature control with a deviation of approximately ± 1.5

C. The furnace measures 42 cm in length (32 cm coil length); the internal furnace diameter (bore) is 50.8 mm. The furnace motion is controlled using a stepper motor coupled to a ACME lead screw whose rotation causes a counterweight to move up or down at desired speed. The counterweight transfers the vertical motion to the furnace via a wire - pulley system. A National Instruments Labview VI controls furnace motion and records the temperature, pressure, and furnace position.

3.2 Zone Refining System

The zone refining apparatus was designed based on existing tellurium zone refining s reported in literature such as in [17, 36]. However, in order to integrate the zone refining process in the purification chain without material handling after vacuum distillation required a few compromises. For instance, the amount of material resulting from the double vacuum distillation step is limited by the volume of the distillation chambers. Therefore, the length of the zone refining boat was limited to approximately 30 cm which is relatively short compared to the 1.6 m reported by other research groups (as described in [36]). The resulting lower zone length over charge length ratio l/L is disadvantageous in terms of purification efficiency as described in Section 2.3.3. However, due to the relatively high purity yield from the double distillation step, this on drawback is acceptable.

3.2.1 Mechanical Design

The overall zone refining setup with key dimensions is shown in Fig. 3.2. The entire apparatus is installed on a metal plate and may be slightly tilted to avoid matter transport, as described in Section 2.3.4.

The length of the zone refining boat and the distance between the two hot zones in the furnace determine the necessary horizontal movement range of the furnace to accommodate both zones traveling the entire length of the zone refining boat. Rails and furnace tube
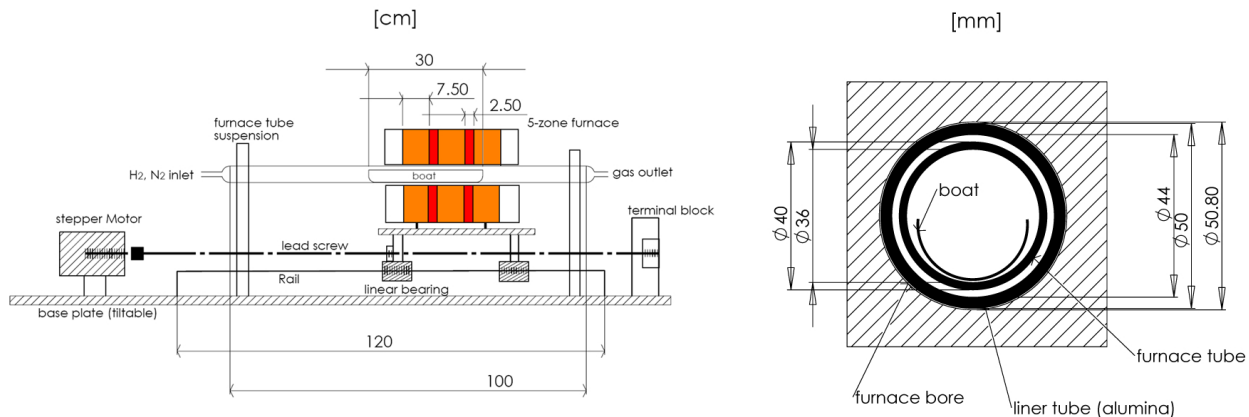
Figure 3.2: Schematic representation of zone refining setup. Furnace cross section shown on left side; overall setup with key dimensions on right side.

length have been dimensioned accordingly, with additional length for future flexibility. The furnace tube suspension was placed relatively close together to simplify the alignment of the furnace tube relative to the furnace bore. The furnace tube is kept in place by a split-ring clamping hanger cushioned on thermal adhesive tape and mounted on a threaded rod so that the vertical position can be fine-tuned. The horizontal position can be adjusted by unscrewing the base plate of the threaded rod.

The 5 zone furnace is mounted on a horizontal translation stage on rails. The vertical motion is controlled by a threaded ACME rod connected to a Trinamic Pan Drive 109-57 stepper motor. The zone refining furnace tube is equipped with N_2 and H_2 gas purge capability. The gas can be passed through a bubbler after passing through the furnace tube, thereby cleaning the purging-gas chemically of toxic substances (i.e. $H_2Se(g)$). The flow rate is measured and adjusted upstream of the furnace tube by a Swagelock VAP-G2-04M-1-8 flow meter, allowing up to 40 l/h air at standard conditions. The H_2 is supplied by an ultra high purity UHP300 T-size bottle and is passed through a Mr. Hydrogen platinum plate hydrogen purification system before entering the furnace tube. The possibility for other

gases, i.e. argon, is built-in as well.

The five zone tube furnace was custom built by Mellen company and has 5 independent temperature zones of 3 / 1 / 3 / 1 / 3 inches long. Each one is independently powered and its respective temperature measured with individual S-type thermocouples. The coils are powered by 24 V and draw 525 / 175 / 525 / 175 / 525 Watts, respectively. The maximum temperature of the furnace is 1300 C.

An alumina Al_2O_3 liner tube is tightly inserted into the furnace bore to shield heavy metal ions coming from the heating coils (see Fig. 3.2). The inner diameter of the liner tube is 44 mm to permit some clearance between the stationary furnace tube (outer diameter 40 mm) and the furnace attached liner tube (inner diameter 44 mm). The inner diameter of the furnace tube is 36 mm in diameter to admit the zone refining ampoule resulting from the vacuum distillation step (described in Section 3.3) with an outer diameter of 31 mm.

3.2.2 Electric Wiring

The furnace and the transformer converting 208 V AC to 28 V AC was provided by Mellen company. The electric wiring was done in-house and is shown in Fig. 3.3. The components of the furnace control are housed in an electric box illustrated by the dash-dotted line in Fig. 3.3. The 208 V power, and a security ground, are provided by a three prong outlet. The two lines are connected through a main breaker before they are are passed through a two-phase relay and fed to the transformer. This relay is steered by an over-temperature controller for security reasons. Once the temperature exceeds an adjustable limit (i.e. 1200 C) the relay output of the over temperature controller shuts so that the 2 phase relay loses its 24 V power supply and shuts off the main 208 V power supply. The security ground is connected to the box for proper grounding meanwhile the transformer provides up to 70 A at 28 V on its secondary side. The 0 V outlet is connected to a grounded distribution block (DB) from which 5 wires leave to the respective zones (coils). The 28 V outlet is fed to a

distribution block from which 5 individual wires are passed through 25 / 15 / 25 / 15 / 25 ampere fuses. Each line is then switched with a Continental SVDA-3V50 solid state relay controlling the power of each zone via pulse-width modulation (PWM) before leaving to the respective coil.
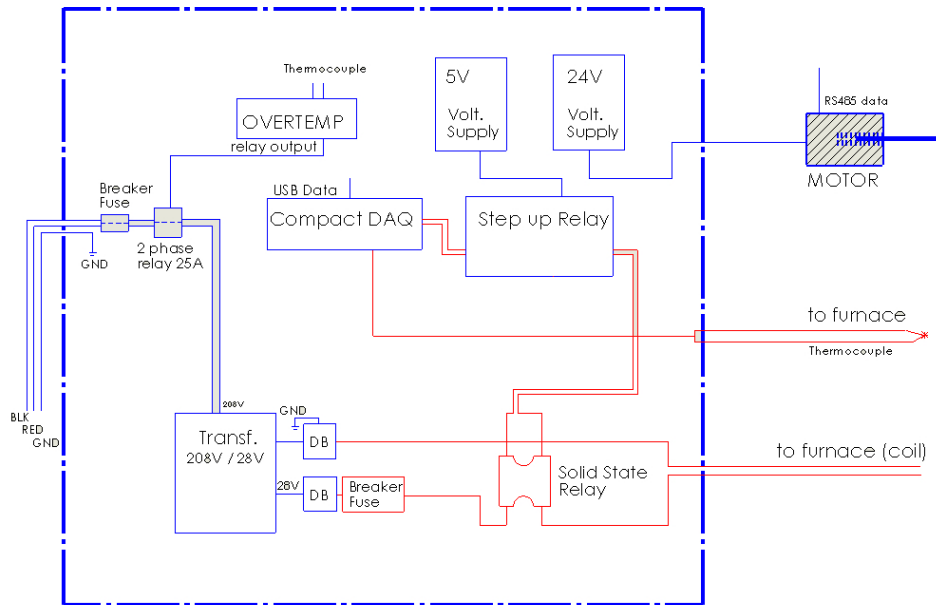
Figure 3.3: Electric wiring of zone refining apparatus. Simplified schematic representation of overall setup; red represents wiring that is present five times for each zone.

The logic signal for the temperature control is provided by a LabView Virtual Interface (VI). A National Instruments mini data acquisition system (miniDAQ) equipped with two NI9211 units read out the S-type thermocouples, and two NI9263 units provide the logic signal calculated from the temperature control algorithm. The logic signal (5V or 0V), however, is limited to 1 mA so that it has to be amplified to be able to open the solid state relays. In turn, these relays require 15 mA to open the secondary side, which is done by a pFET step-up circuit shown in Fig. 3.4. A 5 V power source supplies the necessary amperage of 15 mA for each line individually to open each solid state relay. Furthermore, the 24 V source in the electric box supplies the necessary power for the stepper motor and for the over-temperature relay steered by the over-temperature controller.

power supply

+ 5V -

Step up Relay

S

pFET
V(GS)<5V
I(SD)>15mA

G

PWM signal 0/5V
max 1mA

+

5V, max 1mA

D

R=1kΩ

-

+

5V, >15 mA

-
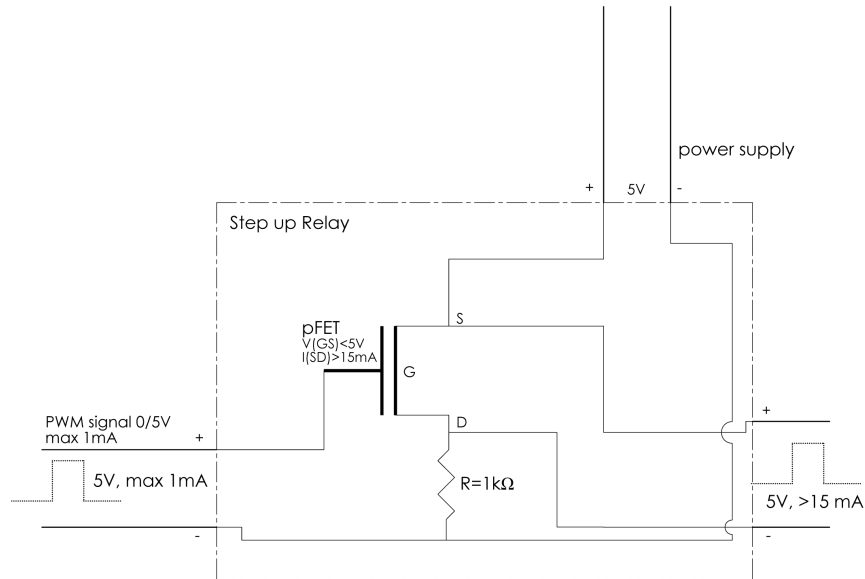
Figure 3.4: Electric wiring of step-up relay.

The data signal for the stepper motor is provided via the RS232 port from a PC. The corresponding logic signal is generated in the same LabView VI as is the temperature control.

3.2.3 Software Design

The LabView VI, written by Tyler Krehbiel, simultaneously controls the horizontal furnace position and the temperatures of each individual zone. Thus, velocity, target position and temperatures can be manually selected or alternatively programmed as a recipe. Then, the programmed recipe can be saved and stored on the hard drive. The interface can iterate (cycle) over a defined part in the recipe, making it particularly adapted to zone refining. The iterated parts of the recipe correspond to the different passes whereas the initial and terminal parts of the recipe represent the heating up and cooling down phases.

Temperature control is performed by an adapted proportional integral derivative (PID) controller. The heating duty cycle, which is the output variable of the controller algorithm, is calculated as the sum of a proportional, an integral and a derivative contribution. The integral and the derivative contribution is modified from traditional implementation to achieve the desired results. The integral contribution is capped to an adjustable threshold value to

46

prevent integral windup, which may lead to significant temperature over shoot. The derivative contribution is scaled down as the temperature approaches the set point temperature to prevent temperature oscillations and effects from thermocouple noise. Experiments show that the temperature is controlled with an error of less than 1.0 C.

The linear motion of the furnace is determined by an ACME lead screw with a step of 5 rotations per inch. The position control uses the micro step controllability of the PanDrive stepper motor whereby A rotation is partitioned into 200 steps, which are repartitioned into 64 micro steps. The LabView program calculates the micro step frequency according to the preprogrammed recipe at a frequency of 10 Hz and communicates it to the PanDrive via the RS-232 port. The furnace can be displaced at a speed of up to several cm per second. One micro step is translates into 4.0 μm, which is essentially sufficient for the present application. There is basically no lower boundary to the velocity; the micro steps can be spaced out arbitrarily. However, the motion becomes less smooth as the speed is reduced.

3.3   Ampoule

The ampoule design has evolved as the vacuum distillation method has been perfected. Factors such as the width and the length of the neck proved to have a significant impact on the distillation rate but finally were chosen to satisfy practical reasons as well. The length of the neck had to be significantly stretched in order to make the torch seal process easier and more reliable. Also note that elongated necks turned out to be advantageous to easily open the target ampoule (zone refining ampoule) exposing the molten material to the gas flow. Alternatively, Dremel diamond blades can crack open shorter ampoule necks. Next, single, double and triple distillation ampoules with up to four chambers were used. The basic limitation is given by the vertical range of the distillation furnace, which limits the overall length of an ampoule to approximately 90 cm depending on whether the furnace needs to be entirely retractable or not.

The outer diameter of the ampoule is basically determined by the vacuum system piping, which is laid out for quick connect fits for 38 mm (OD) ampoules. Adapters could, however, be used for different diameters, but this has not been attempted. Since the zone refining process exhibits a relatively long boat for a reasonable purification efficiency, the target ampoule (the ampoule where the material is deposited during the final vacuum distillation step) was chosen to be 30 cm long. Also, the bottom chamber was dimensioned so that it presents double the volume of the target ampoule. Given that the raw material is loaded loosely and that each distillation step has an ideal yield of roughly 80 %, the target ampoule should therefore be filled far less than 50 % after double distillation.

Due to the limited ampoule length, and to shorten the vacuum distillation process, the vacuum distillation - zone refining ampoule was only laid out for two distillation steps. Two steps turned out to be manageable in one day (three steps are not), which turned out to be extremely advantageous so that the vacuum system could remain on and material did not have to be remelted after cooling down the furnaces over night.

The final design is shown in Fig. 3.5. Particularly for zinc, a special design was developed as material interactions lead to glass cracking. Also, Zn zone refining exposed to a gas stream was not successful so that a design that allows argon back-filled enclosed zone refining was introduced. For more details, please refer to Section 5. The design shown in Fig. 3.6 presents a heavier wall weight on the zone refining part, which is slightly elongated to provide room for the sealing plug and the quick fit connect for the back-filling operation.
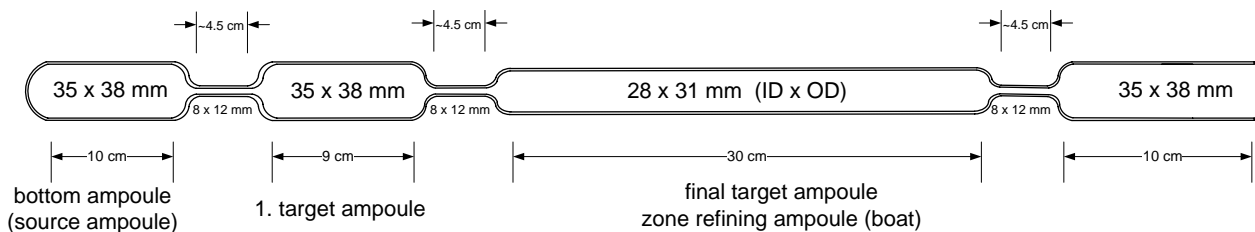
Figure 3.5: Vacuum-distillation / zone-refining ampoule design with key dimensions.

Due to material compatibility issues between Zn, Cd and glass ware, zone refining with-
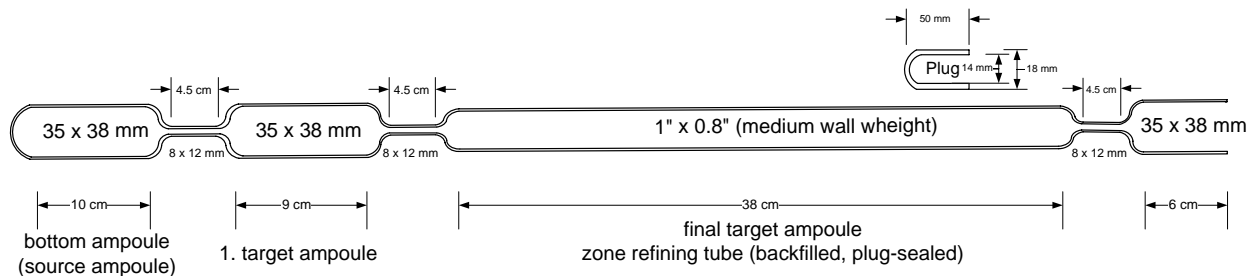
Figure 3.6: Zinc vacuum distillation / Ar back-filled zone refining ampoule with key dimensions.

out preceding vacuum distillation was attempted in graphite boats. The boats were manufactured by POCO graphite and are actually made of Fabmate composite material. Fabmate is a trade name, high-strength, machinable product designed for clean room applications. It is thermally stable for applications with temperatures up to 500 C in the presence of oxygen and up to 2500 C in an inert atmosphere, which is a significant advantage over classical graphite crucibles. The design used for Cd and Zn zone refining is shown in Fig. 3.7.
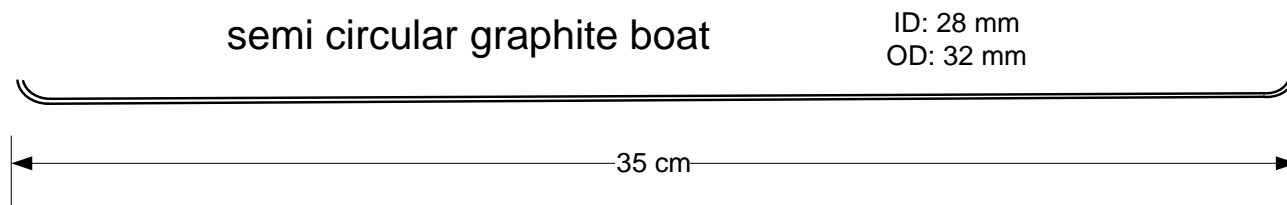
Figure 3.7: Cd zone refining graphite (Fabmate) boat with key dimensions.

Chapter 4

Experimental Procedure

Described in chapter 4 are the experimental procedures relating to glassware / graphite cleaning, vacuum distillation and finally purity analysis. The special procedures performed for cadmium and zinc are discussed separately.

The material purification process started with chemical cleaning the inside of the quartz / Pyrex ampoule in a Class 1000 clean room (Section 4.1). The cleaned ampoule was then coupled to a glove box via a modified quick connect. The glove box was continuously purged with N_2 to reduce the humidity and minimize raw material oxidation. The raw material then was transferred into the ampoule, by dropping the material particles into the bottom chamber of the ampoule. The raw material was stored in plastic bags in plastic jars as they were purchased. They were kept in a fume hood and the material never handled prior to loading it into the ampoule and therefore, a preliminary cleaning step in boiling isopropanol, for instance, was omitted. the The ampoule was then quickly transferred to the vacuum system, which was pumped overnight to evaporate residual isopropanol from the ampoule cleaning step. Next, the vacuum distillation process was performed (Section 4.2), the final step resulting in an internally coated zone refining ampoule. Then, the distilled material was melted to form a rod at the bottom of the zone refining ampoule. Finally, the final zone refining ampoule was cracked opened on the sides and placed horizontally (or slightly tilted) in the zone refining furnace tube, and the zone refining step (Section 4.3) was performed. Due to particular material properties of cadmium and zinc, the conceived experimental

procedure had to be adapted for Cd and Zn, respectively (Sections 4.4 and 4.5).

4.1 Ampoule / Graphite Cleaning

The quartz and Pyrex ampoules were cleaned in the class 1000 clean room. In a first step, a 1 : 1 : 1 sulfuric-acid:hydrogen-peroxide:deionized-water (DI) solution (piranha solution) was used as an etchant to remove organic impurities. After thorough DI rinsing, a chromic acid (potassium dichromate ($K_2Cr_2O_7$) in sulfuric acid) was used to clean the glassware of remaining organic residues. After another DI rinsing, a 5% hydrofluoric acid (HF) etch to remove a layer of the quartz, along with any metallic impurities present, completed the ampoule cleaning. After extensive rinsing with deionized water, the ampoule was rinsed with isopropanol and allowed to dry in the clean room. The quartz used was GE quartz custom fabricated by Quartz Scientific. The Pyrex ampoules were fabricated by the scientific glassblower from the KSU chemistry department, Jim Hodgson.

The graphite boats for Zn and Cu made of Fabmate were custom fabricated by Poco-Graphite (Entigris company). The recommended cleaning procedure used consisted of a 10 min etch in a standard HF solution with 10 parts di-ionized water and one part HF. A next step consisted of a cascade DI water rinse for a minimum of 15 minutes. Finally, the Fabmate parts were dried in a clean oven at 300 C for thirty minutes. If organic contamination was present, a degreasing procedure consisting of a chloroform, acetone and a methanol dipping sequence is recommended.

4.2 Vacuum Distillation

After a vacuum was drawn overnight, the residual isopropanol had presumably evaporated. The vacuum at this point typically reached levels in the low 10^{-6} torr range. The furnace was then ramped up to the appropriate pre-distillation (PD) temperature (see Table 4.1) for a low temperature initial pass. The predistillation temperature has to be optimized satisfying opposing effects. This temperature was chosen low enough to prevent raw material from

melting and to keep the raw material surface area large. The temperature, however, has to be as high as possible to evaporate a maximum of high volatility impurities. Impurities out-gassed during this step were essentially evacuated by the vacuum system. After the initial 30 -45 minute low temperature pass (furnace translation rate shown in Table 4.1), the furnace was (3.8 cm/min) returned to zero, where the bottom of the ampoule was aligned with the top insulation shutters of the furnace.

Table 4.1: Parameters for Cd, Zn and Te vacuum distillation.[a]

	PD. Temp.	PD Transl. rate	Dist. Temp.	Dist. rate	Dist. rate (ZR chamber)	DM Temp.
	[C]	[cm/h]	[C]	[g/min]	[g/min]	[C]
Cd	340	114	460	1.15	1.2	430
Zn	400	76	560	1.4 - 1.65	0.85 - 0.9	460
Te	300	76	525	1.3-2	1.3 - 1.6	460

[a]Abbreviations: Pre-distillation (PD), Distillation (Dist) and Downmelt (DM). Pre-distillation translation rates given in [cm/h] since they are not function of mass loaded. Distillation rates are given in [g/min] as they are calculated as a function of mass of charge. The distillation rate given factors in a desired residue of $\approx 10\%$ - 20 %. The rate for distillation into the zone refining (ZR) chamber is given separately since the distillation distance is significantly longer.

With the furnace at the zero position, the temperature was ramped to the appropriate distillation temperature (Table 4.1) at a rate of 15 C/min. The furnace was then quickly raised (7.6 cm/min) to the top position to cover the entire 1. target chamber, see Fig. 4.1 (a). The furnace was kept at this position for typically 1 minute to clean the target chamber from possible contamination (thin coating) resulting from the pre-distillation step. The furnace was then quickly lowered (7.6 cm/min) to the distillation starting position shown in Fig. 4.1 (b). At this point, the top of the 1. target chamber was exposed to convective cooling, which provided the necessary heat evacuation for condensation. As the furnace was slowly lowered, a second portion of the ampoule reached the optimal temperature for condensation. The condensed material deposited on the chamber walls in an annular form. The rate at which the furnace was lowered was determined as a function of the charge mass loaded and was consequently reported in [g/min]. Given the mass loaded into the ampoule and the distance the furnace needed to travel during the distillation step (given by the geometry of

the ampoule), a translation rate was calculated. For simplicity, the distillation rates shown in Table 4.1 are adjusted so that the calculated translation rate (or distillation time) leads to a residue of approximately $10\% - 20\%$ wt as shown in Fig. 4.1 (c). At the end of the distillation run, the temperature was lowered and the furnace was slowly lowered below the zero position.
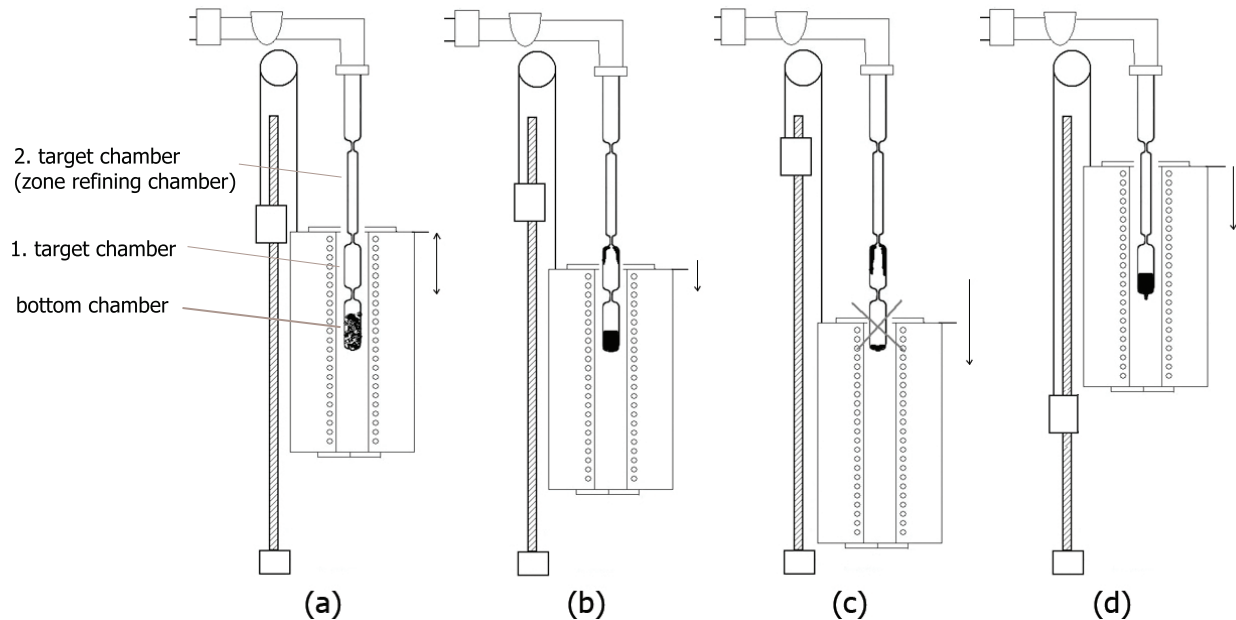
Figure 4.1: Vacuum distillation steps, from left to right: (a) Pre-distillation step, (b) distillation step, (c) furnace retraction for flame torch sealing, (d) final distillation in zone refining ampoule.

With the ampoule still evacuated, a hydrogen-oxygen torch was used to seal the quartz neck between the evaporation chamber and the condensation chamber. When Pyrex ampoules were used, a natural gas-oxygen torch was used, mainly because of the lower melting temperature of Pyrex.

The furnace position was then raised in order to cover the "1. target chamber" that had become the lowest one. The temperature was raised again to the down melt (DM) temperature (see Table 4.1) to down-melt the distilled material to the bottom of the chamber. The ampoule was then ready for the next distillation stage.

The following distillation step was conducted similarly except for omitting the low tem-

perature pre-distillation step. This is because the down melt procedure is believed to suffi-ciently out gas remaining high volatility impurities. The situation immediately before the actual second distillation process is shown in Fig. 4.1 (d).

After the second (final) distillation step, bottom and top neck of the zone refining target ampoule are torch sealed to conserve the vacuum in the target ampoule. Therefore, a down melt step in vertical position of the zone refining ampoule is omitted.

Over the entire process, the vacuum system was run a full pumping speed. The vacuum level reached was essentially depending on the outgassing rate of impurities into the vacuum system and eventual leakage. Of course, pressure, position and furnace temperature were recorded by the LabView VI.

4.3   Zone Refining

The zone refining step required a few preparation steps: First, the proper quartz furnace tube for the respective material had to be mounted on the split ring clamps and adjusted relative to the furnace bore. Then, the bubbler downstream of the furnace tube had to be filled with DI water, or a 5% NaOH solution if hydrogen was blown through the furnace tube. Next, the furnace tube was cleaned from contamination from previous runs by a hot temperature furnace pass by setting all five zones to 800 C, and translating the furnace at 10 cm/h over the entire path length under a steady gas flow of 50 l/h$_{air}$. Temperatures clearly higher than the temperatures present during the upcoming zone refining cleaned the furnace tube from any contamination that may become volatile during zone refining. Also, the filled zone refining ampoule had to be melted down as shown in Fig. 4.2 (a)-(b) before necks could be cracked open. For that purpose, the ampoule was placed into a furnace ideally covering the entire ampoule and raising the temperature above the melting point of the loaded material. The temperature was slowly lowered after down melting to avoid ampoule cracking.

In a subsequent step, the prepared zone refining ampoule (or Fabmate boat) was loaded

into the furnace tube. The ampoule was cleaned on the outside with isopropanol first to remove contamination from handling the ampoule. The location of the ampoule in the furnace tube was given by the position of the hot zone when the furnace was at its original position. Typically, zone refining movement was directed by moving the furnace toward the original position. The hot zone therefore had to be able to pass the edge of the ampoule entirely so that the freezing interface could be advanced all over the charge.

Furnace tube and gas supply piping then were purged to replace oxygen. If hydrogen was used, the gas supply piping and the H_2 purifier also had to be thoroughly purged with 50 psi N_2 for at least 2 hours. The platinum plate hydrogen purifier was then turned to 400 C. Once the temperature had reached steady state, after five more minutes to be sure all the air was removed, the purifier purging valve could be closed, and the H_2 gas supply valves could be opened, thereby adjusting the upstream H_2 pressure to 200 psi maximum. Before switching the gases, the pressure to the atmosphere of the gas supply pipes upstream of the purifier was released as recommended, then the N_2 supply was shut off.

It took approximately 1 h before the purified H_2 gas flow reached its nominal value. Once the flow rate was stabilized, the zone refining recipe was started. First, the ampoule material was leveled with an extended hot zone using all five furnace zones. The step between Fig. 4.2 (b) and (c) illustrates the leveling process. If chemical purification involving H_2 was used, this step was extended to multiple passes in order to sufficiently expose a maximum of liquid material to the gas stream.

The subsequent step was the actual zone refining step as illustrated in Fig. 4.2 (c). The temperature of zone B (hot zone) of the five zone furnace was set sufficiently high to melt a portion of the charge between 3 cm and 6 cm long while the adjacent zone temperatures were set to reduce heat transfer along the charge. The hot zone was moved along the charge at a translation rate between 3 cm/h and 6 cm/h. Typically, between 10 and 20 zone refining passes were performed. An exemplary recipe plot is shown in Fig. 4.3 with only 3 passes, as taken from the LabView interface.
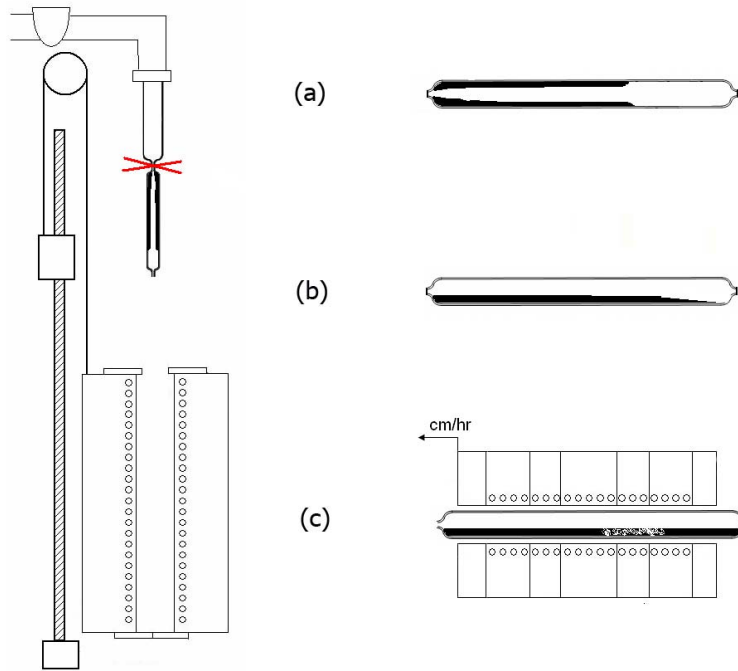
Figure 4.2: Zone refining procedure illustration. (a) distilled material deposited in annular form in zone refining chamber, (b) down-melted material ready for zone refining, (c) zone refining step where melt zone is slowly moved along the charge.

The temperature set point values were experimentally determined since they proved to be a strong function of the charge cross section. Accordingly, measured temperature profiles of commonly used temperature set points for all three materials are given in appendix E. Typically, a temperature set point value was chosen intentionally high, in order to start the process. The zone refining zone length was then monitored, the zone refining recipe was adjusted occasionally, and the temperature was stepwise reduced to achieve the desired zone length. This procedure is practiced because a longer zone initially is beneficial according to the considerations developed in Section 2.3.3. Note that the purification efficiency may benefit from a contracting melt zone as impurities from the extremities are impeded from back contaminating the center part with a shortened zone. Increasing the zone length has to be avoided since it will reverse the segregation purification effect.
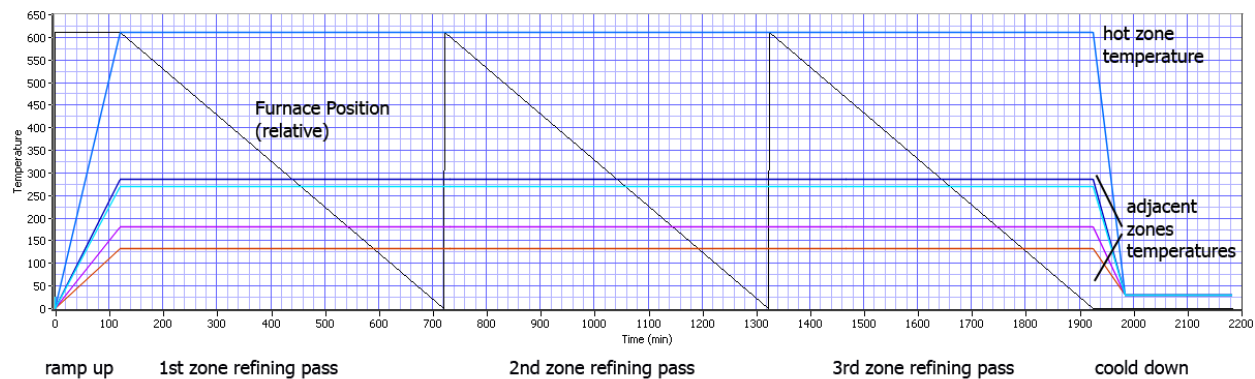
Figure 4.3: Example of a zone refining recipe. Relative furnace position plotted on top of temperature evolution.

After the last pass, the temperature was slowly ramped down and the gas stream switched to N_2 to keep the furnace tube dry. The gas flux could also be switched from H_2 to N_2 during the zone refining run to preserve high purity H_2. Before switching the gases, the gas supply pipes had to be vented after the H_2 supply was shut off and before the N_2 supply valve was opened in order to prevent H_2 back flow in the N_2 lines.

4.4   Special Case: Cadmium

Due to cadmium's toxicity, the vacuum distillation was performed in the enclosed and vented vacuum distillation stage and a gas mask was typically worn for the ampoule neck sealing operation. The glassware used was made of Pyrex due to the incompatibility of Cd and quartz at elevated pressures. Given the lower melting point of Pyrex, a natural gas flame torch was used for sealing off the ampoule necks.

While the solid metals zinc and tellurium do not adhere to the glassware, cadmium strongly bonds to Pyrex. Zone refining, where a large interface between material and boat is present is challenged; therefore Cd zone refining in a Fabmate boat was performed similar to Te zone refining under H_2 flow, to absorb oxygen traces from the gas stream.

4.5   Special Case: Zinc

Due to zinc's strong affinity for oxygen, zone refining had to be performed in an Ar back-filled Pyrex ampoule. Thus, the ampoule loaded with zinc as shown in Fig. 4.2 (a) was cut open on the uncoated side. The ampoule was then connected to a vacuum / back fill system using a quick flange connector. A vacuum was drawn using a roughing pump and a liquid nitrogen sorption pump down to the 10^{-6} torr range. High purity argon passing through a Nupure noble gas mini-purifier was used to backfill the ampoule to ≈ 20 torr. The procedure was repeated at least four times to minimize the oxygen content in the ampoule. Finally, the ampoule was sealed with a Pyrex plug as shown in Fig. 3.6 using a natural gas torch. A slight vacuum was required at this point so that the glass collapsed onto the plug for a proper seal.

For zone refining without preceding vacuum distillation, the loaded graphite (Fabmate) boat was inserted into a cleaned shell Pyrex tube, and the same backfilling procedure was performed. From this point on, the procedure was similar to the zone refining procedure described above, and N_2 was typically used to purge the furnace tube at a flow rate of less than 1 L/h air.

The number of passes was chosen individually for each run; typically in the range between 10 and 20 as recommended in most of the reviewed literature. Also the duration of H_2 exposure for Cd and Te was chosen from run to run based on time limitations and conclusions drawn from previous runs. Finally, the translation rate was set between 3 and 6 cm/h, as reported to be ideal in the literature, depending on timing constraints.

4.6   Impurity Analysis

The impurity analysis including sample preparation was performed by Shiva Tech, EAG labs using glow discharge mass spectroscopy (GDMS). From the specified location, a 20 mm x 2 mm pin was cut using liquid cooled diamond saw (blade saw). The high speed cutting liquid used is a mineral oil based proprietary fluid from Allied High Tech, which

was diluted with water at a ratio of 50 : 1. Once the pin was cut, it was etched in a 10% bromine:methanol solution for approximately 30 seconds. The prepared sample was inserted into the sample holder and the GDMS analysis was performed. The detected concentrations were given in ppm wt for the 74 elements tested for or the respective detection limit if the element remained undetected (Appendix A).

Due to detection limits in the ppm range for certain elements, further analysis on select elements may be performed using laser ablation mass spectroscopy where no sample preparation is required. The depth of analysis can be chosen and is determined by how long the sample is exposed to the laser prior to using mass spectroscopy. Focusing on select elements presents detection limits in the ppb range; if a full scan is performed, the detection limits are, however, higher than those for GDMS.

Chapter 5

Results and Discussions

The complete results of glow discharge mass spectroscopy (GDMS) analysis are tabulated in Appendix A. Note that purity numbers are always expressed relative to the 74 elements tested for; therefore, due to significant detection limit values, the measured purity is strictly given by an interval stating a lower and an upper boundary. If not otherwise mentioned, however, the lower number underestimates the purity by adding the detection limit values of undetected impurities. Cd and mostly Zn suffer from relatively high detection limits, which leads to a larger purity range.

Purity levels are typically given in percentages [%] weight. The purity level is calculated based on the impurities detected as

$$Purity = 100\% - \sum_i C_i, \tag{5.1}$$

where C_i are the individual impurity concentrations.

Using GDMS, tantalum (Ta) was used as the sample holder, whereas indium (In) frequently had to be used as sample binder, depending on the sample size and its consistency. The corresponding detection limits are significantly increased. In the case of cadmium and zinc analysis, a numerical figure for Ta concentrations greater than 1 ppm can be specified leading to a detection limit of 1 ppm. For tellurium on the other side, the corresponding concentration is not specified at all leading to deceivingly lowered detection limits.

5.1 General Results

Glassware cracking was frequently problematic during vacuum distillation and zone refining. In particular, Cd and Zn processing had special issues during vacuum distillation, between first and second distillation step, as the reformed metal plug was reheated. This problem could be strongly mitigated by keeping the material hot and molten at all times.

During zone refining, ampoule cracking with Te occurred, but overall Te zone refining remained a highly successful process. However, Zn zone refining failed 2 out of 3 times due to cracking of the back filled ampoule; Cd zone refining in Pyrex was not further pursued since the purified metal could not be separated from the glass ware.

The glass cracking tendency of Cd and Zn may be explained, as reported in the literature by anomalous expansion of zinc and cadmium near the melting point" [42]. Especially when performing zone refining, sufficient room for expansion is given in the present work, so cracking is likely linked to a reaction of Cd and Zn, respectively, with the glassware.

5.1.1 Vacuum Distillation

Vapor pressure data for relevant elements are given as equation fit coefficients in Appendix B. Furthermore, the evolution of the vapor pressure of the three materials of interest as a function of temperature is shown in Fig. 5.1. Notably, the vapor pressure curve flattens out as the temperature increases. Therefore, distillation under vacuum greatly reduces the temperature requirements. Lowering the pressure below $\approx 10^{-5}$ torr, however, presents a diminishing return in reducing the evaporation temperature. Theoretically, the purification efficiency for most of the prominent impurities should be very favorable due to vapor pressures orders of magnitudes different from those of the material of interest as shown in Appendix B.

In general, the distillation rates observed strongly varied as indicated in Table 4.1. The main reason for the fluctuations was the different impurity concentration and shapes of the loaded raw materials. The other key parameter seems to be the geometry of the ampoule,

61
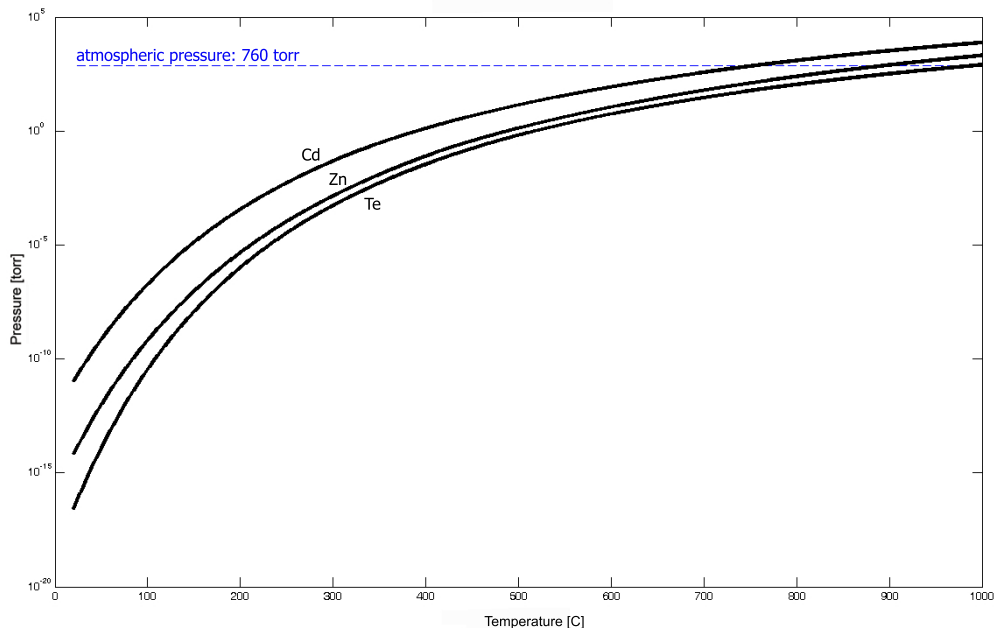
Figure 5.1: Vapor pressure evolution for Cd [43], Zn [43] and Te [44] as a function of temperature. The respective intersection point with the atmospheric pressure of 760 torr designates the atmospheric boiling point: $T_b(Cd) = 767°C$, $T_b(Te) = 988°C$ and $T_b(Zn) = 907°C$.

that is mainly the distance between evaporation and condensation site. On the other hand, the distillation rate seemed to be independent of the vacuum pressure as predicted by Eq. (2.2).

As described in the literature for vacuum distillation, the condensation rate was significantly lower than the evaporation rate. Tiny droplets visibly formed on the ampoule inside wall and conglomerated to a larger droplet that finally ran back down to the evaporation ampoule. After a metal layer had formed, presumably the same process continued to occur. Condensation rate and solidification rate, however, are likely higher on a pre-coated surface than on bare glass, as described in Section 2.2.2. Consequently, in terms of the kinematics, the process is either condensation or solidification limited.

As an example, take the second distillation run from Zn-VD-17, where ≈ 230 g of Zn was distilled in 5 h at an average pressure of 2×10^{-6} torr. The observed average distillation

rate of $\approx$ 0.8 g/min compares to the estimated evaporation rate. Using Eq. (2.2) with $T = (273 + 560)$ K, $P_v = 5.09$ torr [43], $a = 1$, and $\tilde{m} = 65.4$ g/mol, the estimated evaporation rate is 0.80 g/min/cm (with an ampoule cross section of 9.6 cm^2) or 7.70 g/min. Consequently, the rate of evaporation compared to the rate of actual distillation (solidification) presents a ratio of about 10 : 1. This high ratio is desirable according to [21] who states the liquid falling back into the evaporation zone of the melt leads to a continuous washing of the solid surface, removing impurities rejected during the solidification.

The distance between the evaporating material and the condensation site strongly affected the actual distillation rate. As indicated in Table 4.1, the rates for distillation into the zone refining ampoule (as opposed to distillation into the first target ampoule, see Fig. 4.1) were significantly lower for Zn and Te, whereas the transport distance did not seem to be a large factor for Cd. The distance for vapor transport imposed by the ampoule geometry measured up to 20 cm in the early stages of the second distillation step. Since the distillation rate likely starts out low and and reaches a maximum at the end of the distillation step where the distance is the smallest, then the reported distillation rate represents only an average.

Due to the slow initial distillation rate, there was a risk that if the translation rate of the furnace were badly calculated, a plug of material would form at the bottom of the target ampoule and hardly any material would be at the top. The run could not be extended in that case but had to be done over again; hence sufficient time has to be factored in to thoroughly redistribute the material vertically in the ampoule.

The mean free path length for Cd, Zn and Te can be calculated using Eq. (2.3). Using conservative values for the pressure, tabulated values for the atom diameter, and the respective distillation temperatures given in Table 4.1 1.87 cm for Cd, 2.70 cm for Zn and 2.37 cm for Te emerged[1], which are all smaller than the characteristic distance of the ampoule of $\approx$ 15 cm. Therefore, it is likely that atoms experience 5 to 10 collisions before reaching

---

[1]Pressure: $P = 1 \times 10^{-6}$ torr, Temperatures: $T_{dist, \, Cd} = 460$ C, $T_{dist, \, Zn} = 560$ C, $T_{dist, \, Te} = 525$ C; Atom diameters: $d_{Cd} = 210^{-8}151$ cm, $d_{Zn} = 210^{-8}134$ cm, $d_{Te} = 210^{-8}140$ cm

the condensation site, which categorizes the distillation as *viscous*.

GDMS purity analysis from vacuum distilled material suffers from a key flaw. Because the material after distillation typically was down-melted to form a plug, an advancing freezing front potentially introduces significant segregation. Therefore, the purity numbers measured at a certain location may differ strongly from an average value. Raw material purity measurements performed using GDMS suffer from the same problem, since shots typically were molten to form a solid plug.

Fig. 5.2 shows the plotted data record from the tellurium distillation run Te-VD-29. The plot on top represents the first distillation run, which started out with the pre-distillation run at 300 C. The furnace was pre-heated, and the motion was started once the pressure reached a vacuum in the lower 1×10^{-6} torr range.

After the pre-distillation run at 300 C, the temperature was ramped up to 525 C, and the furnace was moved up again to clean the target ampoule from any coating from the pre-distillation run. The temperature was sufficiently high to raise the pressure, which can be attributed to a removed coating evaporating into the vacuum system. The furnace was then slowly lowered over a selected distance, and the Te was distilled. The pressure slowly approached a steady state level ideally in the low 1×10^{-7} torr range.

After the furnace was retracted, and the bottom ampoule sealed off, the furnace was re-raised to "down melt" the distilled material to the bottom of the lowest ampoule. This step was performed manually and not shown in Fig. 5.2. The position of the furnace at this point was reset to 0.

The second distillation step is shown in the lower plot in Fig. 5.2. The second distillation run began with the high temperature cleaning step, which raises the pressure level into the low 1×10^{-6} torr range. Of note, the distance traveled by the furnace during the second distillation run was much longer (≈ 25 cm) than in the first step (≈ 5 cm) since the material was distilled into the elongated zone refining ampoule.

Small temperature spikes in both plots in Fig. 5.2 can be explained as a consequence
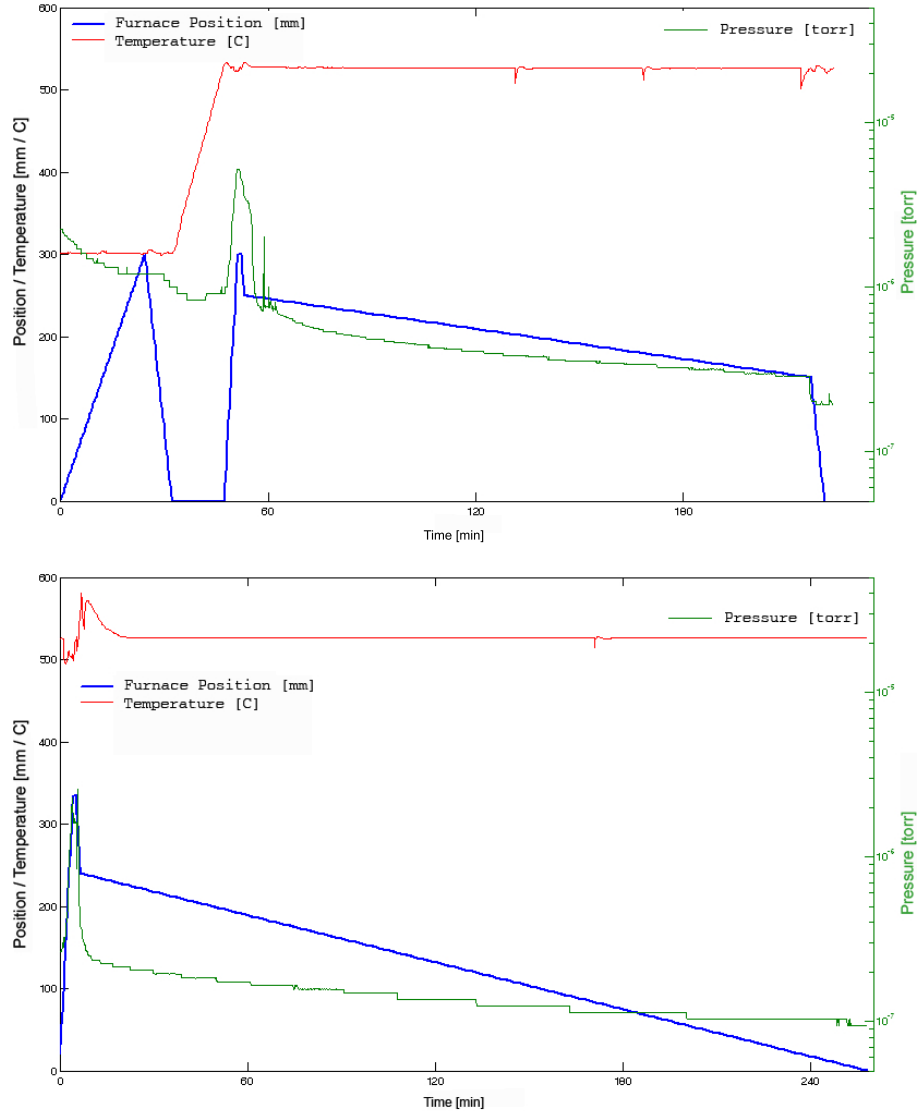
Figure 5.2: Distillation record taken from tellurium double vacuum distillation Te-VD-29. The top plot represents the first run including a low temperature pre-distillation run. The down melt procedure is not shown; position 0 was reset before the second run where a pre-distillation step was omitted.

of the experimenter intervening when the alumina insulations were temporarily removed for process inspection. Larger temperature fluctuations resulted as the alumina insulations passed a neck that temporarily lets cool air into the furnace causing the control algorithm to temporarily overshoot.

In general, but especially for zinc, the metal should be kept in its molten state after the

"down melt" process in between the first and the second distillation steps. If the material solidifies, it will form a plug at the bottom of the ampoule that may crack the ampoule once re-heated due to material expansion. A flame torch was used to keep the ampoule hot as the furnace was raised up, leaving the bottom chamber sticking out at the bottom of the furnace.

5.1.2   Zone Refining

The zone refining furnace retracted from tellurium zone refining is shown in Fig. 5.3. The five thermocouple wires sticking out on top of the furnace indicate the five temperature zones.
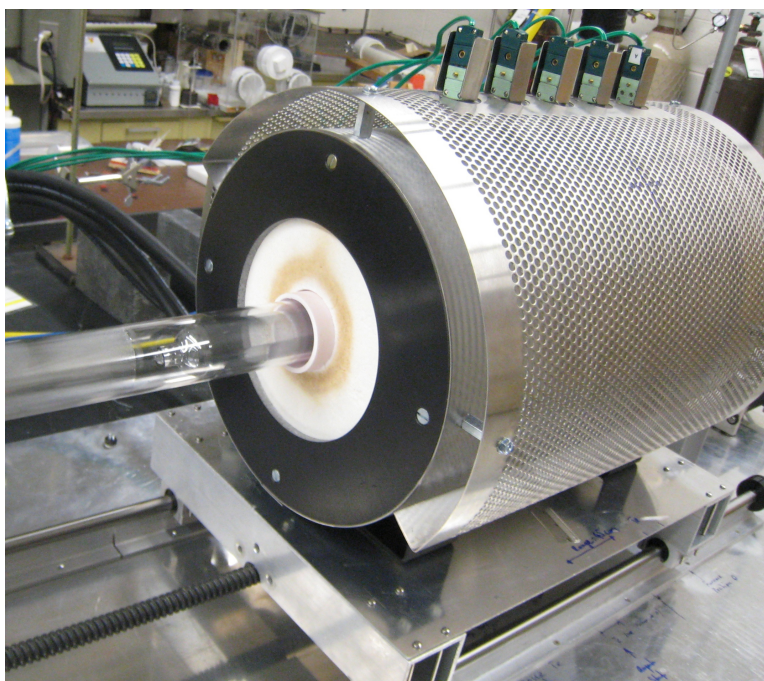
Figure 5.3: Zone refining furnace tube loaded with tellurium zone refining chamber from Te-VD-ZR-24.

Initially, double-zone refining with two staggered melt zones was planned. However, preliminary temperature profiles were recorded to determine the appropriate temperature set points and due to axial heat transfer in the alumina liner tube, the glassware, and eventually also in the charge, the resulting temperature profile was relatively flat; thus only

single-zone zone refining could be performed. The temperature at the center of both hot zones could not be kept at a temperature low enough to divide two well-defined melt zones.

Finding the temperature set points required to form a 3 to 6 cm long melt zone proved to be rather difficult. The measured temperature that is used for the control algorithm is taken right next to the heating coils and differs greatly from the temperature that the charge experiences at the center of the furnace tube as indicated in the profiling plots from typical temperature set points in Appendix E. Furthermore, axial heat transfer in the charge strongly depends on the material cross section and therefore the mass loaded. Therefore, set points had to be determined individually during each zone refining run. For each zone refining run a set of relatively high set points was used initially, and the temperatures were reduced subsequently to optimal values.

Furthermore, the zone refining melt zone fluctuated in length as the zone was translated. Typically, it was longer at the edges where heat transfer in the charge mainly occurred on one side. This phenomenon was most pronounced with Cd and Zn, which can be explained by their thermal conductivity values being 30 to 40 times larger than that for Te (see Appendix C).

Matter transport as described in Section 2.3.4 was minimal, very likely due to surface tension effects and relatively low charge heights. Using Fabmate (graphite) boats, however, the need to compensate for matter transport by tilting seemed more important than with glassware, which may be attributed to low interface forces between Fabmate and the liquid metal. Typically, the zone refining runs were started in a horizontal position and tilted if any matter transport problem was observed.

To avoid material oxidation, zone refining in the loaded zone refining ampoule was attempted without cutting open the edges, thereby conserving the vacuum. However, the high vapor pressures forming in the ampoule led to vapor transport so that the melt zone evaporated out, and the material condensed at the edges of the ampoule, so no segregation purification could be achieved. Instead of a vacuum, argon back-filled zone refining was

67

realized with Zn, where the ampoule was backfilled in order to suppress the vapor pressure of the material that is being purified (Section 5.3).

5.2   Cadmium

Cadmium at elevated temperatures as required for vacuum distillation and zone refining is incompatible with quartz. Therefore, carbon coated quartz ampoules were initially used for vacuum distillation, a process soon discarded because it impeded visibility of the distillation process, and possibly caused contamination. Pyrex ampoules were used instead, which proved to be a good alternative. Also, the high volatility of Cd allowed for a vacuum distillation temperature of only 460 C which is lower than the annealing temperature of Pyrex (505 C).

The drawback of Pyrex appeared when harvesting the distilled material out of the opened ampoule. Cd proved to be extremely ductile and bonded to the glassware. Even cooling down the loaded ampoule to liquid nitrogen temperatures did not allow the Cd to separate from the Pyrex. Shiva Tech, however, managed to isolate a Cd pin for GDMS analysis using a diamond blade saw. This technique could be used to extract the purified plug so that distillation in Pyrex remains a viable alternative. The cooling liquid described in Section 4.6 may be used to cool the diamond blade; if so, the cutting step should be followed by a 30 sec etch in 10% bromine:methanol solution.

Due to strong affinity of Cd to oxygen, the literature suggests using H_2 as protective gas. Other than N_2 or Ar, hydrogen binds traces of oxygen in the gas stream and thereby avoids undesirable Cd oxidation.

5.2.1   Vacuum Distillation Results

Single and double Cd distillation were performed in Pyrex ampoules, and samples of the purified materials were sent out for GDMS analysis. A table of concentrations of select elements is shown in Table 5.1.

Table 5.1: Single and double Cd distillation results. Only a selection of elements are shown; purities given in ppm wt; - : not tested for, < : detection limit reached. For a complete table, please refer to AppendixA.

Element	Raw	Cd-VD-6 (one stage)	Raw	Cd-VD-8 (two stage)	Cd-VD-8 (laser ablation)
Cl	-	0.2	-	< 0.001	
Cu	< 0.01	< 0.005	-	< 0.005	
Zn	< 0.01	< 0.005	-	< 0.005	
As	< 0.003	< 0.005	-	< 0.005	
In	-	< 0.1	-	< 0.1	< 1
Sn	< 0.01	< 0.01	< 0.3	< 0.01	
Sb	< 0.001	< 0.005	-	< 0.005	
Te	-	< 0.1	-	< 0.1	
Ta	-	< 1	-	< 1	0.002
Hg	-	2.4	-	< 0.005	
Tl	< 0.002	0.03	-	< 0.005	
Pb	< 0.01	0.35	-	< 0.005	
⋮		⋮		⋮	
Total min.		**2.98**		**0.00**	
Total max.		**4.43**		**1.47**	
Best Case [%]		**99.99970**		**100.00000**	
Worst Case [%]	**3N (spec.)**	**99.99956**	**5N (spec.)**	**99.99985**	

The single distilled material in Cd-VD-6 using 3N starting material only had Cl, Hg, Tl and Pb in detectable quantities. The latter two were were not found in detectable quantities in the raw material, which is somewhat puzzling. Contamination is assumed to be minimal during the vacuum distillation process, so the raw material purity values are questionable, or may be attributed to segregation in either one of the samples. The overall result of 5N6 purity after a single distillation run seems, however, very impressive. The rather high concentration of Hg in the distilled material may be explained by its chemical resemblance to Cd given by a similar number of valence electrons and a comparable vapor pressure at the distillation temperature of 460 C (see Fig. B.4). The presence of Hg as an impurity in Cd has not been reported in any of the papers reviewed related to Cd purification.

The reported distillation efficiencies from literature listed in Table 2.2 are ambiguous for Pb; however Tl and Cl should be efficiently removed by vacuum distillation. Finally, the run Te-VD-6 was timed slightly too long, and only a minimal, loose and dusty residue was left behind. The lower volatility elements Tl and Pb (see Fig. B.4) may therefore potentially even be better purified by a well-timed distillation run or by a subsequent second distillation step.

Double distillation starting with 5N specified material proved to be extremely effective as demonstrated in Cd-VD-8, shown in Table 5.1. A GDMS full scan did not detect any impurity elements in the distilled material, so the purity level is characterized by the upper boundary given by the sum of the detection limits. The purity therefore lies within 5N9 and 100%. The most significant detection limits are given by Ta < 1 ppm, Te < 1 ppm and In < 0.1 ppm where only the latter is reported to be electrically active in CdZnTe [11]. Te is not a concern since it will likely not harm CdZnTe growth.

Additional laser ablation mass spectroscopy results focusing on tantalum (Ta) and indium (In) were performed promising detection limits in the ppb range. However, only Ta could be quantified to 0.002 ppm while In could not be clearly quantified due to noise from the very dominant Cd signal. Effectively, In has a mass-to-charge ratio (m/z) of 115 which is surrounded by ^{114}Cd and ^{116}Cd isotopes which naturally occur in 28.7% and 7.5%, respectively. Therefore, broadened peaks from those Cd isotopes prevent mass sepctroscopy from achieving lower detection limits for In, given by 1 ppm. However, Cu, Ga, Hg, Ag and Sn were all detected above 0.01 ppm according to the laser ablation mass spectroscopy results, but are not specified further since only analysis for In and Ta was purchased. Notably, those elements did not get detected in the GDMS analysis performed.

In summary, by taking the improved result for Ta of 0.002 ppm and 0.01 ppm for Cu, Ga, Hg, Ag and Sn from the laser ablation results, together with the detection limit for In of 0.1, 6N5 purity is found as a conservative estimate. This result is still strongly affected by detection limits; if only the actually detected impurities in laser ablation Cu, Ga, Hg, Ag and Sn (all ≈ 0.01 ppm) are taken into account, the calculations result in 7N5 purity.

5.2.2 Zone Refining Results

Because Cd adheres to Pyrex, vacuum distillation followed by zone refining in Pyrex was considered not feasible. Cd zone refining could, however, be performed in a Fabmate boat using 5N starting material without preceding vacuum distillation. The results of the GDMS

analysis of the zone-starting and zone ending extremity plus the center part are listed in Table 5.2.

Table 5.2: Cd zone refining results. Only a selection of elements are shown; purities given in ppm wt; - : not tested for, < : detection limit reached. For a complete table, please refer to AppendixA.

Element	Raw	Cd-ZR-Fabmate-s (starting edge)	Cd-ZR-Fabmate-c (center part)	Cd-ZR-Fabmate-e (ending edge)
Si		0.008	< 0.001	0.004
Cl	-	< 0.001	< 0.001	0.004
Cu	-	0.02	0.05	0.11
Zn	-	< 0.005	0.04	0.03
Ag	0.6	0.1	< 0.01	< 0.01
In	-	< 0.1	< 0.1	0.18
Sn	-	< 0.01	0.02	< 0.01
Te	-	< 0.1	< 0.1	0.08
Ta	-	< 1	< 1	< 1
Pb	-	< 0.005	< 0.005	0.01
⋮		⋮	⋮	⋮
Total min.		**0.13**	**0.11**	**0.42**
Total max.		**1.68**	**1.66**	**1.77**
Best Case [%]		**99.999987**	**99.999989**	**99.99996**
Worst Case [%]	**5N (spec.)**	**99.99983**	**99.99983**	**99.99982**

The procedure started with an extended melt-zone run to melt the material shots to a solid rod followed by 16 zone refining passes under continuous H_2 flow at an inclination of $1°$ approximately. Only an Ag concentration of 0.6 ppm was specified in the raw material which was efficiently reduced as predicted by the literature (Table 2.2). According to Table 2.3, Ag (in Cd) is one of the few cases with a segregation coefficient greater than unity which is confirmed by the fact that the concentration was highest in the starting edge. Si is reported to be difficult to remove using zone refining which is confirmed by increased concentrations in both extremities compared to the center part; however, the concentration level is relatively insignificant. The main impurities detected in the center part are Cu and Zn with segregation coefficients k close to unity of 0.58 and 0.4, respectively (Table 2.2). The Sn detected in the center part is surprising since it is not detected in either of the extremities. The detected concentration of Te might be due to cross contamination, furthermore, it's presence should not harm CdZnTe crystal growth.

In summary, zone refined Cd in Fabmate boats is a viable alternative to vacuum distilla-

tion. The key advantage is that the Cd easily falls off of the Fabmate boat and does not stick to the Pyrex. If it can be assumed that Ta, Te and In are present in ppb concentrations, so the present purity levels achieved in the center part would be at least 6N5, possibly up to 6N9.

5.2.3   Combined Vacuum Distillation and Zone Refining Results

Combined vacuum distillation and zone refining was not attempted.

5.3   Zinc

Other than the tendency to crack glassware, the zinc distillation rate proved to be relatively slow. Furthermore, despite the melting point of Zn (419.5 C) being lower than that of Te (449.51 C), a higher vacuum distillation temperature for Zn (560 C) than tellurium (525 C) proved necessary to achieve an acceptable distillation rate. Apparently, Zn does not readily condense unless the vapor intensity is extremely high or the condensation site is pre-coated as reported by [16].

Raising the temperature of the furnace above the Zn melting point, revealed that the Zn shots did not change their appearance and did not fall together to form a continuous liquid. The relatively high surface tension of liquid Zn of ≈ 750 mN/m (comparison: Te 186 mN/m) may be the reason for this phenomenon. Alternatively, impurities gathering at the surface may explain this phenomenon and the high temperature requirements.

Zn distillation seems to be particularly dependent on the distance between evaporation and condensation site; thus, early phase of the distillation process for Zn proved to be especially ineffective due to the larger distance.

Pertinent literature offers little on Zn zone refining or vacuum distillation. In a first attempt in this study, zone refining was performed under N_2 flow. The Zn seemed to react slowly with the nitrogen or with oxygen traces so that the zinc-oxide (nitride) covered Zn rod would not melt any more. Alternatively, argon flow was not successful, likely due to

traces of oxygen leaking into the gas stream. As a solution, Ar backfilled zone refining runs were successfully performed.

Zone refining without preceding vacuum distillation showed that the Zn shots did not collapse to a continuous liquid by raising the temperature, similar to vacuum distillation. However, combined heat and mechanical agitation proved to be an effective method to overcome the surface tension that kept the liquid Zn shots separated. A continuous liquid is necessary so that segregation may purify the center part of the metal rod efficiently.

Quartz ampoules cracked on a regular basis during zone refining runs. Using Pyrex, which seems to be a little less brittle, mitigated this problem. However, the temperatures required for the Zn vacuum distillation (560 C) are higher, and the temperatures required for zone refining ($\approx$ 460 C) are close to the Pyrex annealing temperature (505 C) where sodium escapes from the glass, likely contaminating the Zn.

5.3.1 Vacuum Distillation Results

4N rated raw material was used for first Zn vacuum distillation runs. The vacuum distillation in run Zn-VD-1 was redone seven times (designated: h) to determine the temperature and timing requirements. The material was downmelted using the furnace and the H_2 torch. A power loss occurred during one distillation run attempt. As a result, the vacuum had to be secured by closing valves. Comparing the purity of the used raw material to the single distilled material (seven attempts) reveals that several impurities were introduced, although some of the most prominent starting impurities Pb, Tl and Cd were effectively reduced. In particular, Si and Fe were introduced in significant quantities so that the distilled material and the starting material both had high 4N purities only. According to Table 2.4, Fe should be efficiently removed using vacuum distillation, whereas no information on Si is available. Disadvantageous segregation conditions in the raw material and distilled material plug may explain the apparent contamination, however, no segregation coefficients for impurities in Zn are available to support this statement. Alternatively, contamination can not be entirely

excluded since Si and Fe are very common elements.

Table 5.3: Zn vacuum distillation results along with the purification coefficient S_C. Only a selection of elements are shown; purities given in ppm wt; - : not tested for, < : detection limit reached. For a complete table, please refer to AppendixA.

Element	Raw	Zn-VD-1h one stage	S_C	Zn-VD-2c three stage	S_C	Raw	Zn-VD-7 three stage	S_C
B	0.01	0.02	-100%	< 0.001	> 90%	< 0.001	< 0.001	
Na	0.03	0.13	-333%	0.007	77%	< 0.005	0.03	
Mg	0.01	0.17	-1600%	< 0.005	> 50%	< 0.005	0.007	
Al	0.13	0.72	-454%	0.004	97%	0.002	0.06	-2900%
Si	0.28	2.7	-864%	0.05	82%	< 0.005	0.07	
P	0.009	0.01	-11%	< 0.005	> 44%	< 0.005	< 0.005	
S	0.61	0.57	7%	< 0.05	> 92%	< 0.05	< 0.05	
Cl	0.18	0.25	-39%	0.01	94%	< 0.01	0.06	
Ca	< 0.01	0.1		< 0.01		< 0.01	0.03	
Ti	< 0.005	0.04		< 0.005		< 0.005	< 0.005	
V	< 0.001	0.002		< 0.001		< 0.001	< 0.001	
Cr	0.04	0.42	-950%	< 0.01	> 75%	< 0.01	0.02	
Mn	0.12	0.13	-8%	< 0.005	> 96%	< 0.005	< 0.005	
Fe	2	7.2	-260%	< 0.01	> 100%	0.05	0.02	60%
Co	0.02	0.13	-550%	< 0.005	> 75%	< 0.005	< 0.005	
Ni	0.11	1.4	-1173%	< 0.01	> 91%	< 0.01	< 0.01	
Cu	2.1	0.35	83%	1.3	38%	< 0.05	< 0.05	
Ga	< 0.01	< 0.01		< 0.01		< 0.01	0.34	
Ge	< 0.05	< 0.05		< 0.05		< 0.05	0.08	
Y	< 0.005	< 0.005		< 0.005		< 0.005	0.06	
Mo	< 0.01	0.38		< 0.01		0.03	< 0.01	> 67%
Ag	0.59	< 0.05	> 92%	< 0.05	> 92%	< 0.05	< 0.05	
Cd	3	0.86	71%	< 0.05	> 98%	0.25	< 0.05	> 80%
In	0.02	< 0.005	> 75%	< 0.005	> 75%	< 0.005	< 0.005	
Sn	0.36	0.2	44%	< 0.01	> 97%	0.07	< 0.01	> 86%
Sb	0.02	0.01	50%	< 0.01	> 50%	0.5	0.02	96%
Te	0.64	0.24	63%	< 0.01	> 98%	0.06	< 0.01	83%
La	< 0.001	0.06		< 0.001		< 0.001	< 0.001	
Tm	< 0.001	< 0.001		< 0.001		< 0.001	0.007	
W	0.18	0.51	-183%	< 0.005	97%	0.01	0.007	30%
Re	< 0.005	0.08		< 0.005		< 0.005	< 0.005	
Pt	0.02	0.13	-550%	0.008	60%	< 0.005	< 0.005	
Tl	3.9	0.62	84%	0.03	99%	0.06	< 0.01	> 83%
Pb	12	0.74	94%	< 0.05	> 100%	0.11	< 0.05	> 55%
⋮	⋮	⋮		⋮			⋮	
Total min.	26.38	18.17		1.41		1.14	0.81	
Total max.	27.84	19.66		3.17		2.81	2.51	
Best Case [%]	99.99736	99.99818		99.99986		99.99989	99.99992	
Worst Case [%]	99.99722	99.99803		99.99968		99.99972	99.99975	

Using the same 4N rated raw material, a triple distillation run was performed in Zn-VD-2c. The large chunk material had to be downmelted initially using the flame torch. The first distillation step was done twice (designated: c) to optimize the yield. As opposed to the one stage distillation experiment, the purification efficiency was very high for all impurity elements except for Cu, which was present at 1.3 ppm. Along with the high detection limit for Ta of 1 ppm, those two elements draw the material purity down to high 5N levels instead

74

of mid 6N. Clearly, the sequence of downmelting, vacuum power outages and re-attempting a distillation run seems to introduce impurities, and must be avoided.

Oddly, Cu was removed more efficiently in the one stage run than in the three stage distillation run. According to the literature (Table 2.4), Fe should be efficiently removed from Zn by vacuum distillation, which indicates that Fe may have been introduced in Zn-VD-1h. Lastly, the high distillation removal efficiency reported in the literature (Table 2.4) of Pb was confirmed in both runs.

Using higher purity 5N rated Zn material shots, another three stage distillation run Zn-VD-7 was performed, shown in Table 5.3. Generally, the large number of elements detected in the triple distilled material, that remained undetected in the raw material, is surprising. Heavier elements such as Pb, Sb, Cd etc. were removed or reduced relatively efficiently, whereas lighter elements such as Al, Si, Ga were introduced. No potential source for Ga introduction could be imagined. Hypothetically, if introducing contamination could be avoided and undetected materials are assumed to be absent (rather than down to the detection limit), 7N5 purity would be achieved, indicating that if the introduction of elements could be avoided, Zn vacuum distillation would be very promising.

As always in the case of vacuum distillation GDMS data, disadvantageous segregation conditions may explain the elements found at higher concentration in the distilled material as compared to the raw material. Unfortunately, GDMS data may falsely indicate contamination.

In summary, Zn vacuum distillation seems to lack repeatability to a certain extent and purity results seem somewhat erratic. However, the potential for successful purification is given as indicated by the elements that could be removed successfully.

5.3.2   Zone Refining Results

Combined vacuum distillation and zone refining was difficult due to glassware cracking, those issues previously discussed. In fact, two out of three attempts failed. To analyze the zone

refining purification efficiency for Zn, an enclosed Ar backfilled zone refining experiment in a Fabmate boat was performed. The Fabmate boat was enclosed in a Pyrex shell ampoule that was back-filled with ≈ 0.2 atm of Ar and plug sealed as shown, still attached to the vacuum system, in Fig. 5.4. The run consisted of two extended zone passes where the ampoule was mechanically agitated to break the surface tension of the Zn shots, followed by 15 actual zone refining passes. The impurities in the two extremities and the center part were analyzed using GDMS.

Figure 5.4: Zinc shots loaded into Fabmate boat, enclosed in Pyrex shell, backfilled with argon, plug sealed.

A selection of impurity concentrations is listed in Table 5.4. Given that the Cd concentrations in all three measured parts is significantly higher than that specified for the raw material by the manufacturer. Likely, the indicated material quality is very conservatively specified. Alternatively, the high Cd contamination could be from cross contamination. Table 2.4 reports Cd to be a good candidate for zone refining removal in Zn, which is confirmed by the increased concentration in the ending edge. Furthermore, Si proved to

be another good candidate for zone refining, having a segregation coefficient greater than unity, reflected by the increased concentration in the starting edge. On the other hand, Fe is reported to be a bad candidate for zone refining in Zn, which is confirmed by a relatively flat profile. Similarly, Cr did not have strong segregation and was therefore only slightly removed.

Table 5.4: Zn zone refining results. Only a selection of elements are shown; purities given in ppm wt; - : not tested for, < : detection limit reached. For a complete table, please refer to AppendixA.

Element	Raw	Zn-ZR-Ar-Fabmate-s (starting edge)	Zn-ZR-Ar-Fabmate-c (center part)	Zn-ZR-Ar-Fabmate-e (ending edge)
Si	-	0.31	< 0.005	< 0.005
Cr	-	0.02	0.01	0.03
Fe	-	0.03	0.03	0.04
Cd	0.2	0.65	0.54	2.9
In	-	=< 0.05	=< 1	=< 0.05
Ta	-	< 1	< 1	< 1
⋮		⋮	⋮	⋮
Total min.		1.01	0.58	2.97
Total max.		2.82	3.34	4.78
Best Case [%]		99.99990	99.99994	99.99970
Worst Case [%]	5N (spec.)	99.99972	99.99967	99.99952

In and Ta are listed due to their significant detection limits. Both are only present in ppb levels. It can therefore be assumed that the center part presents low 6N purity. Furthermore, the presence of Cd can be tolerated for the growth of CZT crystals. Conclusively, zone refining alone presents a viable option since combined vacuum distillation and zone refining is challenged by glassware cracking.

5.3.3   Combined Vacuum Distillation and Zone Refining Results

Finally, to assess the combined vacuum distillation and zone refining efficiency, a run in a Pyrex ampoule was performed. The zone refining chamber part was made of medium wall weight Pyrex which prevented cracking. Once the material was vacuum deposited in the zone refining chamber, the ampoule was cut open on one side and backfilled with ≈ 0.2 atm of Ar, and sealed with a plug. Next, 5 extended zone passes followed by 20 short zone passes were performed. The center part of the zone refined material was GDMS analyzed, as listed in Table 5.5.

Table 5.5: Zn zone refining results. Only a selection of elements are shown; purities given in ppm wt; - : not tested for, < : detection limit reached. For a complete table, please refer to AppendixA.

Element	Raw	Zn-VD-ZR-Ar-17c (center part)
Al	-	0.01
Si	-	0.03
Fe	0.2	< 0.01
Cd	-	0.19
In	-	=< 0.05
Sn	-	0.02
Ta	-	< 1
:		:
Total min.		**0.25**
Total max.		**2.07**
Best Case [%]		**99.99998**
Worst Case [%]	**5N (spec.)**	**99.99979**

Only Cd had poor removal and was detected in significant quantities. It can be assumed that Fe and Cr were successfully purified in the vacuum distillation step, since zone refining alone was not effective for those two elements, as shown in Table 5.4. In fact, Fe is reported to be removed effectively using vacuum distillation as listed in Table 2.4. The minor presence of Si is in line with the previously discussed Zn zone refining experiment. The presence of Sn is rather unexpected since its purification efficiency in vacuum distillation is reported to be good, as listed in Table 2.4.

In summary, the purification level reached is strongly affected by the detection limits of In and Ta, again. Assuming those two to be in the ppb range, the achieved purity starting with 5N material using combined vacuum distillation and zone refining in an enclosed argon atmosphere yields high 6N purity material. Notably, the procedure used involved a lot of steps and was challenged due to frequent glassware cracking. Finally, the high temperatures of 560 C during the vacuum distillation step may have contaminated the Zn with sodium escaping from Pyrex, which is not analyzed in GDMS.

5.4 Tellurium

Vacuum distillation with tellurium using the multi-chamber ampoule worked as predicted. Te distillation was relatively fast, up to 2 g/min as stated in Table 4.1. Moreover, no

cracking incidents occurred during vacuum distillation.

As reported in the literature, N_2 or H_2 could be used as protective gas, and H_2 additionally acts as a chemical purification agent duting zone refining. The duration of H_2 exposure was typically limited to the extended zone passes after which the gas stream was switched to N_2 reduce high purity H_2 gas usage.

5.4.1   Vacuum Distillation Results

Single, double and triple distillation runs with 5N1 raw material were performed to compare their respective purification outcomes, shown in Table 5.6. Accordingly, 6N0, 5N8 and 6N1 purities were achieved, respectively. The purification efficiency S_C in terms of individual elements was consistent for all detected impurities with the exception of selenium. As shown in Fig. B.5, which shows the different vapor pressures at the chosen Te distillation temperature of 525 C, Se has a vapor pressure comparable to that of Te, which only partly explains the purification difficulties. In fact, Cd having a vapor pressure closer to Te than to Se and Cd proved excellent purification efficiencies, so the vapor pressure differential alone can not be used to predict the purification outcome. Likely, the chemical similarity of Se and Te (same number of valence electrons) renders purification difficult.

The main conclusion from Table 5.6 is that triple distillation is not superior to single distillation. However, since timing the distillation run is challenging and a distillation residue of approximately 20% is necessary, two stage distillation was chosen for futher runs. That way, if one run was overdone, the second run could ensure an adequate residue.

Other GDMS measurements from multiple distillations were performed with 3N rated raw material and are summarized in Table 5.7. The results indicate 5N9, 5N2 and 5N6 results for single, double and triple distillation, respectively. The GDMS measured purity of the raw material was 5N8, which questions the efficiency of the vacuum distillation. Specifically, Al, Si, S, Ca, Ba and La demonstrated highly negative purification numbers for

Table 5.6: Single, double and triple Te distillation results along with the purification coefficient S_C. Only a selection of elements are shown, purities given in ppm wt, - : not tested for, < : detection limit reached. For a complete table please refer to AppendixA.

Element	Raw	Te-VD-9 (one stage)	S_C	Te-VD-10 (two stage)	S_C	Te-VD-11 (three stage)	S_C
Na	0.2	0.1	50%	0.02	90%	0.04	80%
Al	0.03	0.009	70%	0.01	67%	0.01	67%
Si	0.02	< 0.005	> 75%	< 0.005	> 75%	0.009	55%
S	-	-	-	-	-	0.006	-
Cl	0.2	0.01	95%	0.02	90%	0.02	90%
Ni	0.2	< 0.005	> 98%	< 0.005	> 98%	< 0.005	> 98%
Cu	0.04	< 0.005	> 88%	0.01	75%	< 0.005	> 88%
Zn	0.01	< 0.005	> 50%	< 0.005	> 50%	< 0.005	> 50%
Se	0.3	0.25	17%	0.8	-167%	0.3	0%
Cd	7	0.05	99%	< 0.005	> 99%	< 0.005	> 99%
Pb	0.08	< 0.005	> 94%	< 0.005	> 94%	< 0.005	> 94%
Bi	0.02	< 0.005	> 75%	< 0.005	> 75%	< 0.005	> 75%
⋮	⋮	⋮		⋮		⋮	
Total min.	**8.11**	**0.45**		**1.03**		**0.39**	
Total max.	**8.66**	**1.03**		**1.57**		**0.92**	
Best Case [%]	99.99919	99.99996		99.99990		99.99996	
Worst Case [%]	99.99913	99.99990		99.99984		99.99991	

single, double and triple distillation. Next, Na, Cl, Fe, Cu and Zn having highly negative purification numbers for single and double distillation only. On the other side, K, Pb and Bi generally had efficient purification.

The discrepancy between rated and measured raw material purity may explain the bad and inconsistent results. The raw material prepared for GDMS analysis was molten to a plug in a small ampoule where the freezing front could have led to significant segregation. Na, Al, Si, Ca, Fe, Cu and Zn had very low segregation coefficients in Te (Table 2.7), which could strongly offset the purity levels within a frozen plug. Consequently, the calculated, favorable purification efficiency for Pb and Bi may even be better since Pb and especially Bi has very low segregation coefficients ($<< 1$) that could mean that the average starting concentration of those two elements is in fact significantly greater. Segregation in the distilled plug after down-melting may further explain inconsistency.

However, assuming that the starting material was 3N only, as it is rated, the purity achieved in the upper 5N range is very acceptable. Se again consistently had low purification numbers S_C. The detected traces of Hg and especially W in the double distillation sample remain a mystery. Contamination from quartz typically only includes Al, Li and Ca [17].

Table 5.7: Incoherent, single, double and triple Te distillation results along with the purification coefficient S_C. Only a selection of elements are shown; purities given in ppm wt; - : not tested for, < : detection limit reached. For a complete table, please refer to AppendixA.

Element	Raw	Te-VD-13 (one stage)	S_C	Te-VD-14 (two stage)	S_C	Te-VD-15 (three stage)	S_C
Na	0.17	0.6	-253%	1.2	-606%	0.2	-18%
Al	< 0.005	0.3	-5900%	1	-19900%	0.07	-1300%
Si	< 0.005	0.04	-700%	0.25	-4900%	0.05	-900%
S	< 0.005	0.05	-900%	0.04	-700%	0.01	-100%
Cl	< 0.005	0.05	-900%	0.07	-1300%	< 0.005	
K	0.1	0.06	40%	0.2	-100%	< 0.01	> 90%
Ca	< 0.01	0.1	-900%	1.3	-12900%	0.02	-100%
Fe	< 0.005	0.03	-500%	0.008	-60%	< 0.005	
Cu	< 0.005	0.95	-18900%	0.4	-7900%	< 0.005	
Zn	< 0.005	0.02	-300%	0.01	-100%	< 0.005	
Se	0.7	0.8	-14%	0.6	14%	0.3	57%
Ba	0.04	1.6	-3900%	1	-2400%	0.1	-150%
La	0.01	0.24	-2300%	0.6	-5900%	0.03	-200%
W	< 0.005	< 0.005		0.04	-700%	< 0.005	
Hg	< 0.005	< 0.005		0.06	-1100%	< 0.005	
Pb	0.7	< 0.005	> 99%	0.01	99%	< 0.005	> 99%
Bi	0.02	< 0.005	> 75%	< 0.005	> 75%	< 0.005	> 75%
:	:	:	:	:		:	
Total min.	1.74	0.78		7.23		4.99	
Total max.	2.27	1.30		7.69		5.47	
Best Case [%]	99.99983	99.99992		99.99928		99.99950	
Worst Case [%]	99.99977	99.99987		99.99923		99.99945	

Finally, irregularities with the GDMS process can not be excluded entirely.

Regarding testing anomalies the starting material got stuck in the ampoule necks prior to the first purification runs and had to be melted down using the flame torch. Also, during the single distillation run of Te-VD-13, vacuum problems occurred, and a quartz piece of unknown origin was found in the bottom ampoule with the residue, which could hint at contamination.

In summary, Te vacuum distillation alone efficiently reduces impurities with the exception to Se as indicated in the literature. Zone refining under H_2 flow is necessary to reduce Se sufficiently to reach 7N purity. However, as demonstrated by the Te-VD-13 run the distillation has to be performed properly and incidents such as vacuum outages are not tolerable. Furthermore, GDMS results from downmelted material has to be interpreted correctly due to segregation.

5.4.2 Zone Refining Results

Since combined vacuum distillation and zone refining worked out well with Te, no exclusive zone refining runs were performed.

5.4.3 Combined Vacuum Distillation and Zone Refining Results

Double distillation followed by zone refining under H_2 flow initially, then under N_2 flow was performed, and GDMS measurements from the two extremities and the center of the charge are taken, shown in Table 5.8. 5N specified starting material was used which was not sent out for GDMS analysis. The Te starting material chunks had to be crushed being cooled by liquid N_2 using a dedicated blender to a size that fell down to the lowest ampoule chamber. Starting material purity values are taken from the material specifications given in terms of an upper boundary ($<$).

Table 5.8: Double vacuum distillation followed by zone refining Te results along with the purification coefficient S_C. Only a selection of elements are shown; purities given in ppm wt; - : not tested for, $<$: detection limit reached. For a complete table, please refer to AppendixA.

Element	Raw	Te-VD-ZR-24s (starting edge)	S_C	Te-VD-ZR-24c (center part)	S_C	Te-VD-ZR-24e (ending edge)	S_C
Na	< 0.22	0.03	86%	0.04	82%	0.07	68%
Mg	< 0.03	< 0.005		< 0.005		< 0.005	
Al	< 0.01	0.01	0%	0.03	-200%	0.02	-100%
Si	< 0.1	0.05	50%	0.2	-100%	0.04	60%
S	< 0.02	0.04	-100%	0.03	-50%	0.03	-50%
Cl	< 0.05	0.02	60%	0.006	88%	0.03	40%
Co	< 0.08	< 0.005		< 0.005		< 0.005	
Cu	< 0.05	< 0.005		0.007	86%	0.006	88%
Se	< 1.2	0.2	83%	0.5	58%	1	17%
:	:	:		:		:	
Total min.		0.35		0.81		1.20	
Total max.		0.98		1.43		1.82	
Best Case [%]		99.99997		99.99992		99.99988	
Worst Case [%]	5N (spec)	99.99990		99.99986		99.99982	

Ultimately, 6N purity levels were achieved for the three samples. A clear segregation effect is visible only for Na and Se and somewhat for Cu. Note that all detected impurities have segregation coefficients smaller than unity (Table 2.7), so the impurities built up in the "ending edge" accordingly. Se has a segregation coefficient close to unity, which was

reflected in the low segregation purification effect. The high base level of Se concentration, however, indicates that the H_2 flow should be extended over the entire zone refining process and not just be limited to the "extended zone" preliminary runs. Impurities such as Na, Al, Si, S and Cu have much lower segregation coefficients and should present far better segregation characteristics, which indicates that the zone refining process was not entirely effective. Presumably, very low concentrations may not get rejected or attracted by the freezing interface in order to lead to a segregation profile. Alternatively, redistribution of impurities by an excessively large melt zone or continuous contamination may be responsible for this inefficiency. Finally, segregation of other impurities might be hidden below the detection limit due to high purity material yield from the double distillation run.

Additionally, combined double vacuum distillation and zone refining runs were performed, and the center parts (only) were analyzed; the selective GDMS results from select elements are shown in Tables 5.9 and 5.10. The 4N specified raw material used came with relatively exhaustive purity analysis data, however, two different lots of raw material were used with slightly different impurity concentrations, separated into two tables.

The combined purification run Te-VD-ZR-20 consisted of double vacuum distillation, 4 extended melt zone passes and 14 actual zone refining passes. The extended zone passes were performed under H_2 gas flow which was switched to N_2 for the 14 actual zone refining passes. The zone refining ampoule experienced cracking during the preliminary downmelt step, likely due to fast cooling rates, so the unaffected Te rod was reloaded into a cleaned open quartz boat. The second run shown in Table 5.9, Te-VD-22-ZR consisted of a double vacuum distillation step followed by 4 extended melt zone passes under H_2 flow followed by 15 short zone passes under N_2 flow. During the last zone refining pass, the zone refining ampoule cracked and fell apart, and some Te ran out in the furnace tube. Meanwhile, the center sample sent out for GDMS analysis should have stayed unaffected.

Both samples show relatively similar impurity contamination with the exception of chlorine Cl which is present at 2 ppm in Te-VD-ZR-20c and only at 0.13 ppm in Te-VD-ZR-22c.

Table 5.9: Te combined vacuum distillation - zone refining results. Only a selection of elements are shown; purities given in ppm wt; - : not tested for, < : detection limit reached. For a complete table, please refer to AppendixA.

Element	Raw	Te-VD-ZR-20c (center part)	Te-VD-ZR-22c (center part)
Na	1.5	0.05	0.03
Mg	0.2	< 0.005	< 0.005
Al	3.3	0.05	0.01
Si	-	0.08	0.06
S	-	0.04	0.03
Cl	-	2	0.13
K	0.5	< 0.01	< 0.01
Cr	0.3	< 0.005	< 0.005
Mn	0.05	< 0.005	< 0.005
Fe	0.55	< 0.005	< 0.005
Ge	< 1	< 0.005	< 0.005
Se	< 0.5	< 0.01	< 0.01
Cd	< 1	< 0.005	< 0.005
Sb	< 1	< 0.05	< 0.05
Hf	< 1	< 0.005	< 0.005
Ta	< 5	Source	Source
Hg	< 1	< 0.005	< 0.005
:	:	:	:
Total min.		**2.22**	**0.26**
Total max.		**2.85**	**0.89**
Best Case [%]		**99.99978**	**99.99997**
Worst Case [%]	**4N (spec.)**	**99.99972**	**99.99991**

Heavy elements such as Hg and Ta etc. were very efficiently reduced in both cases. The fact that Te-VD-ZR-20c had to be reloaded into an open boat may explain the increased Cl concentration. Even if gloves were worn at all times handling the glassware, Cl may have been introduced through salt (NaCl) from the skin. Na was, however, relatively efficiently reduced which is even more surprising since its reported purification efficiency in vacuum distillation and zone refining, respectively, is mostly unfavorable according to Tables 2.5 and 2.6. Otherwise, the purification chain was very successful reducing the purity of both samples to the order of magnitude of the detection limits. Surprisingly, Se was purified down to its detection limit despite its disadvantageous properties relative to the Te purification and results from other Te purification runs performed such as Te-VD-ZR-24. Presumably, different raw material from a different provider, where the Se initial concentration was already relatively low (< 0.5 ppm), may explain the lack of Se detected in both purified samples. Finally, both samples have purities close to 6N, Te-VD-ZR-22c potentially up to 6N7 purity due to the much lower concentration of Cl.

Based on experiences made during the zone refining experiments performed, an additional combined Te purification run was performed extending H_2 exposure over the entire zone refining part to lower the Se concentration. Thus, Te-VD-27-ZR was performed using 4N rated material, double vacuum distillation, 5 extended melt zones and 17 actual zone refining passes. In order to conserve high purity H_2, the H_2 flow was reduced from 4l/h air to 1 l/h air approximately for the last 10 zone refining runs. The GDMS results from the center part are shown in Table 5.10. Amazingly, all elements tested were not detected above their detection limits with the exception of Si and Cl, reflected in a purity achieved in a range between 6N3 and 7N4.

Table 5.10: Te combined vacuum distillation - zone refining results. Only a selection of elements are shown; purities given in ppm wt; - : not tested for, < : detection limit reached. For a complete table, please refer to AppendixA.

Element	Raw	Te-VD-ZR-27c (center part)
Na	3.5	< 0.005
Al	0.2	< 0.005
Si	0.8	0.04
Cl	-	0.02
K	2	< 0.01
Cr	0.2	< 0.005
Mn	0.1	< 0.005
Fe	0.2	< 0.005
Ni	0.8	< 0.005
Ge	< 1	< 0.005
Se	5.5	< 0.01
Cd	< 1	< 0.005
Sn	< 1	< 0.005
Sb	< 1	< 0.05
Ta	< 10	Source
Pb	0.4	< 0.005
Bi	0.4	< 0.005
Th	< 1	< 0.005
:		:
Total min.		**0.06**
Total max.		**0.71**
Best Case [%]		**99.999994**
Worst Case [%]	**4N (spec.)**	**99.99993**

The presence of Si may be partly attributed to the poor segregation efficiency as demonstrated in Te-VD-ZR-24 and shown in Table 5.8. Cl, again, may be due to contamination, or, poor purification efficiency which can not be judged conclusively since its raw material concentration is not specified. Overall, the present run proves that combined vacuum distillation and zone refining under H_2 flow, performed properly, yields high purity Te in the

mid 6N, up to the mid 7N range.

Chapter 6

Conclusion

With the exception of glassware cracking, both vacuum distillation and zone refining proved to be reliable and repeatable processes. The equipment and the control software provided a stable platform to conduct the experimens. However, different raw materials led to very varying distillation rates; different charge heights led to different temperature requirements for zone refining. Therefore, the experiments have to be monitored closely in order to get desired results.

In general, segregation was orders of magnitude less effective than that predicted by segregation coefficients from the literature. Due to the high degree of purity, diffusion in the solid may be more relevant and the rejection or attraction effect of the freezing interface may not be as pronounced. Additionally, only a small number of elements were typically detected in all the three samples so that the segregation effect could not be fully assessed. Alternatively, segregation effects could be hidden below detection limits.

The vacuum distillation could not achieve efficiencies predicted by the vapor pressure differential of the purified element and impurity elements. Elements from the same periodical group (same number of valence electrons) at times showed purification difficulties. However, the vacuum distillation process typically yielded material close to 6N purity which represents an ideal starting material for zone refining.

Double vacuum distillation of cadmium in Pyrex glassware was very effective in purifying 5N starting material to a purity in the range between 6N5 and 7N5 using GDMS and laser

ablation mass spectroscopy data. Alternatively, zone refining in Fabmate exposed to H_2 flow led to a purity (in the center section) between the range of 6N5 and 6N9. The latter process presents the advantage that the Cd easily separates off the Fabmate boat whereas diamond blade cutting is necessary to separate the Cd from the target Pyrex chamber, followed by a 10% bromine:methanol solution etch. Furthermore, the torch sealing of the necks steps necessary for vacuum distillation, which exposes the experimentor to a certain risk of Cd vapor exposure, could be avoided by using zone refining only. The author, therefore, suggests zone refining in Fabmate for Cd ultra purification, and chopping off 5 cm of the extremities on each side. If diamond wire/blade cutting is necessary, the contaminated surface has to be cleaned from contamination using a 10% bromine:methanol solution etch for 30 sec.

Zinc vacuum distillation results, challenged by high detection limits, could not reach 6N purity. Pure zone refining in an enclosed argon atmosphere with 5N starting material yielded material between the range of 5N7 to 6N4 in the center part of the charge. Finally, Ar backfilled enclosed zone refining following double vacuum distillation yielded 5N8, up to 6N8 material. This latter process, however, required a lot of work and proved to be susceptible to glassware cracking. Therefore, the author suggests enclosed Ar backfilled zone refining in Fabmate boats without prior vacuum distillation.

Tellurium purification using combined double vacuum distillation and zone refining under continuous H_2 flow was successful, yielding purity between the mid 6N up to the mid 7N range. Although extra effort was required to perform vacuum distillation and zone refining, the improved results are commiserate with the increased work load.

According to Dr. Mark Harrison, the primary constraints on what physical form the Cd, Zn and Te must have for the CdTe and ZnTe synthesis are: the pieces must be small enough to fit into the ampoule/crucible, but, they should have a surface area as large as possible to minimize contamination. Because of the relatively ductile nature of Zn and especially Cd, those two metals must be cut in shape using a diamond blade/wire saw. The contaminated surface must be cleaned by an etch procedure in a 10% bromine:methanol

solution for approximately 30 seconds. Obviously, to satisfy the correct mass ratio, the mass of the Te must be fine adjusted with small peices which is fesible due to the very brittle character of Te.

6.1 Improvements

Current purification techniques have reached the limits of commercial full-scan mass spectroscopy methods. To further improve the purification, in-house analysis equipment becomes necessary to specifically improve the process and focus on key contaminants. However, some improvements in order to guarantee the outcome based on the current setup can be taken.

First, the entire process should be conducted in a clean-room environment to reduce contamination. The lab facility where the processes are performed is multi-use and other elements including silicon, mercury, iodide, bromine, lanthanum and fluorine are handled. To improve the purity results, more dedicated facilities may be necessary. For instance, the same glove box for material loading for all three elements was used. Also, the same vacuum system was used for Zn and Te, only Cd has a designated vacuum distillation stage due to the need for venting in case of leaking vapors.

To optimize the processes, raw material of consistent composition and grain sizes is required. That way, the timing for the distillation could be fine tuned and the mass ending up in the zone refining ampoule would become consistent. Systematic optimization of parameters such as predistillation and distillation temperatures could be performed. To optimize the zone refining purification without prior vacuum distillation, longer zone refining charges generally have a higher zone refining purification potential.

Significant improvements are related to high cost. Raw material in the 5N range is expensive at approximately $1/g and several kg are required for a systematic optimization. Furthermore, GDMS analysis or the purchase of appropriate mass-spectroscopy laboratory equipment is very costly. Therefore, the need for higher purification has to be proved first.

The attained purification levels and consistencies with current methods may likely be

sufficient to develop consistent and successful CdZnTe crystal growth methods.

Bibliography

[1] T. Schlesinger, J. Toney, H. Yoon, E. Lee, B. Brunett, L. Franks, and R. James, "Cadmium zinc telluride and its use as a nuclear radiation detector material," *Materials Science and Engineering: R: Reports*, vol. 32, no. 4-5, pp. 103 – 189, 2001.

[2] A. Kargar, R. B. Lowell, M. J. Harrison, and D. S. McGregor, "The crystal geometry and the aspect ratio effects on spectral performance of CdZnTe Frisch collar device," in *The International Society for Optical Engineering (SPIE)*, vol. 6706, (San Diego, CA, United states), p. 61J, 2007.

[3] K. Guergouri, R. Triboulet, A. Tromson-Carli, and Y. Marfaing, "Solution hardening and dislocation density reduction in CdTe crystals by Zn addition," vol. 86, (Netherlands), pp. 61 – 5, 1988.

[4] L. Bao, J. Zhu, X. Zhang, and J. Chu, "Effect of annealing on near-stoichiometric and non-stoichiometric CdZnTe wafers," *Journal of Crystal Growth*, vol. 181, pp. 204–209, 1997.

[5] D. S. McGregor and H. Hermon, "Room-temperature compound semiconductor radiation detectors," *Nuclear Instruments and Methods in Physics Research, Section A: Accelerators, Spectrometers, Detectors and Associated Equipment*, vol. 395, no. 1, pp. 101 – 124, 1997.

[6] S. Sze, *Semiconductor Devices - Physics and Technology*. John Wiley & Sons, Inc., 2nd ed., 2002.

[7] N. Tsoulfanidis, *Measurement and Detection of Radiation*. Tylor & Francis, 2nd edition ed., 1995.

[8] G. F. Knoll and D. S. McGregor, "Fundamentals of semiconductor detectors for ionizing radiation," (Pittsburgh, PA, USA), pp. 3 – 17, 1993.

[9] L. Kuchar, J. Drapala, and J. Lunacek, "Purification methods of Cd, Te and CdTe and periodicity of segregation coefficients of admixtures," *Journal of Crystal Growth*, vol. 161, pp. 94–103, 1996.

[10] D. S. McGregor, "Semiconductor radiation detectors." Handouts from NE860 class. Kansas State University, spring semester, 2008.

[11] S. Song, J. Wang, and M. Isshiki, "Preparation and photoluminescence characterization of high-purity CdTe single crystals: purification effect of normal freezing on tellurium and cadmium telluride," *Journal of Crystal Growth*, vol. 236, pp. 165–170, 2002.

[12] B. Wedlock, "Purification of tellurium by distillation," *J. Electrochem. Soc.*, vol. 109, pp. 318–320, 1962.

[13] W. Armarego and D. Perrin, *Purification of Laboratory Chemicals*. Butterworth Heinemann, 4th ed., 1996.

[14] S. Ali, R. Reddy, N. Munirathnam, C. Sudheer, G. Anil, and T. Prakash, "A novel in-situ technique of ultra purification of cadmium for electronic applications," *Separation and Purification Technology*, vol. 52, pp. 288–294, 2006.

[15] D. Favrat and L. Borel, *Thermodynamique et energetique*. Presse Polytechnieque Universitaire Romande, 2005.

[16] L. Holland, *Vacuum Deposition of Thin Films*. John Wiley & Sons, Inc., 4th ed., 1961.

[17] M. Roumie, A. Zaiour, K. Zahraman, J. Charara, A. Fawaz, F. Lmai, and M. Hage-Ali, "Purification of tellurium to nearly 7N purity," *Materials Science & Engineering B (Solid-State Materials for Advanced Technology)*, vol. 131, no. 1-3, pp. 54 – 61, 2006.

[18] W. G. Pfann, *Zone Melting*. New York: John Wiley & Sons, Inc., 2nd ed., 1978.

[19] N. Parr and M. M.I., *Zone Refining and Allied Techniques*. George Newness Limited, London, 1960.

[20] C. Ho, H. Yeh, and L. Yeh, "The optimal variation of zone lengths in multipass zone refining processes," *Separation and Purification Technology*, vol. 15, no. 1, pp. 69 – 78, 1999.

[21] S. Ali, J. Rao, K. Varma, and T. Prakash, "Purification of cadmium up to 5N+ by vacuum distillation," *Bull. Mater. Sci.*, vol. 25, pp. 479–481, 2002.

[22] S. Ali, N. Munirathnam, C. Sudheer, R. Reddy, and T. Prakash, "Purification of cadmium by vacuum distillation and its analysis," *Materials Letters*, vol. 58, pp. 1638–1641, 2004.

[23] S. Ali, N. Munirathnam, C. Sudheer, R. Reddy, M. Reddy, and T. Prakash, "Reduction of trace oxygen by hydrogen leaking during selective vaporization to produce ultra-pure cadmium for electronic applications," *Materials Letters*, vol. 61, pp. 1512–1516, 2007.

[24] S. Kovalevski, V. Kosyakov, and I. Shelpakova, "Cadmium purification by vacuum distillation in the presence of its oxide: thermodynamic modeling and experiment," *Journal of Crystal Growth*, vol. 167, pp. 208–211, 1996.

[25] S. Kovalevski and I. Shelpakova, "High-purity Zinc, Cadmium, Tellurium, Indium and Gallium: Preparation and analysis," *Chemistry of Sustainable Development*, vol. 8, pp. 85–87, 2000.

[26] B. Marthur and A. Singh, "Preparation of quadruple zone refined cadmium," *Indian Journal of Technology*, vol. 27, pp. 218–220, 1989.

[27] I. Shelpakova, V. Kosyakov, S. Kovalevski, and V. Shestakov, "The use of evaporation

in vacuum for purification and analysis of zinc," *Materials Research Bulletin*, vol. 33, no. 2, pp. 173–181, 1998.

[28] M. Isshiki, T. Tomizono, T. Yoshida, T. Ohkawa, and K. Igaki, "Preparation of high purity zinc by vacuum distillation and zone refining," *Japan Institute of Metals*, vol. 48, no. 12, pp. 1179–1179, 1984.

[29] J. A. Beran, *Laboratory Manual for Principles of General Chemistry.* John Wiley & Sons, 2007.

[30] "US Patent 5939042 - Tellurium extraction from copper electrorefining slimes," 1999.

[31] S. Ali, D. Prasad, N. Munirathnam, and T. Prakash, "Purification of tellurium by single-run multiple vacuum distillation technique," *Separation and Purification Technology*, vol. 43, no. 3, pp. 263 – 267, 2005.

[32] N. Munirathnam, D. Prasad, C. Sudheer, and T. Prakash, "Purification of tellurium to 6N+ by quadruple zone refining," *Journal of Crystal Growth*, vol. 254, pp. 262–266, 2003.

[33] D. Prasad, N. Munirathnam, J. Rao, and T. Prakash, "Effect of multi-pass, zone length and translation rate on impurity segregation during zone refining of tellurium," *Materials Letters*, vol. 60, no. 15, pp. 1875 – 9, 2006.

[34] G. Anil, M. Reddy, D. Prasad, S. Ali, N. Munirathnam, and T. Prakash, "Profiling of selenium removal in hydrogen ambient zone-refined tellurium bar using RF-GDOES," *Materials Characterization*, vol. 58, no. 1, pp. 92 – 5, 2007.

[35] N. Munirathnam, D. Prasad, J. Rao, and T. Prakash, "High purity tellurium production using dry refining processes," *Bull. Mater. Sci.*, vol. 28, pp. 309–311, 2005.

[36] N. Munirathnam, D. Prasad, C. Sudheer, A. Singh, and T. Prakash, "Preparation of

high purity tellurium by zone refining," *Bulletin of Materials Science*, vol. 25, no. 2, pp. 79 – 83, 2002.

[37] A. Zaiour, J. Hage-Ali, M. Koebel, and P. Siffert, "Effective and equilibrium evaporation coefficients of some impurities in molten tellurium," *Materials Science and Engineering*, vol. B3, pp. 331–334, 1989.

[38] D. Prakash, D. Sudheer, N. Munirathnam, and T. Prakash, "Tellurium purification: Various techniques and limitations," *Bull. Mater. Sci.*, vol. 25, pp. 545–547, 2002.

[39] A. Bollong and R. Bult, "The ultra purification of tellurium," *Jom*, vol. 41, pp. 39–41, 1989.

[40] B. Schaub and C. Potard, "Purification of tellurium and cadmium," in *N/A*, (Strasbourg, France), pp. 2 – 5, 1971.

[41] I. Cokov, *Unknown Title*. PhD thesis, MISIS, Moscow, 1966.

[42] W. F. Hachkovsky and P. G. Stkelkov, "Anomalous expansion of zinc and cadmium near the melting point," *Nature*, vol. 139, pp. 715–716, 1937.

[43] C. Alcock, V. Itkin, and M. Horrigan, "Vapor pressure equations for the metallic elements: 298-2500K," *Canadian Metallurgical Quarterly*, vol. 23, pp. 309–313, 1984.

[44] R. Machol and E. F. Westrum, "Vapor pressure of liquid tellurium," *J. Am. Chem. Soc.*, vol. 80, pp. 2950–2952, 1958.

[45] R. Honig, "Vapor pressure data from the solid and liquid elements," *RCA Reveiw*, vol. 30, pp. 285–305, 1969.

Appendix A

GDMS Analysis Results

A.1 Cadmium

Run:		Raw	Cd-VD-6	Raw	Cd-VD-8
Raw Material:		Am. Element	Am. Element	Am. Element	Am. Element
		Lot # 1151393149-663	Lot # 1151393149-663	Lot # 1151394349-093	Lot # 1151394349-093
		3N	3N	5N	5N
Purification:		-	1 stage VD	-	2 stage VD
Shiva Job #:		(spec.)	**S09X3298**	(spec.)	**S09X3298**
Element	**Detection Limits**	**Concentration**	**Concentration**	**Concentration**	**Concentration**
	[ppm wt]	**[ppm wt]**	**[ppm wt]**	**[ppm wt]**	**[ppm wt]**
Li	0.001	-	< 0.001	-	< 0.001
Be	0.001	-	< 0.001	-	< 0.001
B	0.001	-	< 0.001	-	< 0.001
F	0.01	-	< 0.01	-	< 0.01
Na	0.001	-	< 0.001	-	< 0.001
Mg	0.001	-	< 0.001	-	< 0.001
Al	0.001	-	< 0.001	-	< 0.001
Si	0.001	-	< 0.001	-	< 0.001
P	0.001	-	< 0.001	-	< 0.001
S	0.005	-	< 0.005	-	< 0.005
Cl	0.001	-	0.2	-	< 0.001
K	0.01	-	< 0.01	-	< 0.01
Ca	0.005	-	< 0.005	-	< 0.005
Sc	0.005	-	< 0.005	-	< 0.005
Ti	0.001	-	< 0.001	-	< 0.001
V	0.001	-	< 0.001	-	< 0.001
Cr	0.001	-	< 0.001	-	< 0.001
Mn	0.005	-	< 0.005	-	< 0.005
Fe	0.005	-	< 0.005	-	< 0.005
Co	0.001	-	< 0.001	-	< 0.001
Ni	0.005	-	< 0.005	-	< 0.005
Cu	0.005	< 0.01	< 0.005	-	< 0.005
Zn	0.005	< 0.01	< 0.005	-	< 0.005
Ga	0.005	-	< 0.005	-	< 0.005
Ge	0.005	-	< 0.005	-	< 0.005
As	0.005	< 0.003	< 0.005	-	< 0.005
Se	0.005	-	< 0.005	-	< 0.005
Br	0.005	-	< 0.005	-	< 0.005
Rb	0.005	-	< 0.005	-	< 0.005
Sr	0.005	-	< 0.005	-	< 0.005
Y	0.005	-	< 0.005	-	< 0.005
Zr	0.005	-	< 0.005	-	< 0.005
Nb	0.005	-	< 0.005	-	< 0.005
Mo	0.005	-	< 0.005	-	< 0.005
Ru	0.005	-	< 0.005	-	< 0.005
Rh	0.005	-	< 0.005	-	< 0.005
Pd	0.01	-	< 0.01	-	< 0.01
Ag	0.01	< 0.01	< 0.01	-	< 0.01
Cd	Matrix	-	Matrix	-	Matrix
In	0.1	-	< 0.1	-	< 0.1
Sn	0.01	< 0.01	< 0.01	< 0.3	< 0.01
Sb	0.005	< 0.001	< 0.005	-	< 0.005
Te	0.005	-	< 0.1	-	< 0.1
I	0.01	-	< 0.01	-	< 0.01
Cs	0.01	-	< 0.01	-	< 0.01
Ba	0.01	-	< 0.01	-	< 0.01
La	0.01	-	< 0.01	-	< 0.01
Ce	0.01	-	< 0.01	-	< 0.01
Pr	0.01	-	< 0.01	-	< 0.01
Nd	0.005	-	< 0.005	-	< 0.005
Sm	0.005	-	< 0.005	-	< 0.005
Eu	0.01	-	< 0.01	-	< 0.01
Gd	0.005	-	< 0.005	-	< 0.005
Tb	0.001	-	< 0.001	-	< 0.001
Dy	0.001	-	< 0.001	-	< 0.001
Ho	0.001	-	< 0.001	-	< 0.001
Er	0.001	-	< 0.001	-	< 0.001
Tm	0.001	-	< 0.001	-	< 0.001
Yb	0.001	-	< 0.001	-	< 0.001
Lu	0.001	-	< 0.001	-	< 0.001
Hf	0.001	-	< 0.001	-	< 0.001
Ta	1	-	< 1	-	< 1
W	0.005	-	< 0.005	-	< 0.005
Re	0.005	-	< 0.005	-	< 0.005
Os	0.005	-	< 0.005	-	< 0.005
Ir	0.005	-	< 0.005	-	< 0.005
Pt	0.005	-	< 0.005	-	< 0.005
Au	0.05	-	< 0.05	-	< 0.05
Hg	0.005	-	2.4	-	< 0.005
Tl	0.005	< 0.002	0.03	-	< 0.005
Pb	0.005	< 0.01	0.35	-	< 0.005
Bi	0.005	-	< 0.005	-	< 0.005
Th	0.005	-	< 0.005	-	< 0.005
U	0.001	-	< 0.001	-	< 0.001
Tot Min	**1.47**		**2.98**		**0.00**
Tot Max	**1.47**		**4.43**		**1.47**
Best Case [%]	**99.99985**		**99.99970**		**100.00000**
Worst Case [%]	**99.99985**	**3N (spec.)**	**99.99956**	**5N (spec.)**	**99.99985**

		Run: **Raw** Am. Element Lot # 1151395149-179 5N	Cd-ZR-Fabmate-s Am. Element Lot # 1151395149-179 5N	Cd-ZR-Fabmate-c Am. Element Lot # 1151395149-179 5N	Cd-ZR-Fabmate-e Am. Element Lot # 1151395149-179 5N
Run: Raw Material: Purification: Shiva Job #:		- (spec.)	1+ 16 ZR H2 zone start extr. S09Z4419	1+ 16 ZR H2 center part S09Z4419	1+ 16 ZR H2 zone end extr. S09Z4419
Element	**Detection Limits [ppm wt]**	**Concentration [ppm wt]**	**Concentration [ppm wt]**	**Concentration [ppm wt]**	**Concentration [ppm wt]**
Li	0.001		< 0.001	< 0.001	< 0.001
Be	0.001		< 0.001	< 0.001	< 0.001
B	0.001		< 0.001	< 0.001	< 0.001
F	0.01		< 0.01	< 0.01	< 0.01
Na	0.001		< 0.001	< 0.001	< 0.001
Mg	0.001		< 0.001	< 0.001	< 0.001
Al	0.001		< 0.001	< 0.001	< 0.001
Si	0.001		0.008	< 0.001	0.004
P	0.001	-	< 0.001	< 0.001	< 0.001
S	0.005	-	< 0.005	< 0.005	< 0.005
Cl	0.001	-	< 0.001	< 0.001	0.004
K	0.01	-	< 0.01	< 0.01	< 0.01
Ca	0.005	-	< 0.005	< 0.005	< 0.005
Sc	0.005	-	< 0.005	< 0.005	< 0.005
Ti	0.001	-	< 0.001	< 0.001	< 0.001
V	0.001	-	< 0.001	< 0.001	< 0.001
Cr	0.001	-	< 0.001	< 0.001	< 0.001
Mn	0.005	-	< 0.005	< 0.005	< 0.005
Fe	0.005	-	< 0.005	< 0.005	< 0.005
Co	0.001	-	< 0.001	< 0.001	< 0.001
Ni	0.005	-	< 0.005	< 0.005	< 0.005
Cu	0.005	-	0.02	0.05	0.11
Zn	0.005	-	< 0.005	0.04	0.03
Ga	0.005	-	< 0.005	< 0.005	< 0.005
Ge	0.005	-	< 0.005	< 0.005	< 0.005
As	0.005	-	< 0.005	< 0.005	< 0.005
Se	0.005	-	< 0.005	< 0.005	< 0.005
Br	0.005	-	< 0.005	< 0.005	< 0.005
Rb	0.005	-	< 0.005	< 0.005	< 0.005
Sr	0.005	-	< 0.005	< 0.005	< 0.005
Y	0.005	-	< 0.005	< 0.005	< 0.005
Zr	0.005	-	< 0.005	< 0.005	< 0.005
Nb	0.005	-	< 0.005	< 0.005	< 0.005
Mo	0.005	-	< 0.005	< 0.005	< 0.005
Ru	0.005	-	< 0.005	< 0.005	< 0.005
Rh	0.005	-	< 0.005	< 0.005	< 0.005
Pd	0.01	-	< 0.01	< 0.01	< 0.01
Ag	0.01	0.6	0.1	< 0.01	< 0.01
Cd	Matrix	-	Matrix	Matrix	Matrix
In	0.1	-	< 0.1	< 0.1	0.18
Sn	0.01	-	< 0.01	0.02	< 0.01
Sb	0.005	-	< 0.005	< 0.005	< 0.005
Te	0.005	-	< 0.1	< 0.1	0.08
I	0.01	-	< 0.01	< 0.01	< 0.01
Cs	0.01	-	< 0.01	< 0.01	< 0.01
Ba	0.01	-	< 0.01	< 0.01	< 0.01
La	0.01	-	< 0.01	< 0.01	< 0.01
Ce	0.01	-	< 0.01	< 0.01	< 0.01
Pr	0.01	-	< 0.01	< 0.01	< 0.01
Nd	0.005	-	< 0.005	< 0.005	< 0.005
Sm	0.005	-	< 0.005	< 0.005	< 0.005
Eu	0.01	-	< 0.01	< 0.01	< 0.01
Gd	0.005	-	< 0.005	< 0.005	< 0.005
Tb	0.001	-	< 0.001	< 0.001	< 0.001
Dy	0.001	-	< 0.001	< 0.001	< 0.001
Ho	0.001	-	< 0.001	< 0.001	< 0.001
Er	0.001	-	< 0.001	< 0.001	< 0.001
Tm	0.001	-	< 0.001	< 0.001	< 0.001
Yb	0.001	-	< 0.001	< 0.001	< 0.001
Lu	0.001	-	< 0.001	< 0.001	< 0.001
Hf	0.001	-	< 0.001	< 0.001	< 0.001
Ta	1	-	< 1	< 1	< 1
W	0.005	-	< 0.005	< 0.005	< 0.005
Re	0.005	-	< 0.005	< 0.005	< 0.005
Os	0.005	-	< 0.005	< 0.005	< 0.005
Ir	0.005	-	< 0.005	< 0.005	< 0.005
Pt	0.005	-	< 0.005	< 0.005	< 0.005
Au	0.05	-	< 0.05	< 0.05	< 0.05
Hg	0.005	-	< 0.005	< 0.005	< 0.005
Tl	0.005	-	< 0.005	< 0.005	< 0.005
Pb	0.005	-	< 0.005	< 0.005	0.01
Bi	0.005	-	< 0.005	< 0.005	< 0.005
Th	0.005	-	< 0.005	< 0.005	< 0.005
U	0.001	-	< 0.001	< 0.001	< 0.001
Tot Min	**1.47**		**0.13**	**0.11**	**0.42**
Tot Max	**1.47**		**1.68**	**1.66**	**1.77**
Best Case [%]	**99.99985**		**99.999987**	**99.999989**	**99.99996**
Worst Case [%]	**99.99985**	**5N (spec.)**	**99.99983**	**99.99983**	**99.99982**

A.2   Zinc

Run:		Raw	Zn-VD-Ih	Zn-VD-2c
Raw Material:		Am. Elements Lot # 1046Zn6334 4N	Am. Elements Lot # 1046Zn6334 4N	Am. Elements Lot # 1046Zn6334 4N
Purification:		-	1 stage VD multipl.downmelts and re-runs	3 stage VD multipl.downmelts and re-runs
Shiva Job #:		S070611114	S070611112	S070611113
Element	Detection Limits [ppm wt]	Concentration [ppm wt]	Concentration [ppm wt]	Concentration [ppm wt]
Li	0.001	< 0.001	< 0.001	< 0.001
Be	0.001	< 0.001	< 0.001	< 0.001
B	0.001	0.01	0.02	< 0.001
F	0.01	< 0.01	< 0.01	< 0.01
Na	0.005	0.03	0.13	0.007
Mg	0.005	0.01	0.17	< 0.005
Al	0.001	0.13	0.72	0.004
Si	0.005	0.28	2.7	0.05
P	0.005	0.009	0.01	< 0.005
S	0.05	0.61	0.57	< 0.05
Cl	0.01	0.18	0.25	0.01
K	0.01	< 0.01	< 0.01	< 0.01
Ca	0.01	< 0.01	0.1	< 0.01
Sc	0.005	< 0.005	< 0.005	< 0.005
Ti	0.005	< 0.005	0.04	< 0.005
V	0.001	< 0.001	0.002	< 0.001
Cr	0.01	0.04	0.42	< 0.01
Mn	0.005	0.12	0.13	< 0.005
Fe	0.01	2	7.2	< 0.01
Co	0.005	0.02	0.13	< 0.005
Ni	0.01	0.11	1.4	< 0.01
Cu	0.05	2.1	0.35	1.3
Zn	Matrix	Matrix	Matrix	Matrix
Ga	0.01	< 0.01	< 0.01	< 0.01
Ge	0.05	< 0.05	< 0.05	< 0.05
As	0.005	< 0.005	< 0.005	< 0.005
Se	0.005	< 0.005	< 0.005	< 0.005
Br	0.005	< 0.005	< 0.005	< 0.005
Rb	0.005	< 0.005	< 0.005	< 0.005
Sr	0.005	< 0.005	< 0.005	< 0.005
Y	0.005	< 0.005	< 0.005	< 0.005
Zr	0.005	< 0.005	< 0.005	< 0.005
Nb	0.005	< 0.005	< 0.005	< 0.005
Mo	0.01	< 0.01	0.38	< 0.01
Ru	0.001	< 0.001	< 0.001	< 0.001
Rh	0.05	< 0.05	< 0.05	< 0.05
Pd	0.05	< 0.05	< 0.05	< 0.05
Ag	0.05	0.59	< 0.05	< 0.05
Cd	0.05	3	0.86	< 0.05
In	0.005	0.02	< 0.005	< 0.005
Sn	0.01	0.36	0.2	< 0.01
Sb	0.01	0.02	0.01	< 0.01
Te	0.01	0.64	0.24	< 0.01
I	0.01	< 0.01	< 0.01	< 0.01
Cs	0.05	< 0.05	< 0.05	< 0.05
Ba	0.01	< 0.01	< 0.01	< 0.01
La	0.001	< 0.001	0.06	< 0.001
Ce	0.001	< 0.001	< 0.001	< 0.001
Pr	0.001	< 0.001	< 0.001	< 0.001
Nd	0.001	< 0.001	< 0.001	< 0.001
Sm	0.001	< 0.001	< 0.001	< 0.001
Eu	0.001	< 0.001	< 0.001	< 0.001
Gd	0.001	< 0.001	< 0.001	< 0.001
Tb	0.001	< 0.001	< 0.001	< 0.001
Dy	0.001	< 0.001	< 0.001	< 0.001
Ho	0.001	< 0.001	< 0.001	< 0.001
Er	0.001	< 0.001	< 0.001	< 0.001
Tm	0.001	< 0.001	< 0.001	< 0.001
Yb	0.001	< 0.001	< 0.001	< 0.001
Lu	0.001	< 0.001	< 0.001	< 0.001
Hf	0.005	< 0.005	< 0.005	< 0.005
Ta	1	< 1	< 1	< 1
W	0.005	0.18	0.51	< 0.005
Re	0.005	< 0.005	0.08	< 0.005
Os	0.001	< 0.001	< 0.001	< 0.001
Ir	0.001	< 0.001	< 0.001	< 0.001
Pt	0.005	0.02	0.13	0.008
Au	0.05	< 0.05	< 0.05	< 0.05
Hg	0.05	< 0.05	< 0.05	< 0.05
Tl	0.01	3.9	0.62	0.03
Pb	0.05	12	0.74	< 0.05
Bi	0.01	< 0.01	< 0.01	< 0.01
Th	0.001	< 0.001	< 0.001	< 0.001
U	0.001	< 0.001	< 0.001	< 0.001
Tot Min	1.839	26.38	18.17	1.41
Tot Max	1.839	27.84	19.66	3.17
Best Case [%]	99.99982	99.99736	99.99818	99.99986
Worst Case [%]	99.99982	99.99722	99.99803	99.99968

Run:		**Raw**	**Zn-VD-7**	**Raw**	**Zn-VD-ZR-Ar-17c**
Raw Material:		Am. Elements	Am. Elements	Am. Elements	Am. Elements
		Lot # 187139-559	Lot # 187139-559	Lot # 1871395149-778	Lot # 1871395149-778
		5N	5N	5N	5N
Purification:		-	3 stage VD	-	2 stage VD
					5+ 20 ZR Ar
Shiva Job #:		S080522017	S080423001		S09Z4419
Element	**Detection Limits [ppm wt]**	**Concentration [ppm wt]**	**Concentration [ppm wt]**	**Concentration [ppm wt]**	**Concentration [ppm wt]**
Li	0.001	< 0.001	< 0.001	-	< 0.001
Be	0.001	< 0.001	< 0.001	-	< 0.001
B	0.001	< 0.001	< 0.001	-	< 0.001
F	0.01	< 0.01	< 0.01	-	< 0.01
Na	0.005	< 0.005	0.03	-	< 0.005
Mg	0.005	< 0.005	0.007	-	< 0.005
Al	0.001	0.002	0.06	-	0.01
Si	0.005	< 0.005	0.07	-	0.03
P	0.005	< 0.005	< 0.005	-	< 0.005
S	0.05	< 0.05	< 0.05	-	< 0.05
Cl	0.01	< 0.01	0.06	-	< 0.01
K	0.01	< 0.01	< 0.01	-	< 0.01
Ca	0.01	< 0.01	0.03	-	< 0.01
Sc	0.005	< 0.005	< 0.005	-	< 0.005
Ti	0.005	< 0.005	< 0.005	-	< 0.005
V	0.001	< 0.001	< 0.001	-	< 0.001
Cr	0.01	< 0.01	0.02	-	< 0.01
Mn	0.005	< 0.005	< 0.005	-	< 0.005
Fe	0.01	0.05	0.02	0.2	< 0.01
Co	0.005	< 0.005	< 0.005	-	< 0.005
Ni	0.01	< 0.01	< 0.01	-	< 0.01
Cu	0.05	< 0.05	< 0.05	-	< 0.05
Zn	Matrix	Matrix	Matrix	-	Matrix
Ga	0.01	< 0.01	0.34	-	< 0.01
Ge	0.05	< 0.05	0.08	-	< 0.05
As	0.005	< 0.005	< 0.005	-	< 0.005
Se	0.005	< 0.005	< 0.005	-	< 0.005
Br	0.005	< 0.005	< 0.005	-	< 0.005
Rb	0.005	< 0.005	< 0.005	-	< 0.005
Sr	0.005	< 0.005	< 0.005	-	< 0.005
Y	0.005	< 0.005	0.06	-	< 0.005
Zr	0.005	< 0.005	< 0.005	-	< 0.005
Nb	0.005	< 0.005	< 0.005	-	< 0.005
Mo	0.01	0.03	< 0.01	-	< 0.01
Ru	0.001	< 0.001	< 0.001	-	< 0.001
Rh	0.05	< 0.05	< 0.05	-	< 0.05
Pd	0.05	< 0.05	< 0.05	-	< 0.05
Ag	0.05	< 0.05	< 0.05	-	< 0.05
Cd	0.05	0.25	< 0.05	-	0.19
In	0.005	< 0.005	< 0.005	-	=< 0.05
Sn	0.01	0.07	< 0.01	-	0.02
Sb	0.01	0.5	0.02	-	< 0.01
Te	0.01	0.06	< 0.01	-	< 0.01
I	0.01	< 0.01	< 0.01	-	< 0.01
Cs	0.05	< 0.05	< 0.05	-	< 0.05
Ba	0.01	< 0.01	< 0.01	-	< 0.01
La	0.001	< 0.001	< 0.001	-	< 0.001
Ce	0.001	< 0.001	< 0.001	-	< 0.001
Pr	0.001	< 0.001	< 0.001	-	< 0.001
Nd	0.001	< 0.001	< 0.001	-	< 0.001
Sm	0.001	< 0.001	< 0.001	-	< 0.001
Eu	0.001	< 0.001	< 0.001	-	< 0.001
Gd	0.001	< 0.001	< 0.001	-	< 0.001
Tb	0.001	< 0.001	< 0.001	-	< 0.001
Dy	0.001	< 0.001	< 0.001	-	< 0.001
Ho	0.001	< 0.001	< 0.001	-	< 0.001
Er	0.001	< 0.001	< 0.001	-	< 0.001
Tm	0.001	< 0.001	0.007	-	< 0.001
Yb	0.001	< 0.001	< 0.001	-	< 0.001
Lu	0.001	< 0.001	< 0.001	-	< 0.001
Hf	0.005	< 0.005	< 0.005	-	< 0.005
Ta	1	< 1	< 1	-	< 1
W	0.005	0.01	0.007	-	< 0.005
Re	0.005	< 0.005	< 0.005	-	< 0.005
Os	0.001	< 0.001	< 0.001	-	< 0.001
Ir	0.001	< 0.001	< 0.001	-	< 0.001
Pt	0.005	< 0.005	< 0.005	-	< 0.005
Au	0.05	< 0.05	< 0.05	-	< 0.05
Hg	0.05	< 0.05	< 0.05	-	< 0.05
Tl	0.01	0.06	< 0.01	-	< 0.01
Pb	0.05	0.11	< 0.05	-	< 0.05
Bi	0.01	< 0.01	< 0.01	-	< 0.01
Th	0.001	< 0.001	< 0.001	-	< 0.001
U	0.001	< 0.001	< 0.001	-	< 0.001
Tot Min	**1.839**	**1.14**	**0.81**		**0.25**
Tot Max	**1.839**	**2.81**	**2.51**		**2.07**
Best Case [%]	**99.99982**	**99.99989**	**99.99992**		**99.99998**
Worst Case [%]	**99.99982**	**99.99972**	**99.99975**	**5N (spec.)**	**99.99979**

Element	Detection Limits [ppm wt]	Raw Am. Elements Lot # 1871395149-329 5N - Concentration [ppm wt]	Zn-ZR-Ar-Fabmate-s Am. Elements Lot # 1871395149-329 5N 1 + 15 ZR in Ar starting extr. S09Z4419 Concentration [ppm wt]	Zn-ZR-Ar-Fabmate-c Am. Elements Lot # 1871395149-329 5N 1 + 15 ZR in Ar center part S09Z4419 Concentration [ppm wt]	Zn-ZR-Ar-Fabmate-e Am. Elements Lot # 1871395149-329 5N 1 + 15 ZR in Ar end extr. S09Z4419 Concentration [ppm wt]
Li	0.001	-	< 0.001	< 0.001	< 0.001
Be	0.001	-	< 0.001	< 0.001	< 0.001
B	0.001	-	< 0.001	< 0.001	< 0.001
F	0.01	-	< 0.01	< 0.01	< 0.01
Na	0.005	-	< 0.005	< 0.005	< 0.005
Mg	0.005	-	< 0.005	< 0.005	< 0.005
Al	0.001	-	< 0.001	< 0.001	< 0.001
Si	0.005	-	0.31	< 0.005	< 0.005
P	0.005	-	< 0.005	< 0.005	< 0.005
S	0.05	-	< 0.05	< 0.05	< 0.05
Cl	0.01	-	< 0.01	< 0.01	< 0.01
K	0.01	-	< 0.01	< 0.01	< 0.01
Ca	0.01	-	< 0.01	< 0.01	< 0.01
Sc	0.005	-	< 0.005	< 0.005	< 0.005
Ti	0.005	-	< 0.005	< 0.005	< 0.005
V	0.001	-	< 0.001	< 0.001	< 0.001
Cr	0.01	-	0.02	0.01	0.03
Mn	0.005	-	< 0.005	< 0.005	< 0.005
Fe	0.01	-	0.03	0.03	0.04
Co	0.005	-	< 0.005	< 0.005	< 0.005
Ni	0.01	-	< 0.01	< 0.01	< 0.01
Cu	0.05	-	< 0.05	< 0.05	< 0.05
Zn	Matrix	-	Matrix	Matrix	Matrix
Ga	0.01	-	< 0.01	< 0.01	< 0.01
Ge	0.05	-	< 0.05	< 0.05	< 0.05
As	0.005	-	< 0.005	< 0.005	< 0.005
Se	0.005	-	< 0.005	< 0.005	< 0.005
Br	0.005	-	< 0.005	< 0.005	< 0.005
Rb	0.005	-	< 0.005	< 0.005	< 0.005
Sr	0.005	-	< 0.005	< 0.005	< 0.005
Y	0.005	-	< 0.005	< 0.005	< 0.005
Zr	0.005	-	< 0.005	< 0.005	< 0.005
Nb	0.005	-	< 0.005	< 0.005	< 0.005
Mo	0.01	-	< 0.01	< 0.01	< 0.01
Ru	0.001	-	< 0.001	< 0.001	< 0.001
Rh	0.05	-	< 0.05	< 0.05	< 0.05
Pd	0.05	-	< 0.05	< 0.05	< 0.05
Ag	0.05	-	< 0.05	< 0.05	< 0.05
Cd	0.05	0.2	0.65	0.54	2.9
In	0.005	-	=< 0.05	=< 1	=< 0.05
Sn	0.01	-	< 0.01	< 0.01	< 0.01
Sb	0.01	-	< 0.01	< 0.01	< 0.01
Te	0.01	-	< 0.01	< 0.01	< 0.01
I	0.01	-	< 0.01	< 0.01	< 0.01
Cs	0.05	-	< 0.05	< 0.05	< 0.05
Ba	0.01	-	< 0.01	< 0.01	< 0.01
La	0.001	-	< 0.001	< 0.001	< 0.001
Ce	0.001	-	< 0.001	< 0.001	< 0.001
Pr	0.001	-	< 0.001	< 0.001	< 0.001
Nd	0.001	-	< 0.001	< 0.001	< 0.001
Sm	0.001	-	< 0.001	< 0.001	< 0.001
Eu	0.001	-	< 0.001	< 0.001	< 0.001
Gd	0.001	-	< 0.001	< 0.001	< 0.001
Tb	0.001	-	< 0.001	< 0.001	< 0.001
Dy	0.001	-	< 0.001	< 0.001	< 0.001
Ho	0.001	-	< 0.001	< 0.001	< 0.001
Er	0.001	-	< 0.001	< 0.001	< 0.001
Tm	0.001	-	< 0.001	< 0.001	< 0.001
Yb	0.001	-	< 0.001	< 0.001	< 0.001
Lu	0.001	-	< 0.001	< 0.001	< 0.001
Hf	0.005	-	< 0.005	< 0.005	< 0.005
Ta	1	-	< 1	< 1	< 1
W	0.005	-	< 0.005	< 0.005	< 0.005
Re	0.005	-	< 0.005	< 0.005	< 0.005
Os	0.001	-	< 0.001	< 0.001	< 0.001
Ir	0.001	-	< 0.001	< 0.001	< 0.001
Pt	0.005	-	< 0.005	< 0.005	< 0.005
Au	0.05	-	< 0.05	< 0.05	< 0.05
Hg	0.05	-	< 0.05	< 0.05	< 0.05
Tl	0.01	-	< 0.01	< 0.01	< 0.01
Pb	0.05	-	< 0.05	< 0.05	< 0.05
Bi	0.01	-	< 0.01	< 0.01	< 0.01
Th	0.001	-	< 0.001	< 0.001	< 0.001
U	0.001	-	< 0.001	< 0.001	< 0.001
Tot Min	1.839		1.01	0.58	2.97
Tot Max	1.839		2.82	3.34	4.78
Best Case [%]	99.99982		99.99990	99.99994	99.99970
Worst Case [%]	99.99982	5N (spec.)	99.99972	99.99967	99.99952

A.3 Tellurium

Run	-	Raw	Te-VD-9	Te-VD-10	Te-VD-11
Raw Material	-	Am. Elements Lot # 1550TE418 4N	Am. Elements Lot # 1550TE418 4N	Am. Elements Lot # 1550TE418 4N	Am. Elements Lot # 1550TE418 4N
Purification	-	-	1 stage VD	2 stage VD	3 stage VD
Shiva Job #		U070112131	S070208051	U070112130	S070208052
Element	Detection Limits [ppm wt]	Concentration [ppm wt]	Concentration [ppm wt]	Concentration [ppm wt]	Concentration [ppm wt]
Li	0.005	-	-	-	< 0.005
Be	0.005	-	-	-	< 0.005
B	0.005	-	-	-	< 0.005
F	0.05	-	-	-	< 0.05
Na	0.005	0.2	0.1	0.02	0.04
Mg	0.005	< 0.005	< 0.005	< 0.005	< 0.005
Al	0.005	0.03	0.009	0.01	0.01
Si	0.005	0.02	< 0.005	< 0.005	0.009
P	0.005	-	-	-	< 0.005
S	0.005	-	-	-	0.006
Cl	0.005	0.2	0.01	0.02	0.02
K	0.01	-	-	-	< 0.01
Ca	0.01	< 0.01	< 0.01	< 0.01	< 0.01
Sc	0.005	-	-	-	< 0.005
Ti	0.005	< 0.005	< 0.005	< 0.005	< 0.005
V	0.005	< 0.005	< 0.005	< 0.005	< 0.005
Cr	0.005	< 0.005	< 0.005	< 0.005	< 0.005
Mn	0.005	< 0.005	< 0.005	< 0.005	< 0.005
Fe	0.005	< 0.005	< 0.005	< 0.005	< 0.005
Co	0.005	< 0.005	< 0.005	< 0.005	< 0.005
Ni	0.005	0.2	< 0.005	< 0.005	< 0.005
Cu	0.005	0.04	< 0.005	0.01	< 0.005
Zn	0.005	0.01	< 0.005	< 0.005	< 0.005
Ga	0.005	-	-	-	< 0.005
Ge	0.005	-	-	-	< 0.005
As	0.01	< 0.01	< 0.01	< 0.01	< 0.01
Se	0.01	0.3	0.25	0.8	0.3
Br	0.01	-	-	-	< 0.01
Rb	0.005	-	-	-	< 0.005
Sr	0.005	-	-	-	< 0.005
Y	0.005	-	-	-	< 0.005
Zr	0.005	-	-	-	< 0.005
Nb	0.005	-	-	-	< 0.005
Mo	0.005	-	-	-	< 0.005
Ru	0.005	-	-	-	< 0.005
Rh	0.005	-	-	-	< 0.005
Pd	0.01	< 0.01	< 0.01	< 0.01	< 0.01
Ag	0.005	< 0.005	< 0.005	< 0.005	< 0.005
Cd	0.005	7	0.05	< 0.005	< 0.005
In	0.005	< 0.005	0.03	0.17	< 0.005
Sn	0.005	-	-	-	< 0.005
Sb	0.05	< 0.05	< 0.05	< 0.05	< 0.05
Te	Matrix	Matrix	Matrix	Matrix	Matrix
I	0.05	-	-	-	< 0.05
Cs	0.005	-	-	-	< 0.005
Ba	0.05	-	-	-	< 0.005
La	0.05	-	-	-	< 0.005
Ce	0.005	-	-	-	< 0.005
Pr	0.005	-	-	-	< 0.005
Nd	0.005	-	-	-	< 0.005
Sm	0.005	-	-	-	< 0.005
Eu	0.005	-	-	-	< 0.005
Gd	0.005	-	-	-	< 0.005
Tb	0.005	-	-	-	< 0.005
Dy	0.005	-	-	-	< 0.005
Ho	0.005	-	-	-	< 0.005
Er	0.005	-	-	-	< 0.005
Tm	0.005	-	-	-	< 0.005
Yb	0.005	-	-	-	< 0.005
Lu	0.005	-	-	-	< 0.005
Hf	0.005	-	-	-	< 0.005
Ta	Source	-	-	-	Source
W	0.005	-	-	-	< 0.005
Re	0.005	-	-	-	< 0.005
Os	0.005	-	-	-	< 0.005
Ir	0.005	-	-	-	< 0.005
Pt	0.005	-	-	-	< 0.005
Au	0.05	-	-	-	< 0.05
Hg	0.005	-	-	-	< 0.005
Tl	0.005	< 0.005	< 0.005	< 0.005	< 0.005
Pb	0.005	0.08	< 0.005	< 0.005	< 0.005
Bi	0.005	0.02	< 0.005	< 0.005	< 0.005
Th	0.005	-	-	-	< 0.005
U	0.005	-	-	-	< 0.005
Tot Min	0.66	8.11	0.45	1.03	0.39
Tot Max	0.66	8.66	1.03	1.57	0.92
Best Case [%]	99.99993	99.99919	99.99996	99.99990	99.99996
Worst Case [%]	99.99993	99.99913	99.99990	99.99984	99.99991

Run	-	Raw	Te-VD-13	Te-VD-14	Te-VD-15
Raw Material	-	MCP	MCP	MCP	MCP
		Mat. Specialt.	Mat. Specialt.	Mat. Specialt.	Mat. Specialt.
		3N	3N	3N	3N
Purification	-	-	1 stage VD	2 stage VD	3 stage VD
Shiva Job #		S070703057	S070703060	S070703059	S070703058
Element	Detection Limits [ppm wt]	Concentration [ppm wt]	Concentration [ppm wt]	Concentration [ppm wt]	Concentration [ppm wt]
Li	0.005	< 0.005	< 0.005	< 0.005	< 0.005
Be	0.005	< 0.005	< 0.005	< 0.005	< 0.005
B	0.005	< 0.005	< 0.005	< 0.005	< 0.005
F	0.05	< 0.05	< 0.05	< 0.05	< 0.05
Na	0.005	0.17	0.6	1.2	0.2
Mg	0.005	< 0.005	0.05	0.18	< 0.005
Al	0.005	< 0.005	0.3	1	0.07
Si	0.005	< 0.005	0.04	0.25	0.05
P	0.005	< 0.005	< 0.005	< 0.005	< 0.005
S	0.005	< 0.005	0.05	0.04	0.01
Cl	0.005	< 0.005	0.05	0.07	< 0.005
K	0.01	0.1	0.06	0.2	< 0.01
Ca	0.01	< 0.01	0.1	1.3	0.02
Sc	0.005	< 0.005	< 0.005	< 0.005	< 0.005
Ti	0.005	< 0.005	< 0.005	< 0.005	< 0.005
V	0.005	< 0.005	< 0.005	< 0.005	< 0.005
Cr	0.005	< 0.005	< 0.005	< 0.005	< 0.005
Mn	0.005	< 0.005	< 0.005	< 0.005	< 0.005
Fe	0.005	< 0.005	0.03	0.008	< 0.005
Co	0.005	< 0.005	< 0.005	< 0.005	< 0.005
Ni	0.005	< 0.005	< 0.005	< 0.005	< 0.005
Cu	0.005	< 0.005	0.95	0.4	< 0.005
Zn	0.005	< 0.005	0.02	0.01	< 0.005
Ga	0.005	< 0.005	< 0.005	< 0.005	< 0.005
Ge	0.005	< 0.005	< 0.005	< 0.005	< 0.005
As	0.01	< 0.01	< 0.01	< 0.01	< 0.01
Se	0.01	0.7	0.8	0.6	0.3
Br	0.01	< 0.01	< 0.01	< 0.01	< 0.01
Rb	0.005	< 0.005	< 0.005	< 0.005	< 0.005
Sr	0.005	< 0.005	< 0.005	< 0.005	< 0.005
Y	0.005	< 0.005	< 0.005	< 0.005	< 0.005
Zr	0.005	< 0.005	< 0.005	< 0.005	< 0.005
Nb	0.005	< 0.005	< 0.005	< 0.005	< 0.005
Mo	0.005	< 0.005	< 0.005	< 0.005	< 0.005
Ru	0.005	< 0.005	< 0.005	< 0.005	< 0.005
Rh	0.005	< 0.005	< 0.005	< 0.005	< 0.005
Pd	0.01	< 0.01	< 0.01	< 0.01	< 0.01
Ag	0.005	< 0.005	< 0.005	0.06	< 0.005
Cd	0.005	< 0.005	< 0.005	< 0.005	< 0.005
In	0.005	< 0.005	< 0.005	< 0.005	< 0.005
Sn	0.005	< 0.005	0.1	0.2	< 0.005
Sb	0.05	< 0.05	< 0.05	< 0.05	< 0.05
Te	Matrix	Matrix	Matrix	Matrix	Matrix
I	0.05	< 0.05	< 0.05	< 0.05	< 0.05
Cs	0.005	< 0.005	< 0.005	< 0.005	< 0.005
Ba	0.05	0.04	1.6	1	0.1
La	0.05	0.01	0.24	0.6	0.03
Ce	0.005	< 0.005	< 0.005	< 0.005	< 0.005
Pr	0.005	< 0.005	< 0.005	< 0.005	< 0.005
Nd	0.005	< 0.005	< 0.005	< 0.005	< 0.005
Sm	0.005	< 0.005	< 0.005	< 0.005	< 0.005
Eu	0.005	< 0.005	< 0.005	< 0.005	< 0.005
Gd	0.005	< 0.005	< 0.005	< 0.005	< 0.005
Tb	0.005	< 0.005	< 0.005	< 0.005	< 0.005
Dy	0.005	< 0.005	< 0.005	< 0.005	< 0.005
Ho	0.005	< 0.005	< 0.005	< 0.005	< 0.005
Er	0.005	< 0.005	< 0.005	< 0.005	< 0.005
Tm	0.005	< 0.005	< 0.005	< 0.005	< 0.005
Yb	0.005	< 0.005	< 0.005	< 0.005	< 0.005
Lu	0.005	< 0.005	< 0.005	< 0.005	< 0.005
Hf	0.005	< 0.005	< 0.005	< 0.005	< 0.005
Ta	Source	Source	Source	Source	Source
W	0.005	< 0.005	< 0.005	0.04	< 0.005
Re	0.005	< 0.005	< 0.005	< 0.005	< 0.005
Os	0.005	< 0.005	< 0.005	< 0.005	< 0.005
Ir	0.005	< 0.005	< 0.005	< 0.005	< 0.005
Pt	0.005	< 0.005	< 0.005	< 0.005	< 0.005
Au	0.05	< 0.05	< 0.05	< 0.05	< 0.05
Hg	0.005	< 0.005	< 0.005	0.06	< 0.005
Tl	0.005	< 0.005	< 0.005	< 0.005	< 0.005
Pb	0.005	0.7	< 0.005	0.01	< 0.005
Bi	0.005	0.02	< 0.005	< 0.005	< 0.005
Th	0.005	< 0.005	< 0.005	< 0.005	< 0.005
U	0.005	< 0.005	< 0.005	< 0.005	< 0.005
Tot Min	0.66	1.74	0.78	7.23	4.99
Tot Max	0.66	2.27	1.30	7.69	5.47
Best Case [%]	99.99993	99.99983	99.99992	99.99928	99.99950
Worst Case [%]	99.99993	99.99977	99.99987	99.99923	99.99945

Run	-	Raw	Te-VD-ZR-24s	Te-VD-ZR-24c	Te-VD-ZR-24e
Raw Material	-	Am. Elements Lot # 1701395143 5N	Am. Elements Lot # 1701395143 5N (crushed)	Am. Elements Lot # 1701395143 5N (crushed)	Am. Elements Lot # 1701395143 5N (crushed)
Purification	-		2 stage VD 3+12 ZR H2/N2 zone starting extr.	2 stage VD 3+12 ZR H2/N2 center part	2 stage VD 3+12 ZR H2/N2 zone ending extr.
Shiva Job #		(spec.)	S090414017	S090414018	S090414019
Element	Detection Limits [ppm wt]	Concentration [ppm wt]	Concentration [ppm wt]	Concentration [ppm wt]	Concentration [ppm wt]
Li	0.005	< 0.005	< 0.005	< 0.005	< 0.005
Be	0.005	< 0.001	< 0.005	< 0.005	< 0.005
B	0.005	< 0.005	< 0.005	< 0.005	< 0.005
F	0.05	< 0.5	< 0.05	< 0.05	< 0.05
Na	0.005	< 0.22	0.03	0.04	0.07
Mg	0.005	< 0.03	< 0.005	< 0.005	< 0.005
Al	0.005	< 0.01	0.01	0.03	0.02
Si	0.005	< 0.1	0.05	0.2	0.04
P	0.005	< 0.01	< 0.005	< 0.005	< 0.005
S	0.005	< 0.02	0.04	0.03	0.03
Cl	0.005	< 0.05	0.02	0.006	0.03
K	0.01	< 0.05	< 0.01	< 0.01	< 0.01
Ca	0.01	< 0.05	< 0.01	< 0.01	< 0.01
Sc	0.005	< 0.05	< 0.005	< 0.005	< 0.005
Ti	0.005	-	< 0.005	< 0.005	< 0.005
V	0.005	< 0.001	< 0.005	< 0.005	< 0.005
Cr	0.005	< 0.01	< 0.005	< 0.005	< 0.005
Mn	0.005	< 0.01	< 0.005	< 0.005	< 0.005
Fe	0.005	< 0.02	< 0.005	< 0.005	< 0.005
Co	0.005	< 0.08	< 0.005	< 0.005	< 0.005
Ni	0.005	< 0.01	< 0.005	< 0.005	< 0.005
Cu	0.005	< 0.05	< 0.005	0.007	0.006
Zn	0.005	< 0.01	< 0.005	< 0.005	< 0.005
Ga	0.005	< 0.05	< 0.005	< 0.005	< 0.005
Ge	0.005	< 0.05	< 0.005	< 0.005	< 0.005
As	0.01	< 0.05	< 0.01	< 0.01	< 0.01
Se	0.01	< 1.2	0.2	0.5	1
Br	0.01	-	< 0.01	< 0.01	< 0.01
Rb	0.005	< 0.01	< 0.005	< 0.005	< 0.005
Sr	0.005	-	< 0.005	< 0.005	< 0.005
Y	0.005	< 0.05	< 0.005	< 0.005	< 0.005
Zr	0.005	< 0.01	< 0.005	< 0.005	< 0.005
Nb	0.005	< 0.01	< 0.005	< 0.005	< 0.005
Mo	0.005	< 0.05	< 0.005	< 0.005	< 0.005
Ru	0.005	< 0.05	< 0.005	< 0.005	< 0.005
Rh	0.005	< 0.01	< 0.005	< 0.005	< 0.005
Pd	0.01	< 0.01	< 0.01	< 0.01	< 0.01
Ag	0.005	< 0.05	< 0.005	< 0.005	< 0.005
Cd	0.005	< 0.05	< 0.005	< 0.005	< 0.005
In	0.005	Binder	Binder	Binder	Binder
Sn	0.005	< 0.5	< 0.005	< 0.005	< 0.005
Sb	0.05	< 0.5	< 0.05	< 0.05	< 0.05
Te	Matrix	Matrix	Matrix	Matrix	Matrix
I	0.05	< 0.1	< 0.05	< 0.05	< 0.05
Cs	0.005	< 0.1	< 0.005	< 0.005	< 0.005
Ba	0.05	< 0.1	< 0.05	< 0.05	< 0.05
La	0.05	< 0.05	< 0.05	< 0.05	< 0.05
Ce	0.005	< 0.05	< 0.005	< 0.005	< 0.005
Pr	0.005	< 0.05	< 0.005	< 0.005	< 0.005
Nd	0.005	< 0.01	< 0.005	< 0.005	< 0.005
Sm	0.005	< 0.01	< 0.005	< 0.005	< 0.005
Eu	0.005	< 0.01	< 0.005	< 0.005	< 0.005
Gd	0.005	-	< 0.005	< 0.005	< 0.005
Tb	0.005	< 0.01	< 0.005	< 0.005	< 0.005
Dy	0.005	< 0.01	< 0.005	< 0.005	< 0.005
Ho	0.005	< 0.01	< 0.005	< 0.005	< 0.005
Er	0.005	< 0.01	< 0.005	< 0.005	< 0.005
Tm	0.005	< 0.01	< 0.005	< 0.005	< 0.005
Yb	0.005	< 0.01	< 0.005	< 0.005	< 0.005
Lu	0.005	< 0.01	< 0.005	< 0.005	< 0.005
Hf	0.005	< 0.01	< 0.005	< 0.005	< 0.005
Ta	Source	< 1	Source	Source	Source
W	0.005	< 0.01	< 0.005	< 0.005	< 0.005
Re	0.005	< 0.01	< 0.005	< 0.005	< 0.005
Os	0.005	-	< 0.005	< 0.005	< 0.005
Ir	0.005	< 0.01	< 0.005	< 0.005	< 0.005
Pt	0.005	< 0.01	< 0.005	< 0.005	< 0.005
Au	0.05	< 0.01	< 0.05	< 0.05	< 0.05
Hg	0.005	< 0.01	< 0.005	< 0.005	< 0.005
Tl	0.005	< 0.01	< 0.005	< 0.005	< 0.005
Pb	0.005	< 0.05	< 0.005	< 0.005	< 0.005
Bi	0.005	< 0.05	< 0.005	< 0.005	< 0.005
Th	0.005	< 0.001	< 0.005	< 0.005	< 0.005
U	0.005	< 0.001	< 0.005	< 0.005	< 0.005
Tot Min	**0.66**		**0.35**	**0.81**	**1.20**
Tot Max	**0.66**		**0.98**	**1.43**	**1.82**
Best Case [%]	99.99993		99.99997	99.99992	99.99988
Worst Case [%]	99.99993	5N (spec.)	99.99990	99.99986	99.99982

Run	-	Raw	Te-VD-ZR-20c	Te-VD-ZR-22c
Raw Material	-	Sig. Aldch.	Sig. Aldch.	Sig. Aldch.
		Lot # 01009AJ	Lot # 01009AJ	Lot # 01009AJ
		4N	4N	4N
Purification	-	-	2 stage VD	2 stage VD
			4 + 14 ZR H2/N2	4 + 15 ZR H2/N2
				(ampoule cracked while ZR)
Shiva Job #			S09Z4419	S09Z4419
Element	Detection Limits [ppm wt]	Concentration [ppm wt]	Concentration [ppm wt]	Concentration [ppm wt]
Li	0.005	< 0.1	< 0.005	< 0.005
Be	0.005	< 0.1	< 0.005	< 0.005
B	0.005	< 0.1	< 0.005	< 0.005
F	0.05	-	< 0.05	< 0.05
Na	0.005	1.5	0.05	0.03
Mg	0.005	0.2	< 0.005	< 0.005
Al	0.005	3.3	0.05	0.01
Si	0.005	-	0.08	0.06
P	0.005	-	< 0.005	< 0.005
S	0.005	-	0.04	0.03
Cl	0.005	-	2	0.13
K	0.01	0.5	< 0.01	< 0.01
Ca	0.01	< 1	< 0.01	< 0.01
Sc	0.005	-	< 0.005	< 0.005
Ti	0.005	< 0.1	< 0.005	< 0.005
V	0.005	< 0.1	< 0.005	< 0.005
Cr	0.005	0.3	< 0.005	< 0.005
Mn	0.005	0.05	< 0.005	< 0.005
Fe	0.005	0.55	< 0.005	< 0.005
Co	0.005	< 0.1	< 0.005	< 0.005
Ni	0.005	< 0.1	< 0.005	< 0.005
Cu	0.005	<0.1	< 0.005	< 0.005
Zn	0.005	< 0.5	< 0.005	< 0.005
Ga	0.005	< 0.5	< 0.005	< 0.005
Ge	0.005	< 1	< 0.005	< 0.005
As	0.01	< 0.5	< 0.01	< 0.01
Se	0.01	< 0.5	< 0.01	< 0.01
Br	0.01	-	< 0.01	< 0.01
Rb	0.005	-	< 0.005	< 0.005
Sr	0.005	-	< 0.005	< 0.005
Y	0.005	-	< 0.005	< 0.005
Zr	0.005	< 0.5	< 0.005	< 0.005
Nb	0.005	< 0.5	< 0.005	< 0.005
Mo	0.005	< 0.5	< 0.005	< 0.005
Ru	0.005	-	< 0.005	< 0.005
Rh	0.005	-	< 0.005	< 0.005
Pd	0.01	-	< 0.01	< 0.01
Ag	0.005	< 0.1	< 0.005	< 0.005
Cd	0.005	< 1	< 0.005	< 0.005
In	0.005	< 0.5	Binder	Binder
Sn	0.005	< 0.5	< 0.005	< 0.005
Sb	0.05	< 1	< 0.05	< 0.05
Te	Matrix	-	Matrix	Matrix
I	0.05	-	< 0.05	< 0.05
Cs	0.005	-	< 0.005	< 0.005
Ba	0.05	< 0.5	< 0.05	< 0.05
La	0.05	< 0.1	< 0.05	< 0.05
Ce	0.005	< 0.1	< 0.005	< 0.005
Pr	0.005	-	< 0.005	< 0.005
Nd	0.005	-	< 0.005	< 0.005
Sm	0.005	-	< 0.005	< 0.005
Eu	0.005	-	< 0.005	< 0.005
Gd	0.005	-	< 0.005	< 0.005
Tb	0.005	-	< 0.005	< 0.005
Dy	0.005	-	< 0.005	< 0.005
Ho	0.005	-	< 0.005	< 0.005
Er	0.005	-	< 0.005	< 0.005
Tm	0.005	-	< 0.005	< 0.005
Yb	0.005	-	< 0.005	< 0.005
Lu	0.005	-	< 0.005	< 0.005
Hf	0.005	< 1	< 0.005	< 0.005
Ta	Source	< 5	Source	Source
W	0.005	< 0.5	< 0.005	< 0.005
Re	0.005	-	< 0.005	< 0.005
Os	0.005	-	< 0.005	< 0.005
Ir	0.005	-	< 0.005	< 0.005
Pt	0.005	-	< 0.005	< 0.005
Au	0.05	-	< 0.05	< 0.05
Hg	0.005	< 1	< 0.005	< 0.005
Tl	0.005	< 0.1	< 0.005	< 0.005
Pb	0.005	< 0.5	< 0.005	< 0.005
Bi	0.005	< 0.5	< 0.005	< 0.005
Th	0.005	< 0.1	< 0.005	< 0.005
U	0.005	< 0.1	< 0.005	< 0.005
Tot Min	**0.66**		**2.22**	**0.26**
Tot Max	**0.66**		**2.85**	**0.89**
Best Case [%]	**99.99993**		**99.99978**	**99.99997**
Worst Case [%]	**99.99993**	**4N (spec.)**	**99.99972**	**99.99991**

Run	-	Raw	Te-VD-ZR-27c
Raw Material	-	Sig. Aldch. Batch # MKAA4003 4N	Sig. Aldch. Batch # MKAA4003 4N
Purification	-	-	2 stage VD 20 + 17 H2
Shiva Job #			S09Z4419
Element	Detection Limits [ppm wt]	Concentration [ppm wt]	Concentration [ppm wt]
Li	0.005	< 0.4	< 0.005
Be	0.005	< 0.5	< 0.005
B	0.005	-	< 0.005
F	0.05	-	< 0.05
Na	0.005	3.5	< 0.005
Mg	0.005	< 0.1	< 0.005
Al	0.005	0.2	< 0.005
Si	0.005	0.8	0.04
P	0.005	-	< 0.005
S	0.005	-	< 0.005
Cl	0.005	-	0.02
K	0.01	2	< 0.01
Ca	0.01	< 0.5	< 0.01
Sc	0.005	< 0.1	< 0.005
Ti	0.005	< 0.1	< 0.005
V	0.005	< 0.1	< 0.005
Cr	0.005	0.2	< 0.005
Mn	0.005	0.1	< 0.005
Fe	0.005	0.2	< 0.005
Co	0.005	< 0.1	< 0.005
Ni	0.005	0.8	< 0.005
Cu	0.005	< 0.5	< 0.005
Zn	0.005	< 0.5	< 0.005
Ga	0.005	< 0.1	< 0.005
Ge	0.005	< 1	< 0.005
As	0.01	< 0.5	< 0.01
Se	0.01	5.5	< 0.01
Br	0.01	-	< 0.01
Rb	0.005	< 0.5	< 0.005
Sr	0.005	< 0.1	< 0.005
Y	0.005	< 0.1	< 0.005
Zr	0.005	< 0.1	< 0.005
Nb	0.005	< 0.1	< 0.005
Mo	0.005	< 0.5	< 0.005
Ru	0.005	-	< 0.005
Rh	0.005	-	< 0.005
Pd	0.01	-	< 0.01
Ag	0.005	< 0.5	< 0.005
Cd	0.005	< 1	< 0.005
In	0.005	< 0.5	Binder
Sn	0.005	< 1	< 0.005
Sb	0.05	< 1	< 0.05
Te	Matrix	-	Matrix
I	0.05	-	< 0.05
Cs	0.005	-	< 0.005
Ba	0.05	< 0.1	< 0.05
La	0.05	< 0.1	< 0.05
Ce	0.005	< 0.5	< 0.005
Pr	0.005	-	< 0.005
Nd	0.005	-	< 0.005
Sm	0.005	-	< 0.005
Eu	0.005	-	< 0.005
Gd	0.005	-	< 0.005
Tb	0.005	-	< 0.005
Dy	0.005	-	< 0.005
Ho	0.005	-	< 0.005
Er	0.005	-	< 0.005
Tm	0.005	-	< 0.005
Yb	0.005	-	< 0.005
Lu	0.005	-	< 0.005
Hf	0.005	< 0.5	< 0.005
Ta	Source	< 10	Source
W	0.005	< 0.5	< 0.005
Re	0.005	-	< 0.005
Os	0.005	-	< 0.005
Ir	0.005	-	< 0.005
Pt	0.005	-	< 0.005
Au	0.05	-	< 0.05
Hg	0.005	-	< 0.005
Tl	0.005	< 0.5	< 0.005
Pb	0.005	0.4	< 0.005
Bi	0.005	0.4	< 0.005
Th	0.005	< 1	< 0.005
U	0.005	< 0.1	< 0.005
Tot Min	0.66		0.06
Tot Max	0.66		0.71
Best Case [%]	99.99993		99.999994
Worst Case [%]	99.99993	4N (spec.)	99.99993

Appendix B

Vapor Pressure Data

The vapor pressure coefficients from Tab. B.1 have been fitted from tabulated vapor pressure data taken from [44, 45]. Eq. (B.1) has to be used to compute the vapor pressure P_v:

$$\log_{10}(P_v) = \frac{A}{T} + B \log_{10} T + CT + D \tag{B.1}$$

where the vapor pressure P_v is given in torr and the temperature in K.

Table B.1: Vapor pressure fit coefficients from [44, 45] fitted with a least square accuracy of $R^2 > 0.99$. [1]Chlorine fit only valid up to -30 C.

	B	Bi	Cl[1]	Hg	P	Re	S	Sb	Se	Si	Te
A	-30600	-10800	-2480	-3250	-6640	-42300	-4750	-13800	-5682	-26100	-10663.1
B	-2.675	-2.547	-14.72	0	0	-2.597	0	-13.36	0	-5.01	-18.6169
C	0	0	0	0	0	0	0	0	0	0	0.0034
D	21.26	18.01	48.25	9.14	13.41	20.77	11.12	54.77	9.937	29.14	64.7314

The vapor pressure coefficients from Tab. B.2 are taken from [43]. The three term fit was chosen if available. Eq. (B.2) has to be used to compute the vapor pressure P_v:

$$\log_{10}(P_v) = A + \frac{B}{T} + C \log_{10}(T) + DT \times 10^{-3} \tag{B.2}$$

where the vapor pressure P_v is given in atm and the temperature in K. Note that for most elements in Tab. B.1 a separate fit is available for the liquid (l) and the solid (s) element. For convenience, the melting point temperature T_m is tabulated as well

Table B.2: Vapor pressure fit coefficients from [43]. If available, three term fit was taken.

	Li	Na	K	Rb	Cs	Cu	Ag	Au	Be	Mg	Ca
T_m [°C]	454	371	337	312	303	1357	1234	1336	1556	923	1123
A_s	7.79	5.298	4.961	4.857	4.711	7.81	9.127	9.152	8.042	8.489	10.127
B_s	-8423	-5603	-4646	-4215	-3999	-17687	-14999	-19343	-17020	-7813	-9517
C_s	-0.7074	0	0	0	0	-0.2638	-0.7845	-0.7479	-0.444	-0.8253	-1.403
D_s	0	0	0	0	0	0.1486	0	0	0	0	0
A_l	8.409	8.4	8.233	8.316	4.165	11.209	5.752	10.298	5.786		
B_l	-8320	-5634	-4693	-4275	-3830	-17427	-13827	-18898	-15731		
C_l	-1.0255	-1.1748	-1.2403	-1.3102	0	-1.4742	0	-1.2222	0		
D_l	0	0	0	0	0	0	0	0	0		

	Sr	Ba	Zn	Cd	Al	Sc	Y	La	Ce	Ga	In
T_m [°C]	1043	983	693	594	932	1670	1750	1193	1058	310	429
A_s	9.226	12.405	8.435	8.405	9.459	6.65	9.735	7.463	6.023	6.657	8.532
B_s	-8572	-9690	-6923	-5944	-17342	-19721	-22306	-22551	-21278	-14208	-12680
C_s	-1.1926	-2.289	-0.7523	-0.8052	-0.7927	0.2885	-0.8705	-0.3142	-0.1127	0	-0.8495
D_s	0	0	0	0	0	-0.3663	0	0	0	0	0
A_l		4.007	5.378	5.242	10.578	5.795	13.745	6.524	5.611	6.754	5.374
B_l		-8163	-6286	-5392	-16946	-17681	-22215	-21977	-21200	-13984	-12276
C_l		0	0	0	-1.3133	0	-2.1235	-0.1667	0	-0.3413	0
D_l		0	0	0	0	0	0	0	0	0	0

	Tl	Ti	Zr	Th	Zn	Pb	V	Ta	Cr	Mo	W
T_m [°C]	577	2073	2125	2100	505	601	2130	3270	2176	2850	3650
A_s	8.994	11.925	10.008	8.668	8.274	8.336	9.744	16.807	6.8	11.529	2.945
B_s	-9624	-24991	-31512	-31483	-15834	-10303	-27132	-41346	-20733	-34626	-44094
C_s	-0.9887	-1.3376	-0.789	-0.5288	-0.7398	-0.8782	-0.5501	-3.2152	0.4391	-1.1331	1.3677
D_s	0	0	0	0	0	0	0	0.7437	-0.4094	0	0
A_l	8.628	16.37	1.584	-18.453	5.262	8.532	6.929				
B_l	-9383	-25229	-28764	-24569	-15332	-10093	-25011				
C_l	-1.0086	-2.6574	1.3555	6.6473	0	-1.075	0				
D_l	0	0	0	0	0	0	0				

	U	Mn	Fe	Co	Ni	Ru	Rh	Pd	Os	Ir	Pt
T_m [°C]	1403	1517	1812	1768	1725	2700	2239	1823	2970	2727	2043
A_s	0.77	12.805	7.1	10.976	10.557	9.755	10.168	9.502	9.419	10.506	4.882
B_s	-27729	-15097	-21723	-22576	-22606	-34154	-29010	-19813	-41198	-35099	-29387
C_s	2.6982	-1.7896	0.4536	-1.028	-0.8717	-0.4723	-0.7068	-0.9258	-0.3896	-0.75	1.1039
D_s	-1.5471	0	-0.5846	0	0	0	0	0	0	0	-0.4527
A_l	20.735		6.347	6.488	6.666		6.802	5.426			21.257
B_l	-28776		-19574	-20578	-20765		-26792	-17899			-30921
C_l	-4.0962		0	0	0		0	0			-3.896
D_l	0		0	0	0		0	0			0

	Pr	Gd
T_m [°C]	1208	1585
A_s	8.859	8.344
B_s	-18720	-20861
C_s	-0.9512	-0.5775
D_s	0	0
A_l	11.917	10.606
B_l	-18693	-20505
C_l	-1.957	-1.3598
D_l	0	0
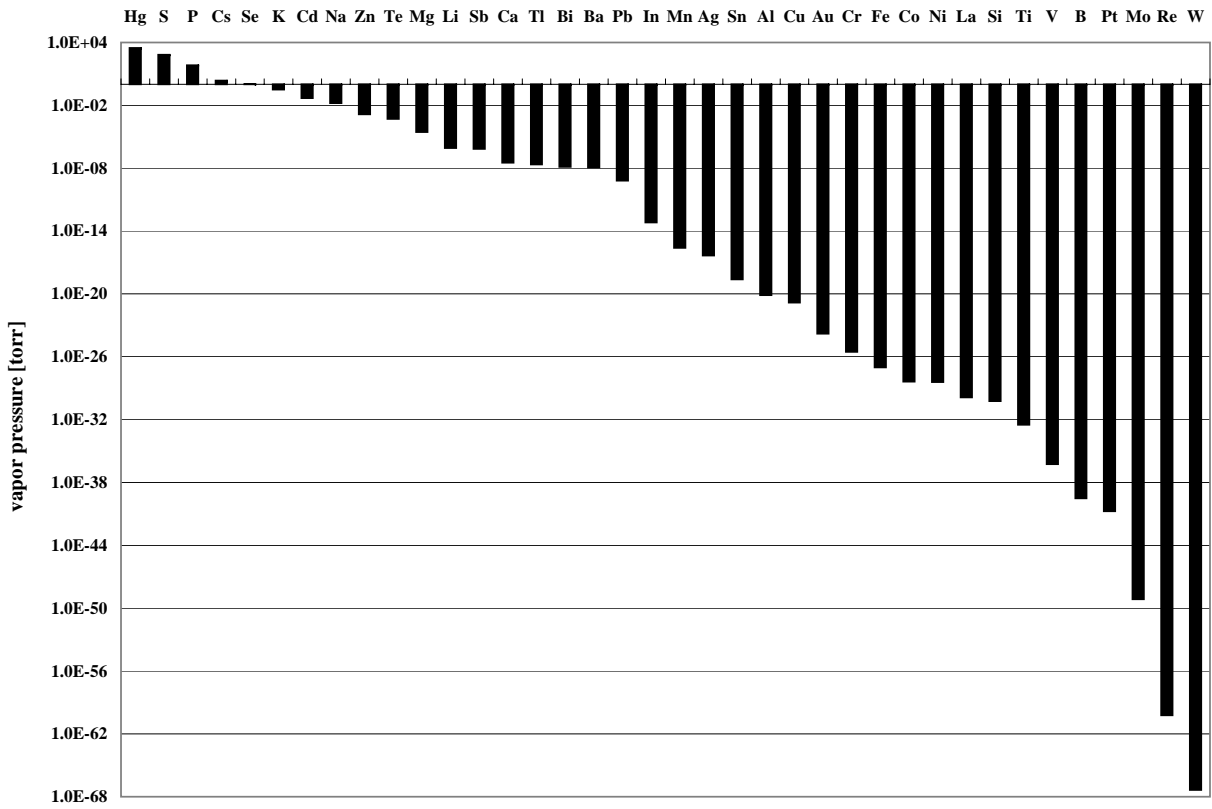
Figure B.1: Vapor pressure for common impurities at 300 C. From [43–45].
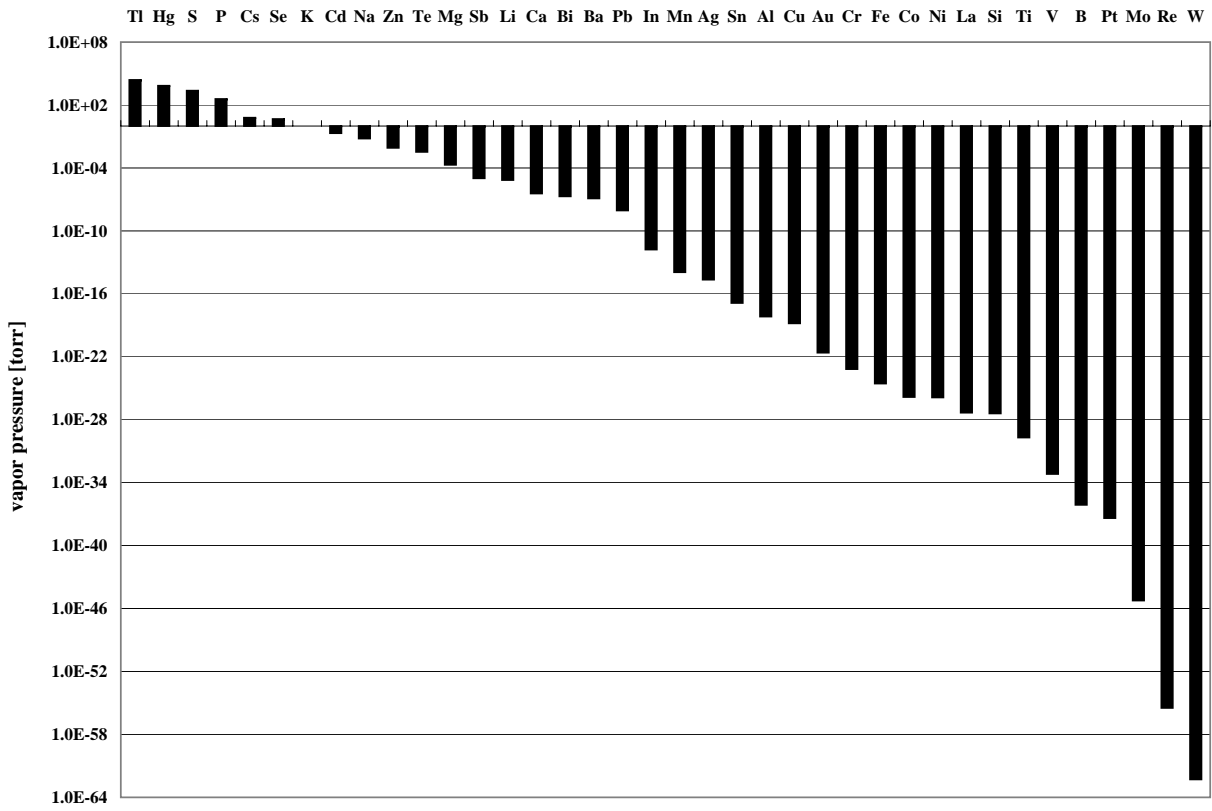
Figure B.2: Vapor pressure for common impurities at 340 C. From [43–45].
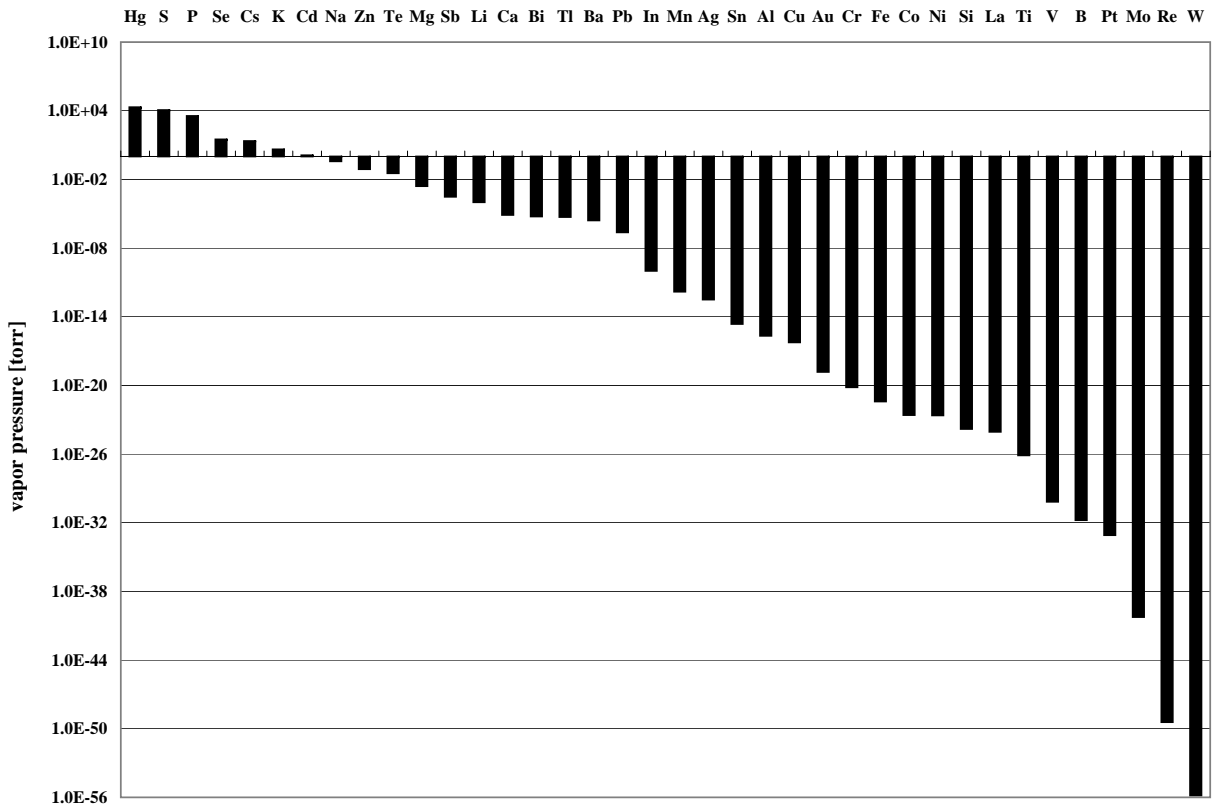
Figure B.3: Vapor pressure for common impurities at 400 C. From [43–45].
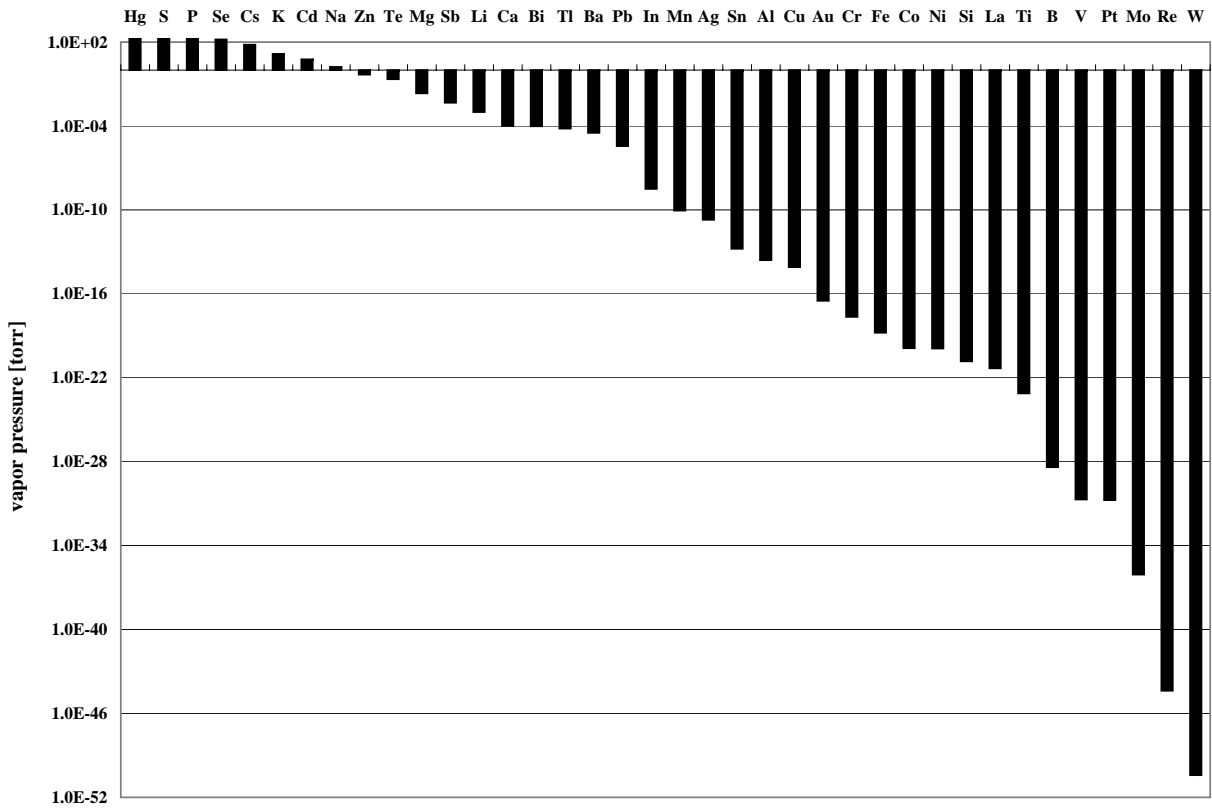
Figure B.4: Vapor pressure for common impurities at 460 C. From [43–45].
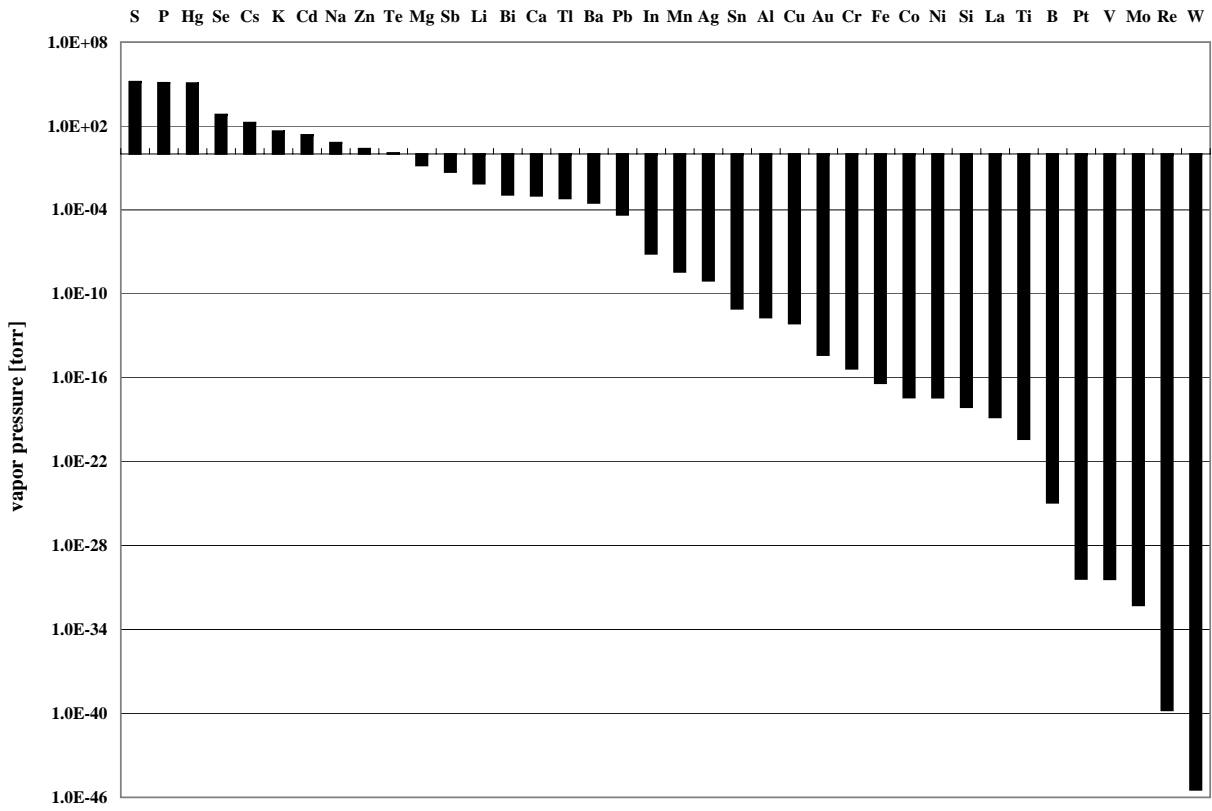
Figure B.5: Vapor pressure for common impurities at 525 C. From [43–45].
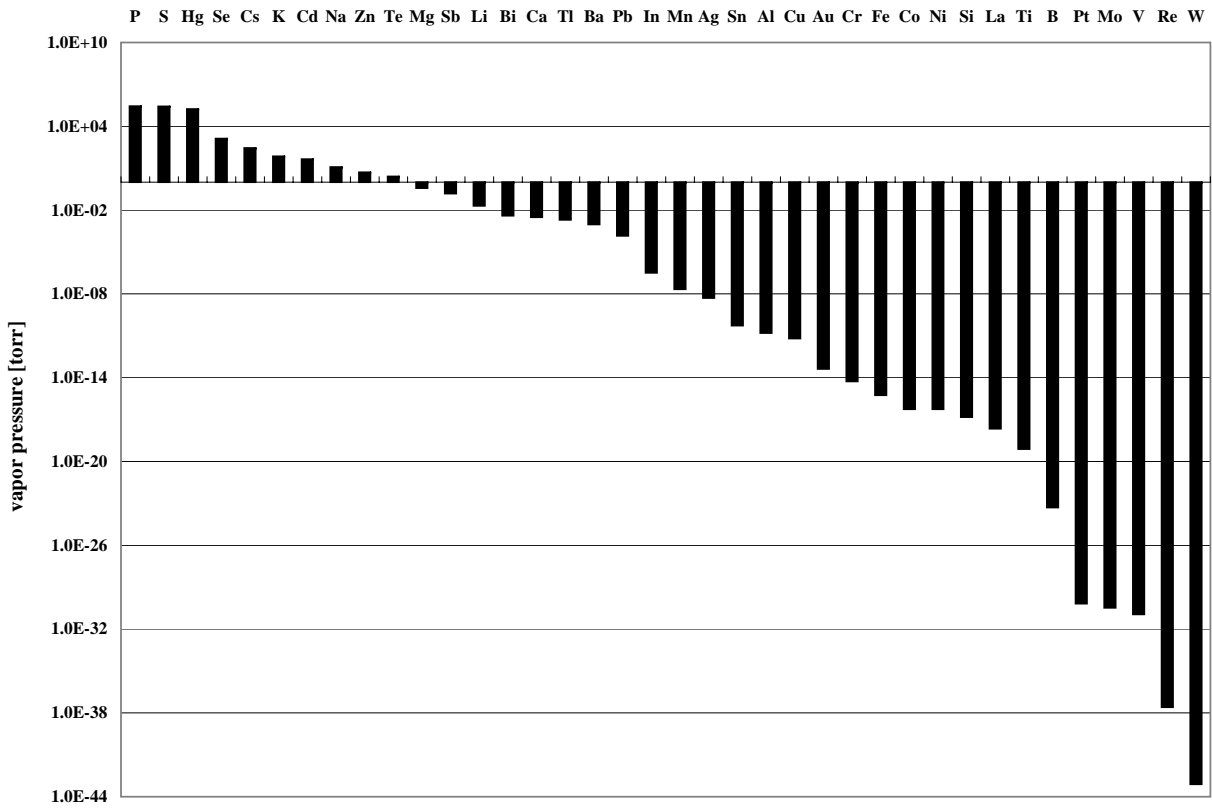
Figure B.6: Vapor pressure for common impurities at 560 C. From [43–45].

Appendix C

Material Properties

Table C.1: Relevant Cd, Zn and Te material properties.

	Cd	Zn	Te
melting point [C]	321.07	419.53	449.51
solid density [gcm^{-3}]	8.64	7.14	6.24
liquid density [gcm^{-3}]	8.00	6.57	5.70
expansion on melting [$-$]	*7.5%*	*8.0%*	*8.7%*
thermal expansion (298 K) [μm m^{-1}K^{-1}]	30.8	30.2	18.2
thermal conductivity (300 K) [Wm^{-1}K^{-1}]	92.0	116	≈ 3
heat of fusion [kJmol^{-1}]	6.21	7.32	17.49
heat of vaporization [kJmol^{-1}]	99.87	123.6	114.1
oxidation standard enthalpy of formation (800 K) [kJmol^{-1}]	-326.1	-372.9	-400

Appendix D

Zone Refining Impurity Distribution Matlab Code

```matlab
function [] = ZoneRefining()

%% Cleaning off:
clear;              % data
clc;                % screen
for Pointer=1:100
    close;          % clean graphic windows
end;

%% Parameter definition
L=30;               % Rod length [cm]:
l=3;                % Zone length [cm]:
eps=0.01;           % Grid length(resolution) [cm]
x=[0:eps:L]';       % Grid
k=0.2;              % Segregation coefficient [−]

%% Variable initialisation
C_0=[];             % Initial Distribution
C_n_1=[];           % (n−1)−th last distribution
C_n=[];             % n−th distribution
C_onepass=[];       % analytical one pass distributoon
C_n_liquid_0=0;     % starting position liquid concentration
C_n_liquid_i=0;     % i−th position liquid concentration
C_n_liquid_i_1=0;   % (i−1)−th position liquid concentration

%% Initial Distribution [ppm]
Concentration=1;                          % 1pp typlical for 6N Tellurium
C_0= Concentration * ones(L/eps+1,1);     % uniform concentration

%% Calculation
C_n_1=C_0;                   % previous concentration first is initial concentration

for n=1:5                    % n: n−th pass
C_n_liquid_0=sum(C_n_1(1:l/eps))/(l/eps);   % Position 0 liquid concentration
```

```matlab
% ZONE REFINING zone
for i=1:(L/eps-l/eps)                    % i-th window freezes out
    if i==1
    C_n_liquid_i_1=C_n_liquid_0;
    end;
    C_n(i)=k*C_n_liquid_i_1;             % i-th window freezes out
    C_n_liquid_i=C_n_liquid_i_1+eps/l*C_n_1(i+l/eps)-eps/l*C_n(i);
    C_n_liquid_i_1=C_n_liquid_i;         % update
end;

% NORMAL FREEZING zone
for i=(L/eps-l/eps+1):(L/eps+1)
    y_tilde=(x(i)-(L-l))/l;              % fraction of the original
                                         % liquid that has frozen
    C_n(i)=k*C_n_liquid_i_1*(1-y_tilde)^(k-1);
end;
    plot(x/L, C_n/C_0);                  % plot over normalized length
    hold on;
    C_n_1=C_n;                           % update
end;

%% Analytical One pass distribution after uniform concentration
% (for verification only)

C_onepass=C_0.*(1-(1-k).*exp((-k*x)/l));
plot(x(1:(L-l)/eps)/L, C_onepass(1:(L-l)/eps));
```

Appendix E

Zone Refining Temperature Profiles

Temperature profiles were recorded and plotted for typical temperature settings applied during the zone refining process of the three materials. The extended hot zone for the leveling and H_2 reaction run as well as the short zone settings for the actual zone refining step were recorded. Temperature settings were fine tuned for each individual run so that the profiles can only be used as a coarse reference. Furthermore, the presence of the charge flattens out the temperature profile mainly due to conduction heat transfer.

The set point temperatures of each zone is plotted as a straight line (red) over the extension of each zone. The temperature measurement taken for the control algorithm is measured right next to the respective heating coils (outside of furnace tube and outside of alumina liner tube) by furnace attached s-type thermocouples. This temperature was typically regulated with a deviation of less than 1.0 C by the PID control algorithm. The temperature in the furnace tube was measured using a quartz rod temperature probe equipped with an s-type thermocouple positioned at the center of the furnace tube.

The measurements were taken with the thermocouple in a stationary position, moving the furnace at 7 cm/h and taking measurements at a set rate. The translation rate was sufficiently slow so that the temperature measurements can be assumed to be quasi steady state.
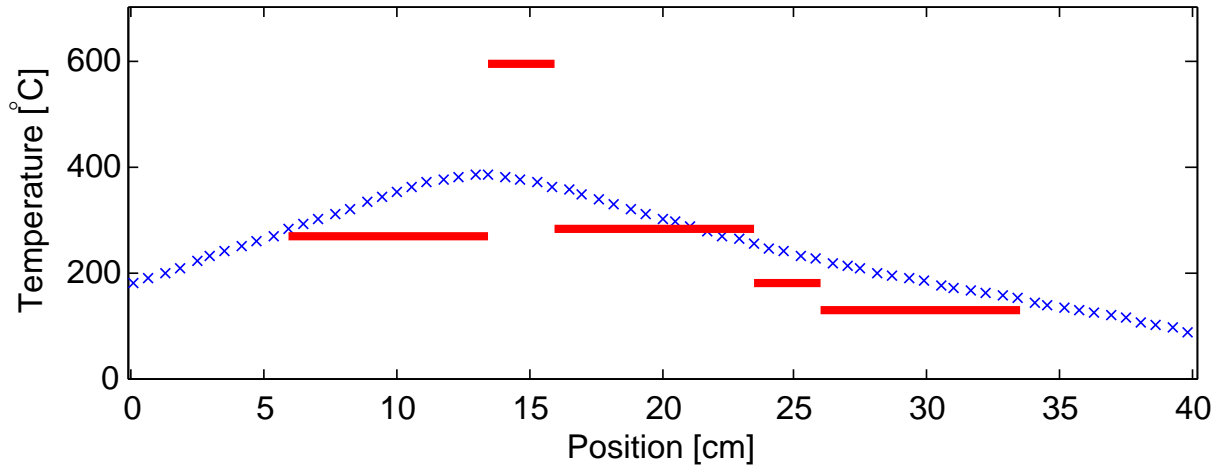
Figure E.1: Temperature profile for Cd zone refining. Origin corresponds to furnace extremity on zone A side; gas flow at ≈ 2 l/h (air) N_2; duty cycles $\approx (0.5/42/0/0/0)$.
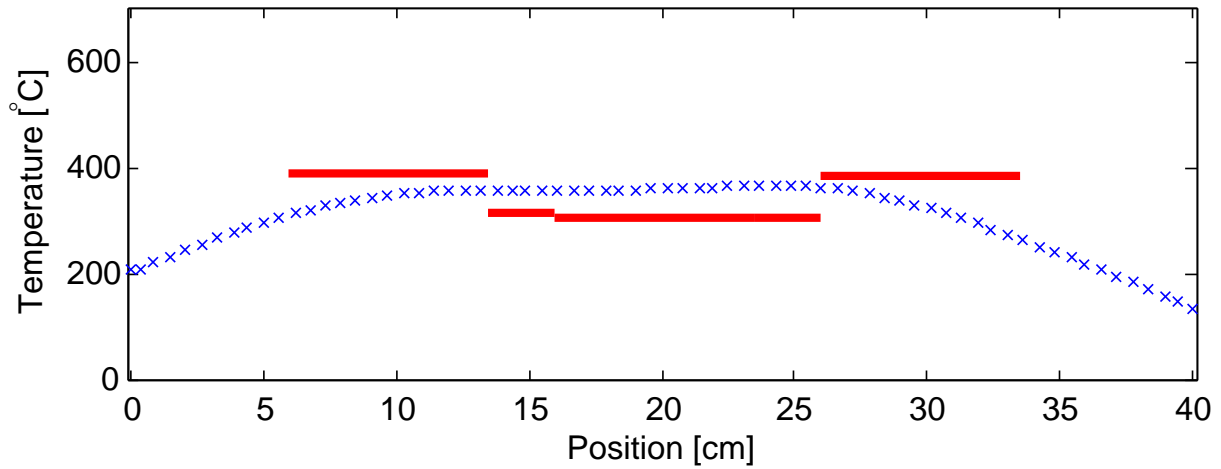
Figure E.2: Temperature profile for Cd leveling and H_2 reaction step. Origin corresponds to furnace extremity on zone A side; gas flow at ≈ 2 l/h (air) N_2; duty cycles $\approx (9.8/0/1.5/0/10.7)$.
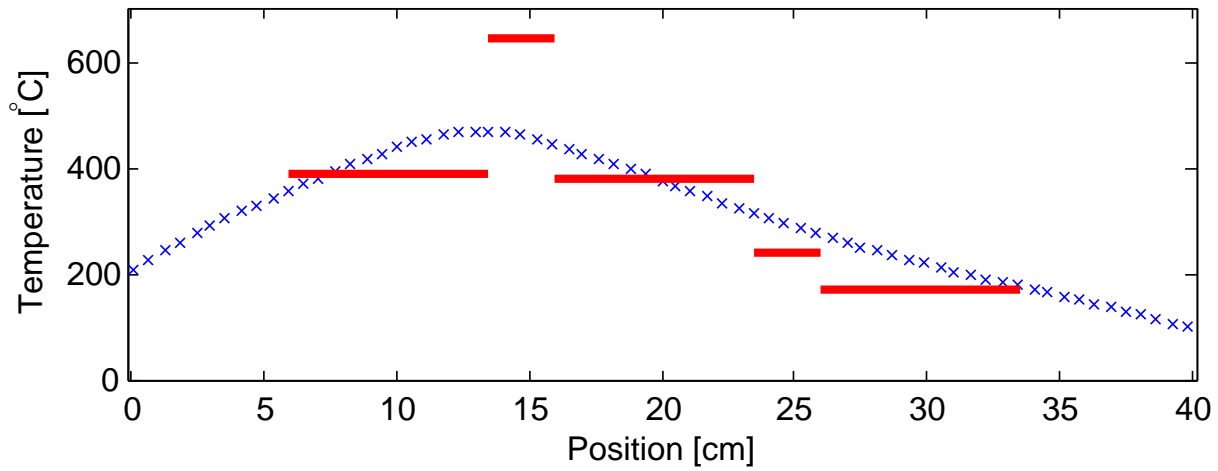
Figure E.3: Temperature profile for Zn zone refining. Origin corresponds to furnace extremity on zone A side; gas flow at $\approx$ 2 l/h (air) N_2; duty cycles $\approx$ (4.8/41/2.8/0/0).
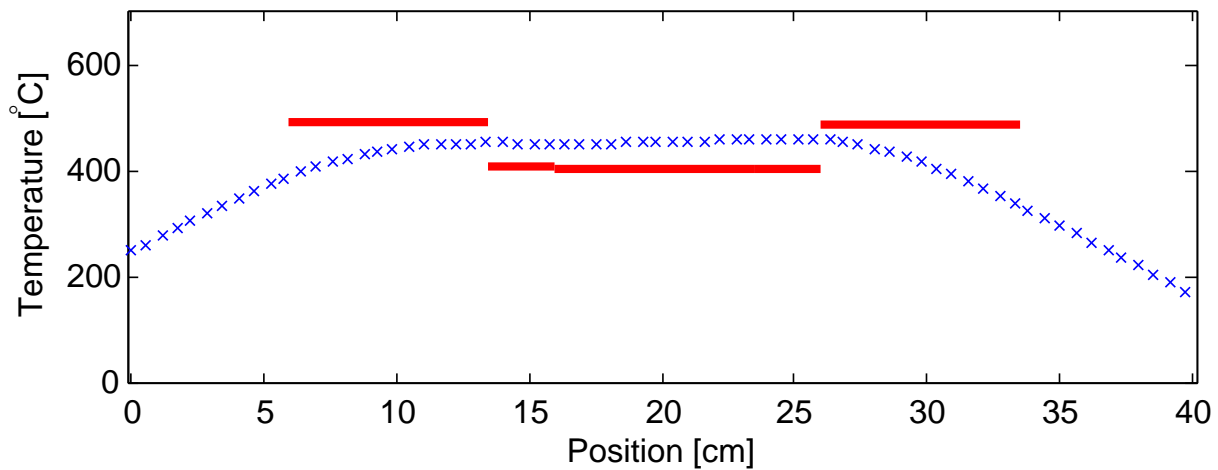
Figure E.4: Temperature profile for Zn leveling step. Origin corresponds to furnace extremity on zone A side; gas flow at $\approx$ 2l/h (air) N_2; duty cycles $\approx$ (13.8/0/3.1/0/14).
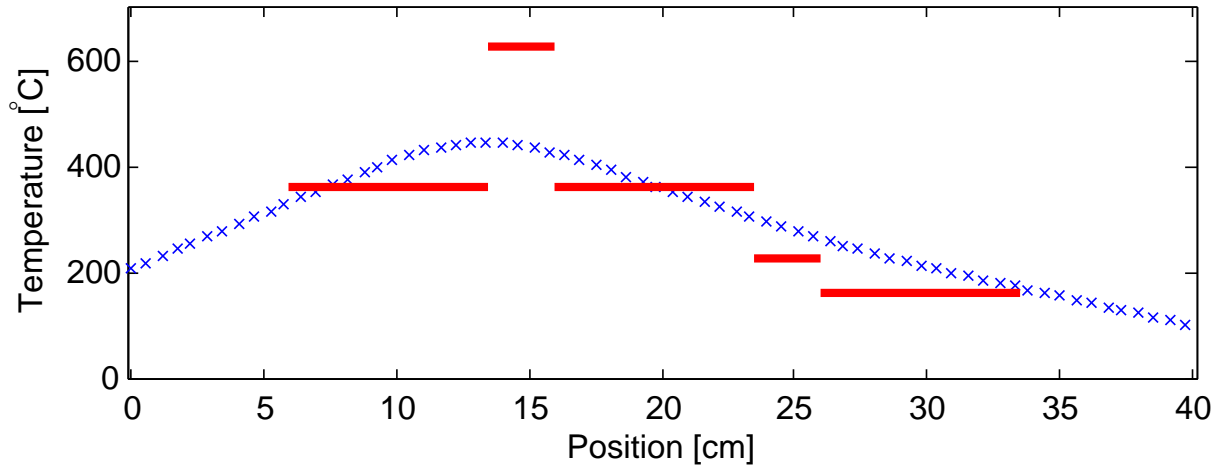
Figure E.5: Temperature profile for Te zone refining. Origin corresponds to furnace extremity on zone A side; gas flow at ≈ 2 l/h (air) N_2; duty cycles $\approx (4.1/44.9/9.3/0/0)$.
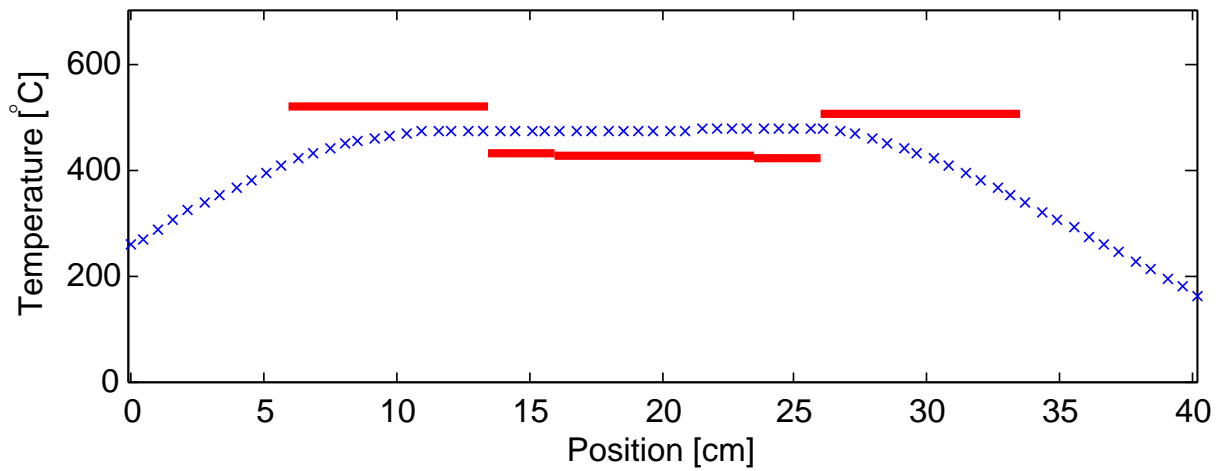
Figure E.6: Temperature profile for Te leveling and H_2 reaction step. Origin corresponds to furnace extremity on zone A side; gas flow at ≈ 2 l/h (air) N_2; duty cycles $\approx (16.1/0/4.3/0/18.8)$.